Université du Québec
Institut national de la recherche scientifique
Énergie, Matériaux et Télécommunications

QUANTUM PHOTONICS SYSTEMS ON CHIP AND IN FIBER

Par

Piotr Roztocki

Thèse présentée pour l'obtention du grade de
Doctorat en sciences, Ph.D.
en l'énergie et des matériaux

Jury d'évaluation

Examinateur externe	Sara Ducci Paris Diderot University
Examinateur externe	Benjamin Sussman University of Ottawa
Examinateur interne	Sharif Sadaf INRS-EMT
Directeur de recherche	Roberto Morandotti INRS-EMT

Acknowledgments

First, I would like to thank my supervisor, Roberto Morandotti. I greatly appreciate his support of my research activities, both academically and financially. I thank him especially for providing state-of-the-art infrastructure for my work, for introducing and supporting me in several academic opportunities, and for allowing me to pursue my own research ideas.

I thank the Natural Sciences and Engineering Research Council of Canada (NSERC) for their financial support via a Vanier Fellowship; INRS for their administrative and financial aid via tuition fee exemption; and the Marconi Society for their academic and financial recognition via a Paul Baran Young Scholar award.

A great thanks to my many mentors, colleagues, and friends in the Ultrafast Optical Processing and Nonlinear Photonics Groups at INRS. In particular, thank you to Prof. Michael Kues, for his ubiquitous mentorship, kind support of my budding research ideas, and thorough feedback on this thesis; Dr. Christian Reimer, for his research support and for teaching me about being a scientist inside and outside the lab; Benjamin MacLellan, for his friendship, his openness to high-risk high-reward ideas, and his help in giving my PhD a second wind; Dr. Stefania Sciara, for her camaraderie as we undertook parallel graduate paths; Bennet Fischer, for his friendship and encyclopedic knowledge of the literature; Dr. Benjamin Wetzel, for his guidance and positive outlook; Dr. Cristina Rimoldi, for her humour and professionalism alike; Dr. Mario Chemnitz, for his enthusiasm for good physics and coffee; Mehedi Islam, for conquering fiber interferometry despite its resistance; Dr. Young Zhang, for his disciplined approach to quantum photonics; Dr. James van Howe, for his kindness and academic support. A special thanks to Rob Helsten, for his second-to-none experimental support as our group's lab manager, his generosity with music knowledge, and his friendship.

I thank Dr. Yoann Jestin, co-founder at our start-up, Ki3 Photonics Technologies, for translating this document's French abstract and summary from English. More importantly, I thank him for believing enough in the quantum photonics technologies presented in this thesis to undertake this start-up journey with me, during which his enthusiasm and support have been invaluable.

I thank Profs. David Moss, Sai T. Chu, and Brent Little, for their collaboration and for providing world-class nanophotonic devices. I also thank Prof. José Azaña, for his kind academic and infrastructural support of our research, as well as his enthusiasm for my ideas.

Finally, my friends and family have been the cornerstone for the completion of this thesis. Among others, I would like to thank Luis, Andrea, Leanne, Allison (especially for her translation assistance), Luca, Caroline, Vi, Rachel, Joanna, and Michał for their support. This thesis is dedicated to my parents, two engineers whose Polish degrees are not recognized in Canada. And yet, their teachings remain the most important that I have received, even into my PhD.

Abstract

Quantum photonics systems hold historical and contemporary relevance towards cutting-edge foundations and applied research, and are relevant to all quantum technology sectors including computing, communications, and sensing. However, in both academia and industry, the development of such systems is significantly, detrimentally impacted by a commercial lack of accessible and standardized components. The quantum photonics supply chain would, in particular, be strengthened by the development of mass-producible, low-footprint, and inexpensive devices compatible with mature infrastructures, like optical fiber and chip-based platforms, and by making use of established degrees of freedom, like time and frequency. These are, to date, unavailable, meaning that the majority of research conducted makes use of home-built sources, signal processing, and characterization modules that oftentimes cannot transition outside laboratories into deployed systems.

The objective of this thesis is to address this lack and to target the development of devices, setups, and techniques for scalable quantum photonics systems. In particular, these will leverage infrastructures from telecommunications and integrated photonics, and will target systems compatible with optical fiber. The thesis objectives span the modules that comprise standard quantum systems, and specifically, target the development of: low-footprint quantum source architectures, low-loss quantum signal processing techniques, and fiber-compatible quantum signal characterization techniques.

A variety of photonics approaches is undertaken to accomplish these diverse objectives, with the main achievements being the realization of: i) a compact photon pair source that does not need an external laser as a pump; ii) a suite of tools for the recovery of interferometric phase, with specific strategies introduced to not decrease quantum signal-to-noise ratios; iii) a scheme for the versatile and coherent control of quantum states that are simultaneously entangled in time and frequency; iv) a radiofrequency-controlled quantum signal characterization technique; and v) an approach for measuring few-photon level optical spectra.

The work was particularly successful in leveraging infrastructure from telecommunications and integrated photonics, confirming that such components can often be used easily, with minimal customization, towards advanced quantum photonics applications.

keywords: *quantum photonics; fiber photonics; integrated optics; photon statistics; quantum signal processing; frequency combs; fiber interferometry; photon pair generation; hyper-entanglement; single-photon spectroscopy*

Résumé

Les systèmes photoniques quantiques ont un impact historique et contemporain par rapport à la recherche fondamentale et appliquée, et sont pertinents dans tous les secteurs des technologies quantiques, y compris l'informatique, les communications et la détection. Cependant, autant dans les universités que dans l'industrie, le développement de tels systèmes est considérablement impacté par un manque de composants standardisés et accessibles commercialement. La chaîne d'approvisionnement de la photonique quantique gagnerait notamment à être renforcée par le développement de dispositifs produits en série, avec un faible encombrement, peu coûteux, compatibles avec des infrastructures matures telles que les plates-formes à fibre optique et à puce, et utilisant des degrés de liberté établis comme le temps et la fréquence. À ce jour, ceux-ci sont indisponibles, ce qui signifie que la majorité des recherches menées utilisent des sources spécialement conçues en laboratoire, ou des modules de traitement du signal et de caractérisation qui souvent ne peuvent pas être utilisés à l'extérieur des laboratoires dans des systèmes déployés.

L'objectif de cette thèse est de combler ce manque et de cibler le développement de dispositifs et de techniques pour des systèmes photoniques quantiques évolutifs. En particulier, nous nous appuieront notamment sur des infrastructures de télécommunications et photonique intégrée, et viseront des systèmes compatibles avec la fibre optique. Les objectifs de la thèse couvrent le développement d'un ensemble de modules qui composent les systèmes quantiques standards et ciblent spécifiquement les architectures de sources quantiques à faible encombrement, les techniques de traitement de signaux quantiques à faible perte ainsi que les techniques de caractérisation de signaux quantiques compatibles avec la fibre optique.

Une variété d'approches photoniques sont utilisées pour atteindre ces objectifs ayant comme cibles: i) une source compacte de paires de photons qui n'a pas besoin d'un laser externe comme pompe; ii) une suite d'outils pour la récupération de la phase interférométrique, avec des stratégies spécifiques introduites pour ne pas diminuer les rapports signal/bruit quantiques; iii) un schéma pour le contrôle polyvalent et cohérent d'états quantiques qui sont simultanément intriqués dans le temps et la fréquence; iv) une technique de caractérisation de signal quantique commandée par radiofréquence; et v) une approche pour mesurer les spectres optiques à quelques photons.

Ces approches ont particulièrement réussi à tirer parti de l'infrastructure de télécommunications et de photonique intégrée, confirmant que ces composants peuvent être utilisés facilement et fréquemment, avec une personnalisation minimale, vers des applications photoniques quantiques avancées.

mots clés: *photonique quantique; fibre photonique; optique intégrée; statistiques de photons; traitement du signal quantique; peignes de fréquence; interférométrie fibrée; génération de paires de photons; hyper-enchevêtrement; spectroscopie de photon unique*

Synopsis

SYSTÈMES PHOTONIQUE QUANTIQUE SUR PUCE ET SUR FIBRE

Introduction

Une grande variété de plates-formes expérimentales a été explorée pour l'étude et l'application des phénomènes quantiques. Pour beaucoup d'entre elles, un premier objectif est d'obtenir un accès répétable à des états quantiques simples - tels que des états de qubit ou de particules uniques. Un deuxième objectif est l'accès à des mécanismes de contrôle cohérents pour ces états. La réalisation de ces objectifs est généralement suffisante pour l'exploration de phénomènes quantiques rudimentaires. Cependant, d'autres problèmes doivent être résolus pour accéder à des questions fondamentales et des technologies plus complexes - comment la plate-forme expérimentale à l'étude peut-elle être dimensionnée, à la fois en nombre et en taille d'états quantiques, ainsi qu'en complexité des circuits de contrôle ? Les états peuvent-ils être transduit efficacement d'une plate-forme à l'autre ?

Ces dernières années, plusieurs plates-formes technologiques quantiques ont connu une maturation et des avancées significatives. Les circuits supraconducteurs sont parmi les plates-formes les plus matures, et ont été utilisés dans la première démonstration de la suprématie quantique. Les technologies quantiques basées sur le contrôle atomique sont également très attrayantes en tant que plate-forme, en partie en raison de leur cohérence et de leur évolutivité. De plus, les spins électroniques, les gaz et autres constituent un éventail de plates-formes avec un accès simplifié aux phénomènes quantiques.

La photonique, en particulier, est une plate-forme centrale pour la physique quantique d'un point de vue historique et contemporain. Les photons, c'est-à-dire les particules fondamentales de la lumière, ont été parmi les premières plates-formes à être utilisées pour la démonstration et la

découverte de phénomènes quantiques. Aujourd'hui, la photonique est une plate-forme clé pour les applications couvrant la majorité, sinon la totalité, des technologies quantiques ; l'optique trouve une utilisation dans toutes les approches pour la génération de nombres aléatoires quantiques, les communications, l'informatique et la détection. La principale raison étant la facilité avec laquelle l'accès et le contrôle de l'état quantique peuvent être obtenus. Cela est dû à la faible décohérence, à l'excellente transmission et aux propriétés de robustesse des photons, l'accès simple à l'intrication qu'ils offrent et à leur compatibilité avec les infrastructures de puces en silicium et de fibres optiques. Néanmoins, l'évolution technique de la photonique quantique fait toujours l'objet d'efforts importants en recherche et développement.

Les études de photonique quantique fondamentale et appliquée utilisent une grande variété de systèmes avec divers composants, objectifs, et degrés de liberté. La présentation d'un « système photonique quantique archétypique » est donc vouée à être une simplification excessive, mais a toujours de la valeur car elle peut tenter de résumer la plupart des systèmes. Ici, je considère que les modules fondamentaux d'un tel système sont : la préparation du signal quantique, le canal de transmission + traitement du signal quantique, et la détection suivie de l'analyse (Figure 1.2). Ce choix de modules tente de souligner l'analogie entre les approches de la photonique quantique et les schémas fonctionnels des systèmes de communication classiques. En effet, les systèmes les plus avancés à ce jour peuvent exploiter le retour d'expérience entre ces différents modules afin, par exemple, de mettre en œuvre des étapes de traitement dépendant de la détection.

Des expériences de photonique quantique ont été mises en œuvre à différentes échelles physiques. La majorité des travaux d'étude sur les états intriqués ont historiquement été réalisés dans des configurations d'optique en espace libre, en utilisant des supports volumineux pompés par des lasers externes. De telles expériences nécessitent généralement de grands espaces et ont une faible portabilité, mais bénéficient d'un accès à des débits de signal élevés (car elles exploitent généralement des processus optiques non linéaires de second ordre très efficaces). Afin d'augmenter la complexité et la facilité d'utilisation, et afin de réduire les empreintes et le coût, les efforts de recherche mondiaux au cours des dernières décennies se sont concentrés sur le développement de la photonique quantique fibrée et sur les plates-formes intégrées. Cependant, des processus moins efficaces sont généralement utilisés dans de tels systèmes (ce qui signifie que des cavités doivent souvent être utilisées pour améliorer les émissions), introduisant un compromis entre les avantages susmentionnés et des taux de signal réduits.

Objectifs et structure de la thèse

Le rythme de développement de la photonique quantique, tant pour l'industrie que pour les universités, est considérablement affecté par le manque de composants accessibles et standardisés. La chaîne d'approvisionnement de la photonique quantique serait également renforcée par la disponibilité de composants produits en masse, à faible encombrement et coût, compatibles avec des infrastructures matures, telles que des plates-formes à base de fibres et de puces, et des degrés de liberté établis, tels que le temps et la fréquence. La disponibilité de tels éléments pourrait également donner accès à de nouvelles applications et concepts de physiques, ainsi qu'à une évolution de la complexité du système, comme l'exigent les nouveaux horizons dans le domaine où l'on envisage la déployabilité dans des environnements hors laboratoire tels que les réseaux de télécommunications et même l'espace.

L'objectif de cette thèse est de combler ce manque et de cibler le développement de dispositifs, de configurations et de techniques pour des systèmes photoniques quantiques évolutifs. En particulier, ceux-ci tireront parti des infrastructures de télécommunication et de la photonique intégrée, et cibleront les systèmes compatibles avec les réseaux de fibre optique. Les objectifs de cette thèse s'inspirent des modules présentés dans la section précédente ainsi que la Figure 1.2 et sont les suivants :

1. **Développement d'architectures de sources quantiques à faible encombrement :**
   Cet objectif se concentre sur les systèmes utilisant des paires de photons intriqués comme signal quantique, où l'état de l'art nécessite généralement des sources massives et/ou des lasers imposants pour la préparation du signal. En utilisant des composants intégrés et à fibre, nous visons le développement d'une nouvelle classe de source portable, un système hybride fusionnant le laser de pompe et la source quantique dans une configuration minimale. Nous caractérisons ensuite les améliorations en termes de stabilité et de performances obtenus grâce à l'utilisation de cette configuration.

2. **Développement de techniques de traitement de signaux quantiques à faibles pertes :**
   Cet objectif se concentre sur le développement de dispositifs et de configurations à base de fibres pour le traitement de signaux quantiques. Les interféromètres jouent un rôle clé dans le traitement du signal quantique, mais leurs réalisations en fibre optique sont sous-développées. Dans le cadre de cet objectif, tout d'abord, nous développons une méthode et un système de

récupération de phase dans des interféromètres à fibre en utilisant des signaux de référence à ondes continues (CW). Nous allons ensuite modifier la méthode pour la rendre mieux adaptée aux expériences de photonique quantique les plus sensibles, en utilisant des signaux de référence d'état cohérent atténués et des signaux de référence pulsés intenses/faibles. Deuxièmement, nous développons un schéma pour le contrôle polyvalent et cohérent d'états quantiques hyper-intriqués en fréquence et en temps.

3. **Développement de techniques de caractérisation de signaux quantiques couplés par fibre :** Cet objectif porte sur la démonstration de techniques de caractérisation de signaux quantiques faisant appel à des infrastructures compatibles avec la photonique fibrée. L'infrastructure basée sur les radiofréquences est très bien développée pour des applications dans le traitement du signal classique et les télécommunications. Nous visons ainsi le développement d'un cadre de caractérisation du signal quantique où, de manière atypique, une entrée de type radiofréquence est considérée comme le degré de liberté de contrôle. Enfin, nous utilisons des composants photoniques facilement accessibles pour effectuer la caractérisation des spectres optiques au niveau de quelques photons.

Sources pour la photonique quantique

Cavités imbriquées à verrouillage de mode actif pour la génération de paires de photons

Ici, nous présentons un nouveau schéma d'excitation à verrouillage de mode intra-cavité qui permet la génération de peignes de fréquence quantique pulsés (PFQ) de haute qualité de manière flexible et efficace. Plus précisément, nous excitons une microcavité non linéaire à l'aide d'une configuration à cavité imbriquée auto-verrouillée et une modulation active pour vérifier l'émission d'états de photons de haute pureté. Il s'agit, à notre connaissance, du premier schéma permettant de générer des peignes de fréquence quantique intégrés pulsés sans avoir besoin d'un laser externe. La polyvalence du schéma ainsi que l'utilisation de composants compatibles avec les puces photoniques en font un pas important vers la réalisation d'une source de peigne quantique pulsée extrêmement compacte.

Le schéma de génération des PFQ pulsés se compose d'une microcavité non linéaire intégrée dans une configuration de type « input-drop » à l'intérieur d'une cavité laser externe plus longue (Figure 3.1). La cavité externe incorpore un modulateur d'amplitude électro-optique actif, un

composant de gain optique et un filtre passe-bande étroit, ce dernier limitant le laser de la cavité à une bande passante correspondant à une seule résonance de la microcavité. Dans notre réalisation expérimentale, la microcavité non linéaire est un résonateur en micro-anneau intégré possédant quatre ports avec une plage spectrale libre de 200 GHz et un facteur de qualité Q de 235 000 (bande passante de résonance de ≈800 MHz), fabriqué dans la plate-forme d'oxynitrure de silicium. Le schéma est également compatible avec une large gamme de structures résonantes, par exemple avec des guides d'ondes et des résonateurs à cristaux photoniques, des micro-disques, des guides d'ondes optiques à résonateurs couplés (CROW) et des microcavités non linéaires de second ordre (tant qu'une configuration « input-drop » est accessible). L'élément d'amplification dans notre réalisation est un amplificateur à fibre dopée à l'erbium (EDFA), et l'élément de verrouillage de mode est un modulateur d'amplitude piloté par un signal radiofréquence (RF). Un isolateur dans la cavité assure une propagation unidirectionnelle des impulsions, et tous les composants sont connectés avec des fibres à maintien de polarisation pour une stabilité environnementale accrue. Le filtre passe-bande étroit (correspondant à la bande de télécommunications H34) limite le laser de cavité à une seule résonance du micro-anneau centrée à 1550 nm.

La longueur de la cavité externe a été choisie de telle sorte que plusieurs (environ 84) modes de fréquence de la cavité externe oscillent dans la bande passante de 3 dB de la résonance unique de la micro-cavité (800 MHz). Les phases relatives des modes de la cavité sont typiquement aléatoires, donnant lieu à des trains d'impulsions turbulents, mais l'introduction de la modulation d'amplitude (à une fréquence égale à l'espacement externe des modes, ici 9,8 MHz, ou ses harmoniques), entraîne des oscillations de mode devenant verrouillé en phase. Cela donne lieu à un train d'impulsions avec un taux de répétition correspondant à la fréquence de modulation, une bande passante optique ainsi qu'une fréquence centrale intrinsèquement adaptées à celles de la résonance de la micro-cavité, permettant une excitation à faible puissance, stable et de faible complexité, même si la fréquence de résonance devait légèrement se déplacer en raison, par exemple, d'instabilités thermiques.

Une fois que la fréquence de modulation correcte (correspondant à l'espacement des modes de cavité) a été identifiée par des balayages de fréquence ou une analyse radiofréquence de l'opération à mode déverrouillé, l'impulsion à mode verrouillé commence immédiatement une fois que le signal de modulation d'amplitude est fourni. Cela correspond à un train d'impulsions stable avec un faible bruit quadratique moyen (RMS) (0,42%, Figure 3.2) qui est capable de fonctionner sans interruption pendant des jours. Alors que la plupart des types de signaux de modulation peuvent être utilisés

ici pour le verrouillage de mode (par exemple, sinus, carré, etc.) s'ils redistribuent l'énergie aux harmoniques de l'espacement des modes de la cavité externe, nous utilisons spécifiquement un signal rectangulaire compte tenu de sa robustesse. La modification de la fréquence de modulation à ±0,001 MHz du taux de répétition n'affecte pas le fonctionnement en mode verrouillé, permettant une plage de contrôle du taux de répétition et démontrant également la flexibilité du schéma.

En modifiant le gain net de la cavité (via le gain de l'amplificateur et/ou les pertes de la cavité), la puissance optique du train d'impulsions d'excitation peut être ajustée, ce qui modifie les caractéristiques du PFQ émis. Un filtre coupe-bande à haute isolation est utilisé pour séparer le champ d'excitation du PFQ pour sa caractérisation. Le signal et les photons libres (ici, de la deuxième paire de résonance éloignée du champ d'excitation) sont acheminés vers des détecteurs séparés, où une fonction d'intercorrélation ($g_{si}^{(2)}(\tau)$, τ étant le délai temporel signal-idler) de leurs détections coïncidentes est mesurée (Figure 3.3 a).

Le rapport de coïncidence sur accident (CAR) des systèmes quantiques est une métrique opérationnelle clé semblable au rapport signal sur bruit des systèmes classiques. Nous extrayons le CAR des fonctions de corrélation que nous avons obtenues, et le mesurons dans notre configuration en fonction de la puissance d'excitation crête couplée dans le micro-anneau (Figure 3.3 b). L'opération de verrouillage de mode a persisté sur toute la plage de puissance testée. Le système atteint un CAR maximum de 110 et montre une diminution attendue avec l'augmentation des puissances laser (causée par une plus grande probabilité de générer plusieurs paires de photons à des énergies d'excitation plus fortes). Le taux de coïncidence présente quant à lui une augmentation prévue avec des puissances d'excitation croissantes et, à une valeur de CAR égale à 11 (suffisant pour, par exemple, des expériences de vérification d'intrication de qubit), nous démontrons des taux de coïncidence de 1,95 kHz. Compte tenu des pertes après la sortie du micro-anneau (11,4 dB par signal/idler), cela correspond à un taux de génération de paires de photons de 363 kHz (0,04 paires par impulsion) pour ce couple de canaux. En réduisant les pertes optiques et en utilisant des microcavités avec une non-linéarité plus élevée, le schéma pourrait ainsi être appliqué pour démontrer des taux de coïncidence plus élevés.

Dans cette conception de source, qui a une bande passante de pompe adaptée à la résonance, la majorité de l'énergie d'impulsion peut se coupler à la résonance pour l'excitation. Par comparaison, pour les schémas laser externes (où les impulsions sont généralement beaucoup plus larges spectralement que la résonance très étroite de 100 MHz), une partie moindre de l'énergie totale

des impulsions se couple dans la résonance. Pour ces schémas externes, les courbes de CAR et de coïncidence (Figure 3.3 b) se déplaceraient donc vers des puissances d'excitation plus élevées (étirées dans une mesure déterminée par le rapport du couplage impulsion/résonance). Cela conduirait à une baisse correspondante de l'efficacité énergétique de la source que le schéma présenté ici parvient à éviter.

Enfin, une caractéristique centrale de ce schéma est le contrôle flexible du taux de génération de PFQ. Ceci peut être accompli sans changer aucun composant à l'intérieur de la cavité, uniquement en modifiant la fréquence du signal de modulation d'amplitude RF. En particulier, en pilotant le modulateur d'amplitude à des fréquences correspondant à des multiples entiers de l'espacement des modes de cavité externe, nous obtenons un verrouillage de mode harmonique stable à différents taux de répétition harmonique (voir, par exemple, la Figure 3.4 avec une modulation à 19,5 MHz, résultant en un train d'impulsions avec 0,95% de bruit RMS).

Fait intéressant, ce contrôle du taux de répétition permet de conserver un CAR élevé tout en augmentant le taux de coïncidence. En utilisant des taux de répétition d'impulsion plus élevés tout en maintenant une puissance de crête d'impulsion d'excitation constante, le taux de coïncidence peut être augmenté de manière linéaire sans modifier la géométrie de la configuration (Figure 3.5 en haut et au milieu). De plus, en caractérisant la pureté des photons émis à partir d'une seule résonance en fonction du taux de répétition du système (Figure 3.5 en bas) et en utilisant une configuration de détection de type Hanbury Brown et Twiss, nous avons trouvé, en moyenne, un nombre de mode effectif de 1,00±0,11 pour les différentes harmoniques de taux de répétition. Cela correspond à un état à deux photons séparables de haute pureté, et confirme également que le schéma excite la résonance du micro-anneau sur toute sa bande passante. Ce résultat de mesure est également d'un intérêt fondamental, car à des taux de répétition plus élevés, moins de modes de cavité sont excités dans la résonance. Le cas limite de ceci, qui n'est pas accessible dans cette configuration, serait potentiellement une excitation monomode (onde continue), communément associée à des photons multifréquences filles (c'est-à-dire l'intrication fréquentielle). Néanmoins, la pureté spectrale ne diminue pas dans les harmoniques étudiées ici.

Traitement du signal quantique

Interférométrie à base de fibres avec signaux de référence lumineux à ondes continues

À l'heure actuelle, une technique de stabilisation courante et peu coûteuse consiste à coupler un laser à onde continue de référence dans l'interféromètre et à mesurer le signal interféré (I_x, Figure 4.1 a). Ce signal varie comme un cosinus ($I_x(\phi) = I_{mid}[1+Vcos(\phi)]$, où l'intensité $I_{mid} = (I_{max}+I_{min})/2$ et V représente la visibilité de l'interférence) et est utilisé pour extraire la phase ϕ de l'interféromètre. Bien qu'expérimentalement simple par rapport à l'état de l'art actuel, une telle approche à une seule longueur d'onde est limitée car plusieurs phases entre 0 et 2π correspondent à la même intensité (c'est-à-dire que la carte de l'intensité à la phase n'est pas une à une sur cette plage, par exemple, les deux phases $\phi = \frac{\pi}{2}, \frac{3\pi}{2}$ correspondent à toutes les deux à I_{mid}). Cela conduit à des ambiguïtés dans la récupération de phase, nécessitant généralement le balayage actif de la longueur d'onde laser ou du retard de l'interféromètre, ce qui rend difficile la reproduction des réglages de phase ou le verrouillage de plusieurs interféromètres sur différentes phases avec une seule source.

Cependant, lorsque la fréquence optique d'un tel signal injecté est modifiée (par exemple, via un modulateur acousto-optique), sa réponse en cosinus est décalée en phase. Cela signifie qu'une composante de fréquence optique légèrement décalée est suffisante pour produire une réponse sinusoïdale décalée de $\pi/2$ par rapport à I_x (c'est-à-dire le signal en quadrature, I_y, Figure 4.1 a). L'ambiguïté de phase est présente lorsque seule I_x est acquis, mais peut être éliminée en mesurant simultanément les signaux orthogonaux I_x et I_y. Lorsqu'ils sont acquis ensemble, I_x et I_y mappent un à un une phase comprise entre 0 et 2π (Figure 4.1 b), permettant la récupération sans ambiguïté de la phase de l'interféromètre. Plus précisément, la relation cosinus-sinus de I_x et I_y permet une reconstruction simple de la phase de l'interféromètre (par rapport à la référence optique) en utilisant :

$$\phi = arctan2\left(\frac{2I_y - I_y^{max} - I_y^{min}}{I_y^{max} - I_y^{min}}, \frac{2I_x - I_x^{max} - I_x^{min}}{I_x^{max} - I_x^{min}}\right) \quad (1)$$

où arctan2 est la fonction arctangente à deux arguments, tandis que I^{max} et I^{min} correspondent respectivement aux maxima et minima d'interférence.

Un très faible décalage de fréquence optique entre les deux signaux injectés est nécessaire pour maintenir une période similaire pour I_x et I_y. Par exemple, pour un interféromètre avec un déséquilibre de 4 ns dans la bande télécom à 1550 nm, un décalage de fréquence de 188 MHz peut être utilisé.

Cependant, la plupart des filtres du commerce ne peuvent pas séparer des fréquences aussi finement espacées pour la mesure simultanée des deux interférences. À cette fin, nous exploitons le degré de liberté de polarisation - facilement contrôlable et propagé avec un « cross-talk » minimale dans la fibre optique - pour préparer un signal de référence où I_x et I_y se déplacent dans des modes de polarisation orthogonaux de la fibre (Figure 4.4). Le signal de référence bicolore est préparé à partir d'une source, qui est divisée en un bras passif et un bras modulé acousto-optiquement (AOM) pour créer les composantes décalées en fréquence et polarisées orthogonalement. Ce signal de référence est introduit dans l'interféromètre. Une fois qu'il est interféré et émis, un séparateur de faisceau de polarisation à fibre standard (plutôt qu'un filtre sur mesure coûteux) est utilisé pour séparer les deux fréquences pour la détection des intensités I_x et I_y. A noter également que ce signal peut être préparé une seule fois et réparti entre plusieurs interféromètres, fournissant une référence commune.

Avec l'utilisation supplémentaire de méthodes de stabilisation passive (amortissement mécanique), les perturbations sont limitées à des fréquences inférieures à la dizaine de kHz. Une électronique numérique portable de qualité grand public est ensuite facilement intégrée dans le système pour la récupération de la phase et la correction en temps réel (de même, l'électronique à faible encombrement peut également fournir le signal de commande l'AOM), avec une accordabilité de phase via un tendeur de fibre dans l'un des bras. Le suivi et la compensation des fluctuations permettent une stabilité de phase à long terme (par rapport à notre référence, c'est-à-dire mesurée en boucle, Figure 4.5), comme requis pour de nombreuses mesures avec de longs temps d'intégration et des références optiques communes (par exemple, la caractérisation de l'état quantique). Alternativement, sans stabilisation en temps réel, si notre signal de référence devait être suivi pendant toute la durée d'une mesure, la phase pourrait être post-compensée/post-sélectionnée. De tels schémas interférométriques de suivi de phase pour la post-compensation sont déjà utilisés dans plusieurs domaines d'application.

Un problème dans les schémas de récupération de phase basés sur l'utilisation d'un seul signal d'interférence (sans échantillonner une composante orthogonale) est que les perturbations de phase ne peuvent pas être résolues de la même manière sur toutes les phases. Cela limite la plage de valeurs de phase interférométriques accessibles, à moins que, par exemple, la fréquence laser de référence ou le retard de l'interféromètre ne soient activement réglés pour suivre les maxima de sensibilité, ce qui introduit malheureusement des problèmes de complexité de configuration et de reproductibilité. En regardant l'exemple d'un signal de référence à une seule couleur (qui, bien

que n'étant pas le plus avancé, a une faible complexité expérimentale comparable à la méthode présentée), la réponse du signal de rétroaction aux changements de phase est décrite par la sensibilité $S \propto \left|\frac{dI_x}{d\phi}\right| = |VI_{mid}sin(\phi)|$. La sensibilité, et par procuration la précision de la récupération de phase (par rapport à la référence optique), peut être considérée comme extrêmement dépendante de la phase, avec des minima aux phases 0 et π. Cela restreint la plage de phases accessibles à l'aide d'un tel signal de retour (Figure 4.6 a).

Au lieu de cela, l'utilisation de notre signal de retour bicolore, composé des composants en phase et en quadrature, rend la sensibilité constante pour toutes les phases. En conséquence, toutes les phases de $[0, 2\pi)$ sont accessibles individuellement (Figure 4.6 a) avec des performances de stabilisation indépendantes de la phase (Figure 4.6 b). Ceci est démontré encore plus directement via l'analyse de déviation du signal d'erreur d'Allan pour différents temps d'intégration (Figure 4.6 c). De plus, nous observons une déviation d'Allan de $5.89 \times 10^{-5}\pi$ rad (en boucle, équivalent à 0,04 nm à longueur d'onde optique de 1550 nm) à un temps d'intégration de 2:11 minutes (et même à des temps d'intégration de 1h09m, cette valeur reste inférieure à $1 \times 10^{-3}\pi$ rad). Cette valeur surpasse la plupart des autres implémentations dans l'état de l'art, et est également unique dans sa stabilisation pratique, peu coûteuse et en temps réel.

Interférométrie à base de fibres avec une référence d'état cohérent atténuée

Un certain nombre d'expériences et de technologies de photonique quantique exigent un nombre minimal de photons de fond (background), que les lasers de stabilisation lumineux (dans les régions de longueur d'onde proches des bandes de signaux quantiques) et un filtrage limité ne peuvent pas toujours fournir, entraînant un « cross-talk » non négligeable. Afin de résoudre ce problème pour des cas d'application aussi délicats, nous étudions la mise en œuvre d'une forte atténuation du signal de référence CW bichromatique (avant l'injection dans l'interféromètre) pour produire une réponse d'interférence à quelques photons (mesurée à l'aide de détecteurs à photon unique).

Pour cela, un atténuateur optique variable à maintien de polarisation est inséré juste avant que le signal de référence bicolore ne soit injecté dans l'interféromètre. Le reste de la configuration est conservé comme sur la Figure 4.4, à l'exception des photodiodes remplacées par deux détecteurs de photons uniques supraconducteurs à nanofils (Quantum Opus, un pour I_x et un pour I_y), connectés à une électronique de conversion temps-numérique (Picoquant Hydraharp). Pour la Figure 4.7, l'étireur de fibre dans le bras de l'interféromètre est ensuite balayé et les temps d'arrivée des photons

à chaque canal sont collectés. Une fenêtre d'intégration mobile est ensuite mise en œuvre en post-sélection pour déterminer à la fois les taux de comptage et la réponse en temps d'intégration du système.

Il s'agit d'une solution intéressante, car le signal de sonde à faible puissance ne nécessite plus de filtres à réjection élevée, ce qui signifie que même les filtres DWDM (multiplexage dense en longueur d'onde) standard peuvent réduire le « cross-talk ». De tels états cohérents atténués ont été étudiés pour la reconstruction de phases d'interféromètres et démontrés expérimentalement dans un schéma de stabilisation à une seule couleur pour se verrouiller sur une phase. Ici, nous étendons ces efforts et étudions l'utilisation de deux états cohérents atténués en quadrature pour la récupération de phase.

En mesurant les sorties de signaux en phase et en quadrature à un port d'interféromètre (Figure 4.7), nous illustrons le compromis, provoqué par les statistiques poissonniennes régissant les états cohérents, entre l'erreur d'estimation de phase et le temps d'intégration du signal (c'est-à-dire, une meilleure estimation de la phase pour des temps d'intégration plus longs et des puissances de signal de référence plus élevées). Ces statistiques donnent lieu à une dépendance de phase dans l'erreur d'estimation de phase (Figure 4.8, une dépendance supprimée lorsque les deux ports de sortie sont utilisés).

Pour les expériences où ces inconvénients peuvent être tolérés en échange d'un « cross-talk » réduit, nous joignons une carte thermique illustrant le compromis entre ces paramètres (Figure 4.9). Expérimentalement, le nombre moyen de photons est le produit du temps d'intégration τ du détecteur, et du taux de flux de photons, Θ, qui peuvent tous deux être limités par des considérations de mise en œuvre telles que la vitesse de dérive de phase maximale présente (v), le taux de saturation du détecteur ou l'erreur d'estimation de phase admissible ($\Delta\phi_{max}$). En pratique, le temps d'intégration doit être choisi de manière à pouvoir résoudre les dérives de phase les plus rapides, tandis que le taux de comptage sera limité par le point de saturation des détecteurs utilisés, la puissance maximale disponible à partir de la référence optique, ou la puissance maximale autorisée qui minimise toujours le « cross-talk » à des limites acceptables.

Interférométrie à base de fibres avec références pulsées lumineuses et faibles

Le laser de référence utilisé dans le schéma de récupération de phase n'a pas besoin d'être à onde continue (après tout, les références CW produisent des photons de bruit de fond sur toutes les fenêtres temporelles de détection). Les sources à mode verrouillé (et surtout les peignes de fréquence stabilisés) ont des longueurs de cohérence suffisantes pour produire des signaux d'interférence (Figure 4.10), une caractéristique déjà exploitée dans le cadre de l'optique classique ainsi que les communications quantiques, et ici implémentée avec notre schéma de référence I_x et I_y.

Pour cette étude, la configuration est identique à celle utilisée avec la référence CW (Figure 4.4), mais avec la source laser d'origine remplacée par une sortie de peigne de fréquence stabilisée (Menlo FC1500-250-WG, taux de répétition de 250 MHz) filtrée jusqu'à une bande passante optique de 200 GHz utilisant des filtres passe-bande et des amplificateurs (Santec et Lightwave 2020, Pritel SPFA). Pour visualiser l'interférence de la référence lumineuse pulsée, nous utilisons une photodiode rapide pour suivre la phase d'impulsion en impulsion ; alternativement, une photodiode plus lente peut s'intégrer efficacement sur le signal si une électronique plus simple/moins chère est requise (Figure 4.10). Ici, les photodiodes intégratrices utilisées (Thorlabs PDA50B, bande passante 2,1 kHz, acquise avec un National Instruments DAQ System PCI 6251 + BNC2090) sont lentes par rapport à la fréquence de répétition du signal et agissent comme un intégrateur de signal. D'autre part, les photodiodes rapides (Finisar XPDV, bande passante 50 GHz) sont connectées à un oscilloscope à large bande passante (Agilent DSO-X 92804A, bande passante 28 GHz, 80 GSa/s) pour reproduire les interférences du train d'impulsions.

Dans la préparation du signal de référence (Figure 4.4), la source est également divisée en deux chemins différents pour introduire un décalage de fréquence avec l'AOM sur l'un d'eux. Afin de réaliser la démonstration de multiplexage temporel illustrée à la Figure 4.11, avant la recombinaison, nous ajoutons une ligne à retard optique pour implémenter une différence de temps relative entre I_x et I_y.L'injection de ce signal de référence temporellement entrelacé dans l'interféromètre peut alors être réglée avec une autre ligne à retard pour permettre un multiplexage temporel avec le signal sous test. Le signal de déclenchement du détecteur est fourni par le train d'impulsions du peigne de fréquence. En post-traitement, les différents canaux temporels (Figure 4.11) peuvent alors être facilement séparés pour reconstruire les signaux respectifs. Les données présentées sont acquises

pendant 120 s avec un temps d'intégration de 100 ms (cela correspond à une moyenne sur plusieurs cycles d'échantillonnage).

Dans le cadre de l'optique quantique, l'utilisation de telles sources pulsées permet de nouvelles fonctionnalités pour les systèmes interférométriques. En particulier, lorsqu'un laser pulsé est utilisé dans notre schéma comme référence, son background photonique induit se limite à des modes temporels distincts qui peuvent être retardés par rapport à l'entrée quantique interférée (c'est-à-dire le « cross-talk » entre le signal quantique et la référence peuvent désormais être encore réduits par un filtrage temporel). Ce background peut ensuite être supprimé via une synchronisation temporelle ou post-sélectionné dans l'analyse.

En réduisant davantage les besoins en ressources, la référence pulsée peut être atténuée au niveau de quelques photons (comme pour l'approche de la Section 4.3) et les composantes en phase et en quadrature du signal de rétroaction peuvent être temporellement retardées les unes par rapport aux autres (via un déséquilibre de fibre accordable sur le bras de l'AOM). Une telle approche, qui ressemble aux techniques d'échantillonnage en quadrature à entrelacement temporel du domaine du traitement du signal numérique, nous permet de récupérer les informations de phase de l'interféromètre en utilisant un seul détecteur à photon unique (Figure 4.11).

Contrôle cohérent des états hyper-intriqués

Nous présentons une approche générale pour manipuler de manière cohérente des systèmes quantiques multipartites discrets de niveau d basés sur l'intrication simultanée de photons en temps et en fréquence, en utilisant des composants de télécommunications à fibres optiques. Les états utilisés ici sont générés dans une plate-forme intégrée, produite en utilisant le processus non linéaire de mélange spontané à quatre ondes dans un résonateur à micro-anneau (le concept de peigne de fréquence quantique). Le même résonateur à micro-anneau est utilisé dans les expériences de source quantique. Comme illustré sur la Figure 4.2 c, en excitant le résonateur non linéaire avec trois impulsions à verrouillage de phase (provenant d'un laser à verrouillage de mode à stabilisation de phase à enveloppe porteuse, Menlo Systems Inc.) et en considérant trois paires de modes de fréquence dans les photons émis, nous générons des états intriqués simultanément dans le temps et

la fréquence. Ceux-ci sont décrits par l'expression suivante :

$$\begin{aligned}|\Psi_H\rangle = & \quad (|1_s,1_i\rangle + |2_s,2_i\rangle + |3_s,3_i\rangle) \otimes (|a_s,a_i\rangle + |b_s,b_i\rangle + |c_s,c_i\rangle) \\ = & \quad |1_s,1_i,a_s,a_i\rangle + |1_s,1_i,b_s,b_i\rangle + |1_s,1_i,c_s,c_i\rangle \\ & + |2_s,2_i,a_s,a_i\rangle + |2_s,2_i,b_s,b_i\rangle + |2_s,2_i,c_s,c_i\rangle \\ & + |3_s,3_i,a_s,a_i\rangle + |3_s,3_i,b_s,b_i\rangle + |3_s,3_i,c_s,c_i\rangle,\end{aligned}$$

où les nombres indiquent les trois cases temporelles (1,2,3) et les lettres indiquent les trois cases fréquentielles (a,b,c), avec les indices s et i se référant respectivement au signal et idler (la normalisation n'est pas montrée ici pour la compacité de l'équation). Cet état hyper-intriqué est bi-séparable, puisque toute mesure de projection effectuée, par exemple, sur la base de tranches temporelles, n'affecte pas le sous-état intriqué de tranches de fréquences et vice versa.

En particulier, pour transformer arbitrairement cet état hyper-intriqué en un autre état, un accès expérimental à ses termes individuels est nécessaire tout en maintenant la cohérence. Pour les états multi-particulaires, cela est techniquement très difficile et nécessite alors des portes quantiques à deux parties qui sont généralement probabilistes.

Cependant, l'utilisation de deux types différents d'intrication discrète énergie-temps (c'est-à-dire, tranche de temps et tranche de fréquence) associés à différentes échelles de temps ouvre la possibilité de cartographier complètement l'état intriqué dans le domaine temporel pour effectuer des manipulations d'état cohérentes en utilisant une modulation électro-optique synchronisée. À cette fin, notre conception utilise une cartographie fréquence-temps (Figure 4.13) réalisée avec un réseau de Bragg à fibre (où chaque réseau reflète une fréquence optique spécifique) placé dans une configuration de boucle auto-référenciée et stable en phase. Le système est composé de six réseaux de Bragg à fibre indépendants adaptés aux six longueurs d'onde de photons (1551.08, 1552.70, 1554.31, 1557.55, 1559.17 et 1560.80 nm), spatialement séparés dans la fibre pour obtenir un délai temporel de 3,96 ns entre les modes de fréquence adjacents (c'est-à-dire, pour introduire la cartographie fréquence-temps).

Après réflexion sur le réseau de Bragg personnalisé, chaque partie de l'état est mappée sur un mode temporel individuel. Chaque coefficient d'amplitude et de phase est ainsi accessible expérimentalement, car les opérations de modulation de phase et d'amplitude peuvent être synchronisées sur les tranches de temps individuelles, conférant des changements aux coefficients d'état. Dans

notre implémentation particulière, nous n'avons transmis qu'une modulation de phase (à l'aide d'un modulateur de phase électro-optique (EOSpace), qui était piloté par un générateur de formes d'ondes arbitraires (Tektronix), synchronisé sur l'horloge de référence de 10 MHz du laser à mode verrouillé), mais la modulation d'amplitude est également possible simultanément dans ce schéma.

Enfin, la cartographie fréquence-temps est inversée de l'autre côté lorsque l'état est à nouveau incident sur les réseaux de Bragg. Tous les décalages de longueur dans la fibre du réseau sont ainsi automatiquement compensés sans qu'aucune rétroaction active ne soit requise.

Caractérisation des signaux quantiques

Interférence quantique contrôlée par radiofréquence

Ici, nous démontrons l'interférence quantique contrôlée par radiofréquence des états intriqués dans le temps de grande dimension, voir la configuration à la Figure 5.1. Une source de peigne de fréquence stabilisée (Menlo FC1500-250-WG, taux de répétition de 250 MHz) est utilisée pour exciter une seule résonance d'une microcavité non linéaire afin de générer des paires de photons enchevêtrés dans le temps (via SFWM, voir Section 2.1) décrits par l'état quantique :

$$|1\rangle_s|1\rangle_i + e^{i\theta_{CEO}}|2\rangle_s|2\rangle_i + e^{i2\theta_{CEO}}|3\rangle_s|3\rangle_i$$

où $|k\rangle$ (k=1,2,3) désigne un état quantique temporel et s et i désignent respectivement le signal et l'idler. Ici, la phase impulsion à impulsion θ_{CEO} est décrite par $\frac{2\pi f_{CEO}}{f_{rep}}$ où f_{CEO} correspond à la fréquence de décalage de l'enveloppe porteuse (voir la Section 2.2, balayable via une entrée radiofréquence dans le système Menlo), et f_{rep} correspond au taux de répétition des impulsions (ici, réglé à la constante de 250 MHz). Les phases du signal et idler de l'interféromètre sont maintenues constantes à 0 rad (par rapport à un signal de référence basé sur un signal CW), θ est alors balayé en modifiant l'entrée radiofréquence sur une plage accessible de 10 à 115 MHz. A la sortie des interféromètres, les photons sont acheminés vers deux détecteurs de photons uniques indépendants.

Il est important de noter que, bien que les mesures quantiques précédentes utilisant ce schéma de stabilisation d'interféromètre aient exploité une référence optique commune à travers les étapes de préparation et de caractérisation de l'état, pour cette mesure, nous utilisons des sources optiques indépendantes pour la préparation de l'état (une source de peigne de fréquence commerciale pulsée)

et la stabilisation de l'interféromètre (une source CW séparée, c'est-à-dire hors boucle, avec une gigue basse fréquence). En particulier, les paramètres du peigne de fréquence sont stabilisés par rapport à des radiofréquences accordables à une référence atomique (dans le cadre d'un système clé en main). Les sources laser utilisées pour la préparation de l'état et la stabilisation de l'interféromètre démontrent un taux de dérive de fréquence relative maximale de ≈270 kHz/heure, correspondant à une dérive de l'interféromètre $< 0{,}01\pi$ rad/heure (ce qui est négligeable par rapport au temps d'intégration total de deux heures pour chacune de nos mesures d'interférences quantiques).

Comme mentionné ci-dessus, lorsque l'excitation à mode verrouillé est utilisée comme une pompe pour préparer un état intriqué temporel, la phase codée dans les qudits correspond linéairement à la phase impulsion à impulsion θ_{CEO}; ainsi, les radiofréquences (en particulier, la référence de fréquence de décalage d'enveloppe porteuse (CEO), qui définit θ_{CEO}) peuvent être des degrés de liberté importants pour, par exemple, la métrologie optique quantique. En utilisant cette source en peigne pour l'excitation des paires de photons signal-idler, ainsi que la source CW indépendante pour stabiliser la phase de l'interféromètre à 0π (Figure 5.1), nous montrons que la radiofréquence CEO est un degré de liberté accessible pour démontrer l'interférence quantique (Figures 5.2 et 5.3).

L'utilisation potentielle de telles mesures d'interférence de faible puissance pour la stabilisation et possiblement l'extraction directe des fréquences CEO du laser à mode verrouillé mérite une étude plus approfondie. La démonstration réussie de l'interférence quantique à l'aide de sources optiques indépendantes pour la référence de la pompe et de l'interféromètre (bien qu'avec des métriques de stabilité très élevées) suggère également que les contraintes pour de telles conceptions de systèmes quantiques peuvent être assouplies.

Spectres à photon unique

La caractérisation des signaux de photons uniques est aujourd'hui largement redevable aux applications classiques qui ont conduit au développement d'infrastructures de fibre optique et d'espace libre commerciales et accessibles. Deux configurations différentes sont étudiées pour la caractérisation du profil spectral émis à partir d'un peigne de fréquence quantique sur puce.

Tout d'abord, un monochromateur à réseau accordable avec une plage de fonctionnement de 1470 à 1620 nm est utilisé en combinaison avec un détecteur de photon unique. Les comptages bruts de photons uniques sont mesurés en fonction de la longueur d'onde du monochromateur

(qui a été à son tour calibré dans le domaine classique, à l'aide d'une source large bande et d'un analyseur de spectre optique). Les pertes optiques à travers ce montage, compensées en analyse, correspondent à 7,3 dB (couplage 1,6 dB, contrôle de polarisation 1,5 dB, monochromateur 4,2 dB). La synchronisation temporelle est déclenchée numériquement après la détection en utilisant le taux de répétition de l'émission de peigne de fréquence quantique comme signal d'horloge.

Deuxièmement, un filtre de longueur d'onde numérique accordable à plus haute résolution, limité à la bande C des télécommunications (bande conventionnelle : 1530-1565 nm), est utilisé pour balayer de la même manière le spectre (suivi à nouveau par un détecteur à photon unique). En utilisant le filtre numérique de longueur d'onde, les pertes optiques sont estimées à 7,3 dB (couplage 1,6 dB, filtre numérique 5,7 dB).

L'étage de détection est composé d'un détecteur de photons uniques idQuantique ID210 à une efficacité quantique de 5% (correspondant à une perte de détection de 13 dB), 10 μs de temps morts, une gigue temporelle de 500 ps et des taux de comptage d'obscurité de 1,3 kHz. Les signaux du détecteur sont acquis avec un convertisseur temps-numérique (PicoQuant HydraHarp 400) avec une résolution temporelle de 1 ps.

Les spectres d'émission reconstruits à l'aide des méthodes décrites ci-dessus sont illustrés à la Figure 5.4. Le peigne de fréquence quantique produit lors de la mesure peut être vu comme couvrant les bandes de télécommunications S, C et L, fournissant des ressources quantiques qui peuvent potentiellement être filtrées en fréquence pour s'adresser à plusieurs utilisateurs différents. Une telle mesure est utile pour déterminer l'emplacement spectral approximatif des résonances, comme cela est nécessaire pour la conception des étapes de traitement du signal quantique qui peuvent suivre une telle source (par exemple, le filtrage des résonances pour la corrélation croisée, l'interférence ou la mesure de tomographie).

Conclusion

En réponse à la faiblesse signalée de la chaîne d'approvisionnement de la photonique quantique et au sous-développement de composants de systèmes quantiques standardisés compatibles avec des infrastructures matures, les objectifs de cette thèse étaient le développement d'architectures de sources quantiques à faible encombrement, le développement de techniques de traitement du signal quantique à faible perte et le développement de techniques de caractérisation de signaux quantiques

compatibles avec les fibres. La réalisation de ces objectifs a été couronnée de succès, les principaux résultats étant résumés ci-dessous.

1. **Développement d'architectures de sources quantiques à faible encombrement :**
   Dans cet objectif, nous avons ciblé le développement d'une nouvelle classe de sources portables, un système hybride fusionnant le laser de pompe et la source quantique dans une configuration compacte. Nos résultats illustrent un concept évolutif qui exploite la caractéristique de bande passante de résonance d'une micro-cavité pour conduire à une excitation adaptée à la bande passante (économe en énergie) stable pour la micro-cavité et le processus de génération de photons SFWM associé. Par rapport aux schémas d'excitation externes, cette solution permet un réglage simple et polyvalent de la fréquence de répétition à laquelle le PFQ est émis, soit électroniquement en modifiant le signal de modulation RF, soit en modifiant la longueur de la cavité externe. Dans cette configuration, il a été démontré que des taux de répétition de pompe plus élevés permettent d'augmenter les taux de production de paires photons tout en maintenant leur pureté et le CAR. De plus, comme les progrès du schéma permettront une impulsion stable à des taux de répétition de verrouillage de mode harmonique plus élevés, moins de modes de fréquence externes seront excités dans la résonance, ce qui ouvrira de nouvelles perspectives pour les études fondamentales dans le régime transitoire entre l'excitation pulsée et l'onde continue (par exemple, la mise à l'échelle des propriétés des paires de photons comme la pureté et la dynamique de verrouillage de mode en fonction de moins de modes excités). De futures extensions du schéma, telles que l'inclusion de techniques de suppression du bruit de supermode, pourraient également permettre la cohérence de phase d'impulsion à impulsion requise pour la réalisation d'une source de peigne de fréquence quantique intriquée à taux de répétition élevé, ainsi que des taux de répétition de pompe plus élevés pour des taux de signal photonique accrus.

   L'approche de la source peut être appliquée à une large gamme de structures résonantes en plus des résonateurs à micro-anneaux non linéaires du troisième ordre, par exemple, les guides d'ondes et résonateurs à cristaux photoniques, les micro-disques, les guides d'ondes optiques à résonateurs couplés et les microcavités non linéaires du deuxième ordre (tant qu'une configuration « input-drop » est accessible). L'excitation adaptée à la bande passante donne également accès à des régimes de pompage de puissance plus élevée, utiles pour, par exemple, la génération d'états multi-photoniques. Alors que nous avons observé un verrouillage de mode

lorsque le modulateur d'amplitude a été remplacé par un modulateur de phase, une sensibilité plus élevée à la fréquence d'entraînement RF et une instabilité opérationnelle occasionnelle ont été observées. Nous avons donc utilisé un montage modulé en amplitude plus robuste ; cependant, le schéma peut probablement utiliser des modulateurs de phase s'il est couplé à des méthodes de synchronisation actives, par exemple des circuits de rétroaction régénératifs.

Réaliser un schéma QFC pulsé pratique dans une configuration laser passive, en utilisant la mise en forme d'impulsions pour améliorer davantage les propriétés quantiques (par exemple, en utilisant des profils temporels atypiques), et en utilisant un résonateur à deux ports où une configuration « input-drop » est inaccessible (par exemple, en poursuivant des techniques de découpage d'impulsions) sont d'autres axes de recherche très attrayants.

2. **Développement de techniques de traitement de signaux quantiques à faibles pertes :**
   Dans cet objectif, nous avons ciblé le développement de dispositifs et de configurations à base de fibres pour le traitement de signaux quantiques. Dans un premier temps, nous avons ciblé la réalisation d'une suite d'outils pour la recherche de phase dans les interféromètres à fibre. Deuxièmement, nous avons ciblé le développement d'un schéma pour le contrôle polyvalent et cohérent d'états quantiques hyper-intriqués en fréquence et en temps.

   Le schéma de l'interféromètre à fibre s'est avéré expérimentalement pratique et permettant la récupération sans ambiguïté de la phase, sans avoir besoin de tramer ou de balayer la fréquence laser de stabilisation. De plus, il a permis de démontrer la stabilité à long terme et l'accès à toutes les valeurs de phase. Nous avons également caractérisé l'utilisation du schéma avec des faisceaux de référence faibles et pulsés, en présentant des stratégies visant à réduire le nombre de photons de fond, ainsi qu'une analyse des considérations opérationnelles pour l'utilisation de telles références. Dans les extensions du schéma, nous nous attendons à ce que les signaux de référence codés en quadrature au niveau du photon unique puissent également trouver des cas d'utilisation appropriés où il est obligatoire d'éviter les processus stimulés (par exemple, les signaux de haute puissance et les puces photoniques complexes) ou où des perturbations minimales du système sont importantes (p. ex. télémétrie quantique).

   La méthode de récupération de phase présentée dans cette thèse est actuellement limitée aux applications d'interféromètre déséquilibré (car des longueurs de bras égales ne peuvent pas fournir le décalage de phase requis dans les composants de signal de référence, ce qui rend d'autres schémas plus adaptés à la stabilisation d'interféromètre équilibré) ; il n'est pas

adapté pour une utilisation avec des lasers de référence avec des puissances optiques instables à moins que des étapes d'étalonnage forcé ou des mises à niveau algorithmiques ne soient incluses (contrairement aux méthodes basées par exemple sur la minimisation des tonalités de tramage) ; et il est mieux adapté aux configurations de type Michelson, car étendre notre méthode à d'autres, par exemple, le Mach-Zehnder, nécessiterait un contrôle de polarisation supplémentaire.

Les futurs travaux sur cette méthode se concentreront sur l'augmentation de la stabilité et de la résolution de phase grâce à l'utilisation d'une plus grande profondeur de bits et d'une électronique plus rapide, en effectuant des mesures de stabilité hors boucle à l'aide de sources optiques supplémentaires et d'une fibre plus longue (détermination de la pertinence du schéma au-delà du traitement du signal cohérent), étendant la portée du schéma démontré aux interféromètres avec plus de bras (comme requis, par exemple, pour la manipulation d'états de grande dimension sans avoir cascader des interféromètres à deux bras) ainsi qu'aux interféromètres intégrés.

Dans le cadre de cet objectif, nous avons ciblé le contrôle cohérent des états hyper-intriqués temps-fréquence. De tels états présentent une grande compatibilité avec les fibres optiques, utilisent des degrés de liberté bien développés et ont un grand potentiel d'évolutivité en termes de dimensionnalité d'état (c'est-à-dire que de nombreux intervalles de fréquence et de temps peuvent être utilisés pour créer de grands états). La conception, basée sur une boucle de fibre auto-référenciée composée de réseaux de Bragg à fibre pour la cartographie fréquence-temps et d'éléments électro-optiques pour la mise en place de masques de phase/amplitude temporels, a permis de réaliser des états de cluster de grande dimension. Il convient de noter que si de nombreuses motivations pour l'utilisation de sources intégrées proviennent de raisons de compacité, l'utilisation d'un résonateur à puce permet de nouvelles fonctionnalités - les espacements de fréquence dans la gamme du GHz qui permettent ici d'adresser des modes de fréquence individuels qui ne sont accessibles que dans de telles échelles de taille microscopique. De plus, la possibilité d'utiliser une boucle auto-référenciée pour l'opération est extrêmement avantageuse pour réduire la complexité du schéma, les seules entrées étant basées sur les radiofréquences et l'ensemble du dispositif étant passif (en plus des pertes optiques) lorsqu'aucune de ces entrées ne sont utilisées.

3. **Développement de techniques de caractérisation de signaux quantiques couplés par fibre :**
   Dans cet objectif, nous avons ciblé des techniques de caractérisation de signaux quantiques faisant appel à une infrastructure ou à des degrés de liberté compatibles avec la photonique sur fibre. À cette fin, nous avons démontré l'interférence quantique contrôlée par radiofréquence d'états intriqués dans le temps de grande dimension préparés à l'aide d'une source intégrée. Alors que les radiofréquences ont été utilisées pour les interférences quantiques, par exemple, dans le traitement de photons intriqués en fréquence en utilisant des modulateurs de phase électro-optiques, l'utilisation d'une radiofréquence de cette manière est atypique. Nous avons réussi à démontrer l'interférence en utilisant des projections dans les bases $|1\rangle + |2\rangle$ et $|1\rangle + |3\rangle$. L'extraction de la fréquence de l'enveloppe porteuse du laser pulsé étant à la base de sa stabilisation et du développement de peignes de fréquence de haute précision, l'utilisation des interférences quantiques pour déterminer et stabiliser cette fréquence serait une future piste de recherche très intéressante.

   Deuxièmement, nous avons utilisé des configurations compatibles avec la fibre pour la caractérisation des spectres à quelques photons. À cette fin, nous avons utilisé à la fois des monochromateurs basés sur des réseaux construits à partir de composants commerciaux en espace libre (couplés à la fibre), ainsi que des filtres spectraux programmables basés sur les télécommunications. Avec les deux configurations, nous avons pu résoudre la sortie d'un peigne de fréquence intégré et utiliser les résultats pour localiser l'emplacement spectral de ses résonances. Depuis l'introduction de cette technique dans notre laboratoire, elle est devenue une étape de routine pour construire chaque nouvelle configuration et vérifier le bon fonctionnement de la source. Cependant, l'un des principaux inconvénients de la technique dans son état actuel, est la résolution accessible relativement faible (10 GHz). Les futurs travaux devraient cibler l'utilisation du traitement du signal optique et électronique, par exemple, grâce à l'utilisation de composants dispersifs et de la synchronisation temporelle, pour obtenir des résolutions plus élevées tout en maintenant la facilité d'utilisation et la compatibilité des fibres.

Enfin, il convient également de noter que plusieurs des développements présentés ici peuvent être pertinents en dehors des systèmes photoniques quantiques. Par exemple, l'architecture de source présentée peut être intéressante pour les lasers à bande étroite compacts et à cadencement serré (comme requis, par exemple, pour des applications biomédicales). Des techniques précises pour la

récupération de phase peuvent être pertinentes pour des domaines tels que la détection distribuée et la tomographie par cohérence optique, avec la possibilité d'utiliser des signaux à quelques photons potentiellement adaptés pour les applications où les lasers à haute puissance ne peuvent pas être utilisés (par exemple, en raison de la sécurité des yeux ou de l'émission stimulée).

En conclusion, nos travaux se sont concentrés sur plusieurs aspects différents des systèmes quantiques, couvrant les sources, le traitement du signal et la caractérisation. Bien qu'il reste encore beaucoup de développement pour la réalisation de technologies photoniques quantiques évolutives et déployables, les objectifs susmentionnés de cette thèse ont été atteints avec succès et, espérons-le, font avancer cet objectif. Nous pensons que le travail a été particulièrement réussi en tirant parti de l'infrastructure des télécommunications et de la photonique intégrée. Ceci est important, car cela nous a permis d'utiliser des chaînes d'approvisionnement robustes et des composants standardisés, vers la création de systèmes compatibles avec les réseaux de fibres optiques (une exploitation similaire d'infrastructures complémentaires est à l'origine de l'essor de la photonique intégrée). Les travaux présentés ici confirment que ces composants peuvent être utilisés facilement, avec une personnalisation minimale, vers des applications photoniques quantiques avancées.

Contents

Acknowledgments **iii**

Abstract **v**

Résumé **vii**

Synopsis **ix**

Contents **xxxi**

List of figures **xxxiii**

Notation and abbreviations **xxxv**

1 Introduction and Motivation **1**
1.1 Research background 1
1.2 Photonics for quantum 3
1.3 Quantum photonics systems 4
1.3.1 System implementations 6
1.4 Thesis objective and structure 8

2 Review of Context **11**
2.1 Integrated quantum frequency combs 12
2.2 Mode-locked lasers 15
2.3 Interferometry 18
2.4 Photon detection and cross-correlation measurements 19
2.5 Photon purity and degree of entanglement 22

3 Sources for Quantum Photonics **25**
3.1 Motivation 26
3.2 Actively mode-locked nested cavities for photon pair generation 28
3.2.1 Technical Approach 28
3.2.2 Results 30

4 Quantum Signal Processing **35**
4.1 Motivation 36
4.2 Fiber-based interferometry with bright continuous-wave reference signals 42
4.2.1 Technical Approach 42
4.2.2 Results 45

4.3 Fiber-based interferometry with an attenuated coherent state reference 48
4.3.1 Technical Approach 48
4.3.2 Results 49
4.4 Fiber-based interferometry with bright and dim pulsed references 51
4.4.1 Technical Approach 51
4.4.2 Results 52
4.5 Coherent control of hyper-entangled states 55
4.5.1 Technical Approach 55
4.5.2 Results 58

5 Characterizing Quantum Signals **59**
5.1 Motivation 60
5.2 Radiofrequency-controlled quantum interference 61
5.2.1 Technical Approach 61
5.2.2 Results 62
5.3 Single-photon spectra 64
5.3.1 Technical Approach 64
5.3.2 Results 65

6 Conclusion and Perspectives **67**

References **73**

A Summary of tabletop-scale, state-of-the-art interferometer stabilization methods **91**

B Candidate's Works **93**

List of figures

1.1 Overview of public funding in quantum technologies 2
1.2 Schematic of the main modules for a typical quantum photonics system 5

2.1 Integrated frequency comb generation using nonlinear microcavities 13
2.2 Common pump approaches for entangled photon generation. 15
2.3 Laser signals with phase-locking present versus absent 16
2.4 Temporal (top) and spectral domain (bottom) visualization of a frequency comb signal 17
2.5 Schematic of a Michelson interferometer 18
2.6 Cross-correlation measurement between a signal and idler photon 21
2.7 Determining the coincidence-to-accidental ratio from a signal-idler cross-correlation measurement 22

3.1 Experimental setup for pulsed quantum frequency comb generation 29
3.2 Characterization of the actively mode-locked pulsed pump 30
3.3 Characterization of the photon pair coincidence-to-accidental ratio 32
3.4 Characterization of the harmonically mode-locked pulsed pump 33
3.5 Properties of generated photons as a function of pump repetition rate 34

4.1 Role of optical phase on the operation of an interferometer 38
4.2 Time-frequency hyper-entanglement 41
4.3 Retrieving fiber interferometer phase using a two-color reference signal 43
4.4 Setup for interferometer phase extraction using a two-color reference 44
4.5 Long-term interferometric phase stability. 46
4.6 Use of the two-color reference signal for phase-independent interferometer stability . 47
4.7 Interferometer phase estimation using attenuated coherent states in quadrature . . . 49
4.8 Phase dependence of the estimation error for the attenuated coherent reference method 50
4.9 Average phase estimation error as a function of photon flux and integration time . . 51
4.10 Interferometry with a pulsed optical reference in quadrature 53
4.11 Use of an attenuated pulsed reference 54
4.12 Analysis of error in the reconstructed phase 55
4.13 Coherent control of time-frequency hyper-entangled states 57

5.1 Setup for the radiofrequency-controlled quantum interference of high-dimensional time-bin entangled states 62
5.2 Quantum interference in the signal-idler coincidence events 63
5.3 Quantum interference measurements for the time-bin encoded photon states 64
5.4 Measured single-photon spectrum for an integrated quantum frequency comb 65

Notation and abbreviations

Abbreviations

INRS	Institut national de la recherche scientifique
CW	Continuous-wave
QFC	Quantum frequency comb
SFWM	Spontaneous four-wave mixing
FSR	Free spectral ranges
CAR	Coincidence-to-accidental ratio
CROW	Coupled resonator optical waveguide
EDFA	Erbium-doped fiber amplifier
RMS	Root mean square
RF	Radiofrequency
BS	Beam-splitter
AOM	Acousto-optic modulator
DWDM	Dense wavelength division multiplexing
CEO	Carrier-envelope offset

Physics Symbols

c	Speed of light
I	Optical intensity
V	Interference visibility
f	Optical frequency
n_g	Effective group index of refraction
K	Schmidt number
N_{eff}	Effective mode number

1 | Introduction and Motivation

1.1 Research background

Quantum mechanics is the physics theory describing the laws of nature at the particle level. It was developed in the early 20th century, but has since not lost notoriety for its accurate description of often counterintuitive phenomena. These include a system's ability to simultaneously exist in multiple states (superposition), or exhibit connection between particles despite physical separation (entanglement) [1, 2]. Many widespread technologies already make use of quantum properties or must consider them in their design, among them transistors [3], lasers [4], and magnetic resonance imaging scanners [5, 6]. However, such devices do not encompass the full technological potential of quantum physics, which in a sense has only begun to be explored due to previous limitations in the availability, scalability, and control of quantum platforms.

Today - over a 100 years since the beginning of the field (and coinciding with the centennial of Einstein's 1921 Nobel Prize for describing the photoelectric effect [7], a key milestone in the theory's development) - interdisciplinary advances in quantum theory have granted vision towards disruptive applications of non-classical phenomena in fields as diverse as communications and cryptography [8, 9, 10], information processing and computing [11, 12, 13], and sensing [14, 15]. Likewise, the systems capable of controlling and harnessing quantum resources have significantly matured. Development milestones have been plentiful in experimental platforms such as trapped ions, superconducting circuits, and photonic systems, among others. Recent globally-renowned achievements include Google's 2019 demonstration of 'quantum advantage' (i.e., using a programmable quantum system to solve a computational problem much faster than known to be possible with any classical methods) with 53 superconducting qubits (i.e., two-level quantum systems) [16]; as well as a second

report of quantum advantage from the academic group of Jian-Wei Pan, demonstrated using a 40-70 photon system [17].

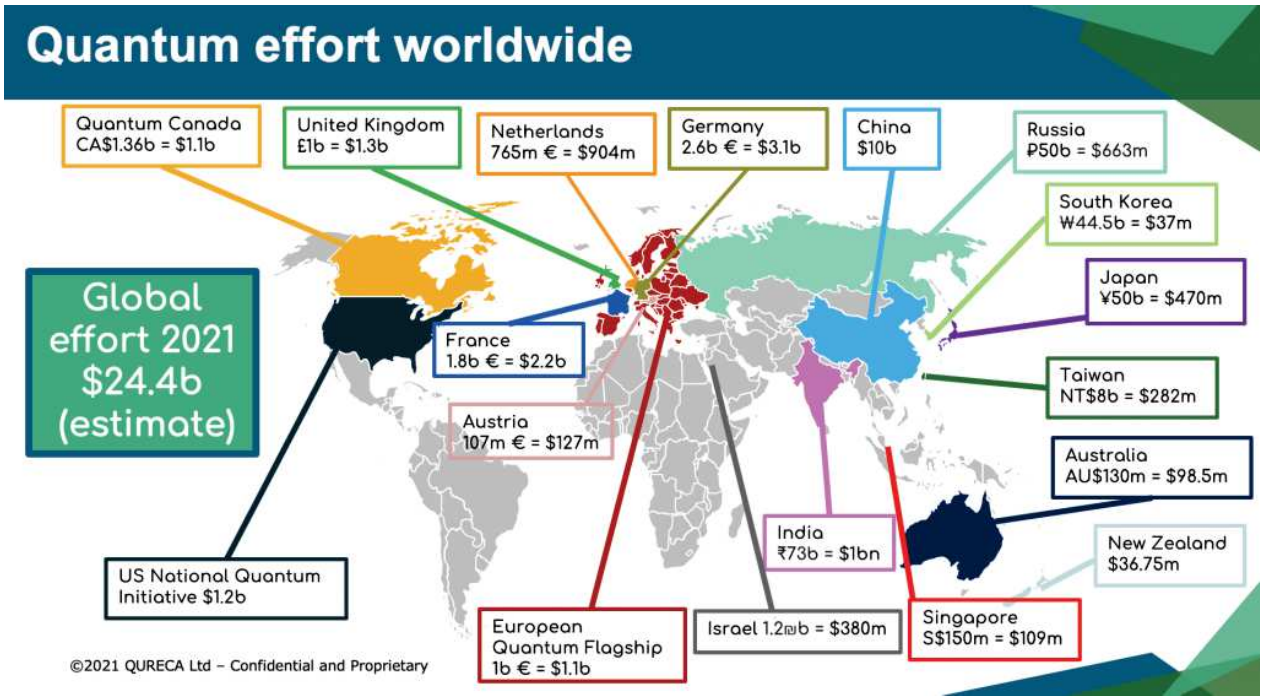

Figure 1.1: Overview of public funding in quantum technologies. Reproduced from Ref. [18], used with permission.

Research into quantum physics has furthermore ceased to be a primarily academic affair, being pursued directly by start-ups (e.g., D-Wave Systems [19], Xanadu Quantum Technologies [20], PsiQuantum [21]) and industrial giants (e.g., Google [16], Amazon [22]) alike, notwithstanding the indirect contributions from hardware vendors and foundries all over the world. Studies into quantum physics and technologies have attracted billions of dollars worldwide in federal and private investment [18], with Canada among the global leaders in investment and research expertise (Figure 1.1). Key to this scale of investment is the perception that, while the development of many advanced quantum technologies has a moderate to high risk of succeeding (varying between applications), the impact of successful technologies would be immense, bringing about disruptive economic, technological, and societal impacts at all levels. For example, quantum computing may potentially revolutionize drug discovery, optimization tasks, and cybersecurity [23, 13], among others, while quantum-based encryption will enable future-proof information security (cybersecurity based on physical laws rather than mathematical intractability [8]). Quantum sensing has already enabled detection capabilities beyond classical limits, which have been, e.g., used to improve gravitational wave detection [24]. The potential impacts of quantum technologies have also inspired reactionary

developments. For example, the potential development of quantum computers, which could compromise widespread encryption approaches, has served as the impetus for the National Institute of Standards and Technology's post-quantum cryptography program [25].

1.2 Photonics for quantum

A large variety of experimental platforms has been explored towards the study and application of quantum phenomena. For many of these, a first goal is to gain repeatable access to simple quantum states - such as single qubit or single particle states. A second goal is access to coherent control mechanisms for these states. Completion of these goals is generally sufficient for the exploration of rudimentary quantum phenomena. However, other issues must be resolved to access more complex fundamental questions and technologies - how can the experimental platform under study be scaled, both in the number and the size of quantum states, as well as in the complexity of control circuitry? Can states be transduced from one platform to another efficiently?

In recent years, several quantum technology platforms have seen significant maturation and advancement. Superconducting circuits are amongst the most mature platforms, also being used in the first demonstration of quantum advantage [16]. Quantum technologies based on ion traps are also very attractive as a platform, due in part to their consistency and scalability [26]. Further, diamond [27, 28], donor [29, 30], and other technologies comprise a host of platforms [13] with ready access to quantum phenomena.

Photonics, in particular, is a central platform for quantum physics from both a historical and contemporary standpoint. Photons, i.e., the fundamental particles of light, were among the first platforms to be used for the demonstration and discovery of quantum phenomena [7, 2]. Today, photonics is a key platform for applications spanning the majority, if not all, of quantum technologies; optics finds use across approaches for quantum random number generation [31, 32, 33], communications [9, 10, 34], computing [17, 20, 13], and sensing [35, 24]. The key reason for this is the ease with which quantum state access and control can be achieved in photonics. Namely, photons:

- Demonstrate **low decoherence**, meaning that they can preserve their quantum states for extended periods of time and spatial propagation

- Have **easily-accessible particle entanglement** when nonlinear optical processes are used for state generation (see Section 2.1)
- Have **numerous degrees of freedom** accessible for state encoding, e.g., polarization, arrival time, optical frequency, orbital angular momentum, path of travel
- Are readily and coherently manipulated using **inexpensive and mature components** (e.g., electro-optics, free-space components, fiber-based filters)
- Propagate at the **speed of light** ($2.998 \cdot 10^8$ m/s in vacuum) and have **excellent transmission properties** especially when the propagation medium and optical wavelength are co-optimized (e.g., in appropriate optical fibers, atmospheric windows)
- Are compatible with established **telecommunications and silicon chip infrastructures**
- Are **robust against radiofrequency interference**

Nevertheless, raising the technical maturity level of quantum photonics is still the subject of active research and development efforts. Photons do not easily interact with other photons, as is required for, e.g., gate operations in information processing. This has necessitated spectacular theoretical developments that have enabled the use of linear optics components towards such operations [36], or the use of simple operations but significant state complexity [37]. Quantum state reproducibility, important towards efficient signal processing (e.g., interference measurements [38]) is another active research area, as is the scalability of state size and control circuitry. The restrictive portability and size of free-space optics has led to concentrated research efforts in platforms such as silicon chips and optical fiber (the work presented in this thesis is among these). This said, many landmark demonstrations have made use of free-space optics, including the recent realization of quantum advantage in photonics [17].

1.3 Quantum photonics systems

Fundamental and applied quantum photonics studies make use of a wide variety of systems, with diverse degrees of freedom, system components, and purposes. Quantum photonics investigations span the scales characteristic of nanotechnologies [38] through to the astronomical [39]. The presentation of an 'archetypical quantum photonics system' is thus doomed to be an oversimplification,

but still holds value as it can attempt to summarize most systems (Figure 1.2). The schematic pictured here attempts to emphasize the analogy between quantum photonics approaches and classical communications system block diagrams [40], with some important caveats outlined below.

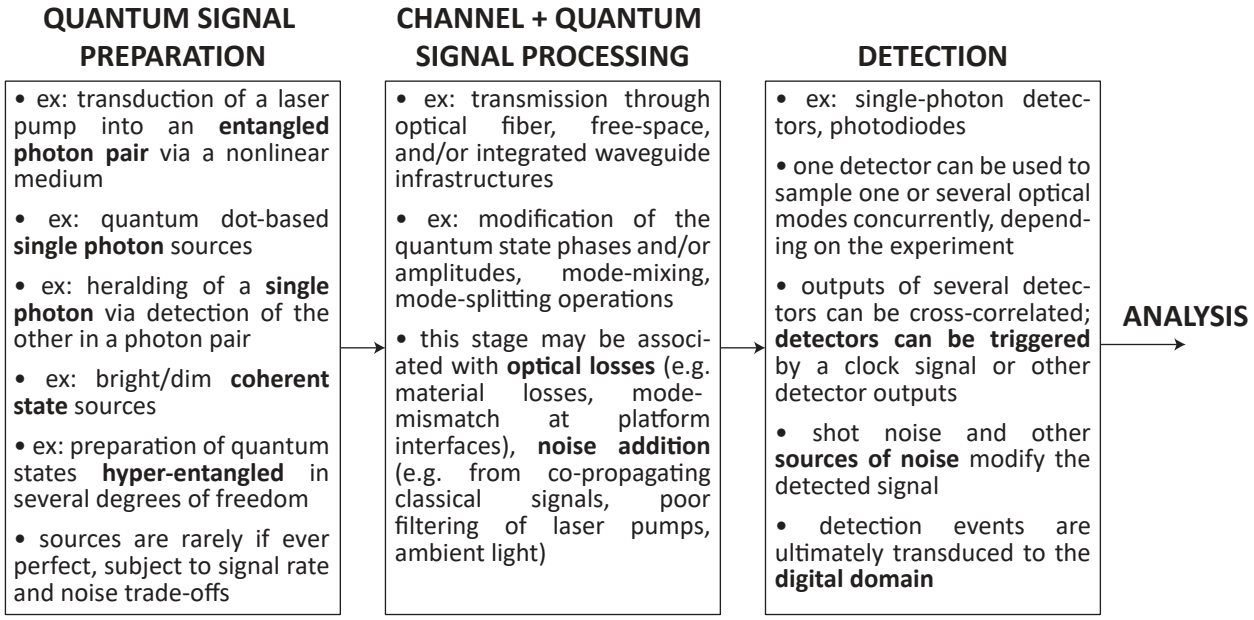

Figure 1.2: Schematic of the main modules for a typical quantum photonics system.

The first stage of a standard quantum photonics system is generating a signal (or several signals), in most cases, a particular quantum state. The characteristics of this state may already be known to the system designer (e.g., they may be targeting the generation of a high-dimensional cluster state [41]) or, alternatively, the system's purpose may be the characterization of a hitherto unknown state. Common quantum states employed in the literature include single photon states, entangled states, and bright/dim coherent states (see Section 1.3.1). While quantum state preparation can be significantly more straightforward in optics than in other platforms, it is still non-trivial and may involve transduction of a classical signal into a non-classical one (as done, e.g., with the use of a pump laser to excite a nonlinear medium, see Section 2.1) in carefully-engineered media such as dispersion-shifted optical fibers [42], quantum dots [43], micro-cavities [38], etc.

Second, the transmission channel and quantum signal processing stages for such a system must inevitably take place within the same module. In particular, non-classical optical states are sometimes referred to as 'flying' quantum information - rather than remaining static, optical states move at the speed of light in a propagation medium and must likewise be processed as they propagate (e.g., via free-space or fiber-based amplitude/phase-shaping components). The transmission chan-

nel is often a major source of optical loss and noise (e.g., from environmental sources [44] or signal cross-talk [45, 46]).

For the majority of applications, keeping the output in the optical domain is not optimal or compatible with the digital infrastructures required to analyze results. Thus, the final stage of quantum photonics systems is usually the transduction of the quantum signal into a more useful domain. Typically, this comprises a 'detection' stage where the optical signal(s) are converted into the electrical domain (e.g., via single-photon detectors, see Section 2.4). From there, the signal(s) may undergo thresholding/analysis in the electrical domain (e.g., noise thresholding, photon-number resolution [47]) or may be converted directly to the digital domain (e.g., via analog-to-digital or time-to-digital converters).

As previously emphasized, the schematic outlined in Figure 1.2 cannot be representative of all systems pursued in the literature. In fact, the most advanced systems to date can make use of feedback between the different modules in order to, e.g., implement detection-dependent processing steps [48]. Nevertheless, this schematic will provide a useful organizational framework for this thesis.

1.3.1 System implementations

Several, often application-dependent, considerations play a role in the implementation of quantum photonics systems. For one, optical losses tend to be far more detrimental to such systems in contrast to their classical counterparts. While optical amplification can often be used in classical photonics with minimal sacrifices to the signal-to-noise ratio, the no-cloning theorem of quantum physics [49, 50, 51, 52], prohibiting the exact replication or 'cloning' of a quantum state, signifies that losses to the signal are generally permanent. Second, detectors often have broadband optical responsivities, meaning that signal crosstalk is a significant concern, especially from other bright sources in the same transmissions channel as the quantum signal. In all, the trade-offs present in such systems (e.g., state complexity versus processing complexity, more intricate circuits versus reduced signal) indicate that treatments of signal and noise in quantum photonics requires great care.

Several types of signals are considered in quantum photonics, with the most common ones being:

- **Coherent states** are pure quantum states corresponding to a single mode of a resonator, equivalent to a coherent superposition of photon number states [2]. Nonlinear processing can turn coherent states into so-called **squeezed states**, which enable noise levels below the standard quantum limit (for one of their quadrature components). Coherent and squeezed states find extensive use in information processing [20], communications [10], and sensing [24].

- **Single photon** sources target the generation of photon number states with a mean of one photon and variance of zero, i.e., minimizing the likelihood of generating vacuum or multi-photon states. Such sources are used towards information processing [38, 36] applications, among others.

- **Photon pair** sources generate pairs of photons highly correlated in arrival time (as well as other degrees of freedom), and are the most accessible route to entangled states (i.e., systems comprised of particles that cannot have their states described independently [1, 2]). Photon pairs find extensive use for information processing [38] and communications [53, 10]; they can also be used as the basis for preparing single-photon states, via the detection of one photon from the pair (i.e., heralding).

- **More complex quantum states** can make use of encoding on multiple discrete levels (high-dimensional entanglement [54, 55], i.e., qudits), entanglement of uncoupled degrees of freedom (hyper-entangled states [56]), or specific state topologies (i.e., graph states, among them cluster states [37, 41]). Complex quantum states are more difficult to prepare, but are in high demand for information processing [37, 41], sensing [35], and communications [57, 53, 10] applications.

Notably, on-demand access to quantum photonic resources (i.e., their deterministic emission) is an important requirement for the scalability of quantum technologies. The development of such capabilities is thus an active research field; approaches being investigated include the use of waveguide/cavity-coupled single quantum emitters (e.g., quantum dots) for deterministic emission [58, 59], as well as the use of probabilistic sources (e.g., ones based on nonlinear optical effects in crystals) enhanced by multiplexing or heralding [48, 38, 60].

In system implementations that make use of few-photon level signals, so called 'photon-counting' approaches, the signal treatment must inherently consider its statistical nature. Photon counts are sampled until the measurement is sufficient to reconstruct the signal - if the signal is sampled in the

time domain, a judicious choice of integration time that balances measurement speed and quality must be determined (see Section 2.4 for some of the associated metrics). Few-photon signals will be primarily considered in this thesis, with a focus on entangled photon pairs. However, coherent states will also be used in certain systems, e.g., as reference signals for interferometric phase reconstruction (see Section 4.3).

As already mentioned, quantum photonics experiments have been implemented at various physical scales. The majority of work studying entangled states has historically been accomplished in table-top free-space optics setups, making use of bulk media pumped by external lasers. Such experiments typically take up large footprints, have low portability, but benefit from access to high signal rates (as they typically exploit efficient second-order nonlinear optical processes). As a means for complexity scaling, lowering footprints, reducing expenses, and increasing ease-of-use, global research efforts within the last decades have focused on developing quantum photonics in the fiber and integrated platforms [61, 62, 38]. However, lower efficiency processes are typically used in such systems (meaning that cavities must often be employed to enhance emission, see Section 2.1), introducing a trade-off between the aforementioned benefits and lowered signal rates.

1.4 Thesis objective and structure

The Quantum Economic Development Consortium recently estimated that for a typical 5 year quantum program, an average of 3 years is spent on equipment sourcing and customization, 1 year is spent on shakedown (i.e., testing and interfacing towards reaching operational status), and only the final year is spent on data collection [63]. The pace of development in quantum photonics, for both industry and academia, is significantly impacted by a lack of accessible and standardized components. The quantum photonics supply chain would also be strengthened by the availability of mass-producible, low-footprint and inexpensive components compatible with mature infrastructures, like fiber and chip-based platforms, and established degrees of freedom, like time and frequency. The availability of such designs could also give access to new physics and applications, as well as increased scalability in system complexity, as required by the new horizons in the field, where deployability in out-of-lab, rugged environments such as telecom networks [64, 65] and even space [66, 67] is envisioned.

The objective of this thesis is to address this lack and to target the development of devices, setups, and techniques for scalable quantum photonics systems. In particular, these will leverage infrastructure from telecommunications and integrated photonics, and will target systems compatible with optical fiber networks. The objectives of this thesis, reflected also via the document's structure, draw from the schematic presented in Figure 1.2 and are as follows:

1. **Development of low-footprint quantum source architectures (Chapter 3):**
   This objective focuses on systems making use of entangled photon pairs as their quantum signal, where the state-of-the-art typically requires large sources or large lasers for signal preparation. By making use of integrated and fiber components, we target the development of a new class of portable source, a hybrid system merging the pump laser and quantum source into one minimal setup (see Section 3.2.1). We go on to characterize the stability and performance enhancements accessible through the use of this setup (see Section 3.2.2).

2. **Development of low-loss quantum signal processing techniques (Chapter 4):**
   This objective focuses on the development of fiber-based devices and setups for the processing of quantum signals. Interferometers play a key role in quantum signal processing, yet their fiber optic realizations are underdeveloped. As part of this objective, first, we develop a method and system for accurate phase retrieval in fiber-based interferometers by making use of bright continuous-wave (CW) reference signals (see Section 4.2). We then go on to amend the method, in an effort to make it better suited towards the most fragile quantum photonics experiments, by making use of attenuated coherent state reference signals (see Section 4.3) and bright/dim pulsed reference signals (see Section 4.4). Second, we develop a scheme for the versatile, coherent control of quantum states hyper-entangled in frequency and time (see Section 4.5).

3. **Development of fiber-coupled quantum signal characterization techniques (Chapter 5):**
   This objective focuses on the demonstration of quantum signal characterization techniques that make use of infrastructures compatible with fiber photonics. Radiofrequency-based infrastructure is very well developed for applications in classical signal processing and telecommunications. We thus target the development of a quantum signal characterization framework where, atypically, a radiofrequency input is the control degree of freedom (see Section 5.2). Finally, we leverage easily-accessible photonics components to perform the characterization of optical spectra at the few-photon level (see Section 5.3).

The thesis Chapters are structured following these objectives, as cross-linked above. For each Section dealing with a particular sub-objective (e.g., interferometry in fiber), there are two sub-sections presenting the Technical Approach and Results, respectively. The motivation for using this structure is to increase readability and to avoid fragmentation of the cause and the effect of our design decisions.

Besides the Chapters listed above, Chapter 2 presents the main context and techniques from the literature that are relevant to the objectives. For the sake of brevity, this Chapter covers only key topics, as the main quantum physics and photonics concepts have been covered in detail by numerous textbooks and review articles (references to noteworthy resources are pointed out explicitly in the text). Chapter 6 presents a short conclusion to the work, a summary of the objective results, with discussion of potential future work interlaced. The Chapter is followed by a list of my published works.

2 | Review of Context

Chapter Abstract:

The development of quantum photonic systems makes use of a broad foundation of concepts spanning laser physics, nanophotonics, quantum optics, and statistics, among others. All of the above cannot be covered in depth here and are, in fact, already detailed in well-established textbooks and review articles. In this Chapter, selected concepts that are especially relevant to this thesis will be summarized. These include the ideas underpinning integrated quantum frequency comb sources, mode-locked lasers, interferometers, and the measurement of few-photon signals.

2.1 Integrated quantum frequency combs

While the low footprint, stability, and new functionalities offered by integrated optics have made it a particularly attractive platform for quantum photonics systems, chip-compatible approaches for the generation and control of complex photon states have largely failed to show scalability. In particular, while integrated squeezed state approaches have seen rapid maturation over recent years [20], other methods have found scaling difficult, as is the case, e.g., for path-entanglement techniques. The realization of multi-partite entangled states [68] is generally still considered very challenging from an experimental point of view. Likewise, the on-chip preparation of high-dimensional (qudit) optical entanglement typically requires highly complex and specialized components. Specifically, N-dimensional path-entanglement requires N coherently-excited, identical sources and complicated circuits of beam-splitters [69, 70], while time-bin-entanglement demands elaborate and stable N-arm interferometers [71].

As highlighted by the versatility and performance of their recent uses in quantum optics [72], integrated frequency combs have offered a unique framework for the generation and manipulation of complex states. Using both integrated optics and established telecommunications components, quantum frequency combs (QFCs) have been recently used to realize and coherently control the first on-chip sources of both multi-photon [73] and entangled high-dimensional [55, 74] states, as well as being the basis for the first high-dimensional cluster states [41]. As such, QFCs provide a promising framework for future quantum information technologies. In this Section, we will review the working principle and recent developments in this platform - note that these have also been covered extensively in recent review articles [72, 75] and theses [76, 77].

In particular, frequency combs are light sources with a broad spectrum comprised of evenly-spaced spectral modes (akin to a 'comb' and also dubbed 'optical rulers'). The precise stabilization of their comb lines revolutionized diverse fields such as spectroscopy and metrology [78], and earned its pioneers the 2005 Nobel Physics prize [79]. However, the challenges associated with the generation of frequency combs via bulky devices motivated investigations into platforms with increased practicality and portability. Towards this end, on-chip nonlinear micro-cavities (see Figure 2.1 a), which can be dispersion-engineered to exhibit a broadband transmission response characterized by equidistant resonances (see Figure 2.1 b), have been employed as the main platform towards integrated frequency comb sources [80, 81]. The development of on-chip frequency combs is an ongoing,

active field, which has already yielded, e.g., mode-locked lasing [82, 83], and carrier-envelope offset self-referenced combs [84], among others (see Ref. [85] for a recent, in-depth review).

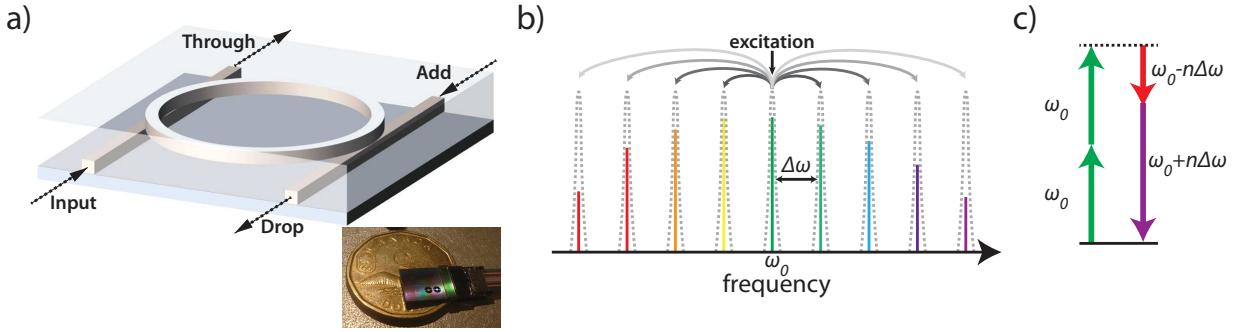

Figure 2.1: Integrated frequency comb generation using nonlinear microcavities. a) A nonlinear micro-ring resonator with four ports. A broadband optical source coupled into the Input port will be filtered by the resonant response of the cavity and leave through the Drop port as a pattern of discrete resonances. Mediated by nonlinear processes, the excitation of such a structure can be used to generate frequency combs. Note the minimal dimensions of such a resonator, which can be fabricated using standard electronics processes to create a compact chip as depicted on the bottom right of panel a (the waveguides are coupled directly to optical fibers, see photograph in the inset). b) Schematic of the resonant transmission response for a nonlinear microcavity, with equidistant resonances spaced by $\Delta\omega$. Also shown is an excitation field coupled to the integrated nonlinear micro-cavity and made, through filtering, to excite only a single resonance at ω_0. Spontaneous four-wave mixing then mediates the annihilation of two excitation field photons and the generation of a daughter photon pair (signal and idler) in the neighboring frequency modes. c) The energy in the spontaneous four-wave mixing process is conserved, meaning that the daughter photons of the quantum frequency comb are spectrally-correlated and emitted symmetrically with respect to the pump resonance.

Many of the principles for the on-chip generation of classical frequency combs were used even in the first demonstrations of on-chip quantum combs. In particular, it was found that when such a nonlinear micro-cavity is excited/pumped with a laser signal at a power below its optical parametric oscillation threshold (i.e., where the contribution of stimulated optical processes is negligible), two-photon states can be efficiently generated [86, 38]. In third-order nonlinear micro-resonators, a process called spontaneous four-wave mixing (SFWM) occurs in response to excitation (see Figure 2.1 b and c), where two pump field photons are annihilated and two daughter photons, called signal and idler, are generated[1] [86]. The daughter photons are created in a quantum superposition of the neighboring frequency comb modes, and are spectrally-correlated due to the energy conservation of SFWM. In order to achieve SFWM, a slight anomalous dispersion is ideally required for phase-matching [88]. A variety of material platforms with third-order nonlinearity, including silicon [89, 90], silicon oxynitride [72, 81], and silicon nitride [74] have been used for on-chip QFC generation. Materials featuring second-order nonlinearity were, in fact, used in the earliest investigations of QFCs, via bulk crystals paired with resonant cavities [91, 92] or electro-optics [93]; more recently,

[1]For simplicity, here we consider a SFWM process that is degenerate in the pump frequency (i.e., the two pump photons have the same frequency). SFWM with pump photons of different frequencies and even polarizations has also been recently demonstrated [87]. See also Ref. [76] for extended discussion.

second-order effects have been used in advanced integrated semiconductor platforms to demonstrate bright QFC generation and control [94, 95].

Micro-cavities can be excited in a variety of ways. One of the most common approaches involves coupling a CW laser to excite a single resonance (Figure 2.2 a). However, active stabilization for such schemes is typically necessary (due to coupling instabilities induced by thermal effects [96]) and often, the pulsed excitation of QFC micro-cavities – i.e., such that the photon pair generation still occurs probabilistically, but in discrete time windows (Figure 2.2 b) – is preferable for quantum technologies (further discussed in Section 3.1). Overall, most approaches continue to rely on pump signals provided by bulk lasers, sometimes with several amplification stages required [41], offsetting any footprint reductions gained from employing on-chip nonlinear media. This has motivated developments into alternative, compact schemes, as investigated in Chapter 3.

Overall, thanks to cavity field enhancement, micro-cavity-based sources [97] can deliver high photon generation rates at low excitation powers, especially when contrasted against plain-waveguide sources [38]. As well, their small cavity footprints translate to resonance spacings (i.e., free spectral ranges, FSRs) on the order of 10's-100's GHz, allowing for the individual resonances of the comb to be addressed using standard telecommunications demultiplexers and spectral filters. This spectral spacing is also compatible with the bandwidths of inter-mode mixing operations realized using off-the-shelf electro-optical modulators [55, 74]. Finally, broadband photon emission at infrared wavelengths (QFC emission has been shown to span the S, C, and L telecommunications bands, see Section 5.3.2), yet with narrow individual linewidths, makes these sources highly compatible with existing fiber and detection components, and potentially even quantum memories, which can have comparable linewidths[2] [86].

These characteristics suggest the strong potential of QFCs for non-classical technologies, and for the scalable preparation and manipulation of complex states. Several multi-channel sources based on QFCs have thus been demonstrated, among them combs of correlated photons [86], cross-polarized photon pairs [87], entangled photon pairs [73, 90, 100], multi-photon states [73], and frequency-bin entangled states [55, 74, 101].

[2]Note that single resonances of integrated cavities tend to correspond to photon durations of the few-nanosecond order; alternative microcavity designs and photon bandwidth manipulation approaches [98, 99] could be employed to modify such characteristics.

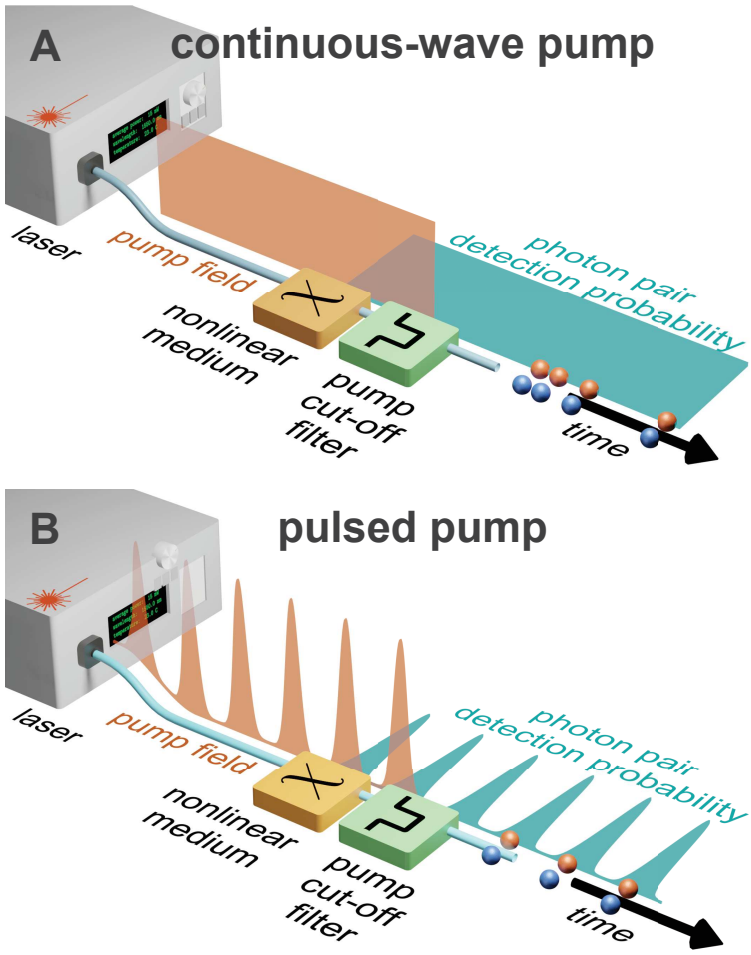

Figure 2.2: Common pump approaches for entangled photon generation. Entangled photons are most commonly generated via the coupling of a bright pump laser with a nonlinear medium, like a nonlinear micro-cavity, where spontaneous parametric processes facilitate the conversion of pump photons into entangled photon pairs. The main pump signals employed in quantum photonics today are a) continuous-wave and b) pulsed lasers. The former introduces a constant probability of generating a photon pair at any time, the latter discretizes this probability into distinct time windows that correspond to the pulsed excitation. Both generally necessitate external lasers.

2.2 Mode-locked lasers

Classical frequency combs, discussed above, are a subtype of mode-locked laser unique in their stability [79, 78]. Mode-locking, also known as phase-locking, refers to establishing a stable phase relation between the oscillating longitudinal modes of a laser [102]. If such a phase relationship is established, the oscillating modes can constructively interfere and the result is a pulse train in the temporal domain with a well-defined pulse power and repetition rate (Figure 2.3 top). Alternatively, if such a phase relation cannot be established, the oscillating modes interfere randomly and the result

is a pulse train with a distribution of pulse powers and repetition rates (Figure 2.3 bottom), not useful for most applications and even destructive towards some[3].

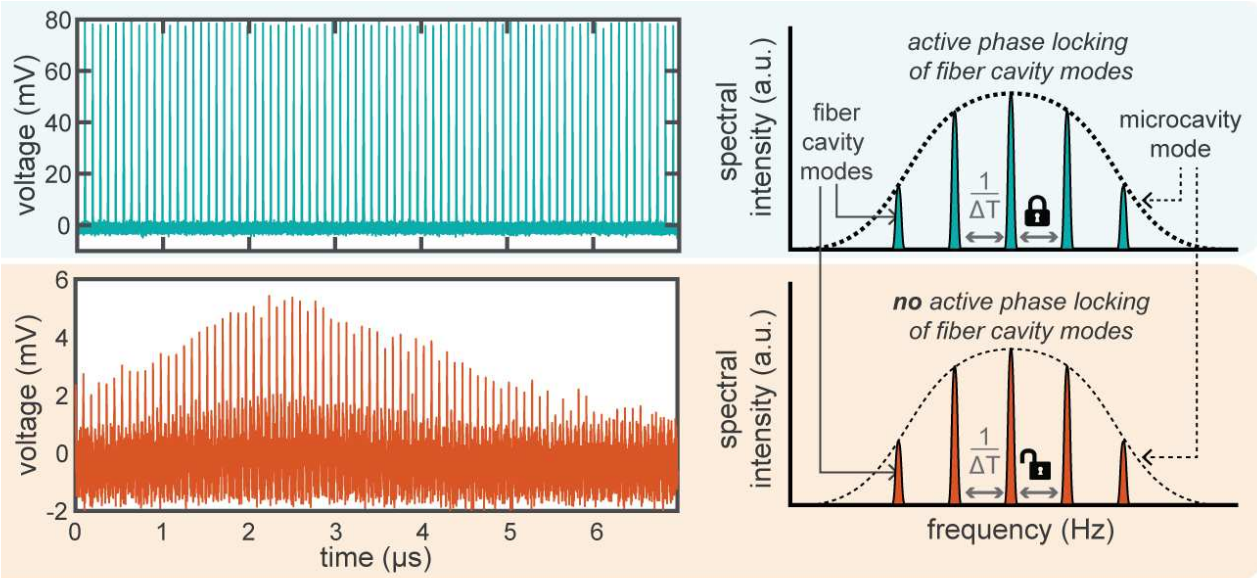

Figure 2.3: Laser signals with phase-locking present (green background) versus absent (orange background). The temporal domain signals can be seen on the left side (acquired using a fast photodiode in the setup from Chapter 3), with schematics of the spectral domain on the right side.

Techniques for establishing such phase relations are mainly divided into *active* and *passive* approaches [102]. Active mode-locking makes use of electro-optic components like phase or amplitude modulators to force a phase relation between the modes amplified in the laser cavity (via coherent side-band generation at an equal spacing to that of the longitudinal modes). Passive mode-locking approaches use the same principle, but instead, rely on nonlinear effects, e.g., saturable absorption, to lock phases between modes. While passive methods are generally preferred for their smaller energy and spatial footprints, active techniques can still prove useful if long-term stability and tight timing is required in the laser's performance (as in the case of pump lasers for quantum sources, as investigated in Chapter 3).

In addition, *harmonic* mode-locking is a variation on active approaches common especially in the telecommunications sector [102]. Here, rather than using a modulation signal frequency corresponding to the spectral spacing of the longitudinal modes, the frequency instead corresponds to an integer multiple (i.e., a harmonic) of this spacing. Locking modes that are further apart, harmonic mode-locking enables the generation of higher repetition rate pulse trains, as required

[3]Such regimes may, however, ultimately prove to be of use for quantum photonics. Their use as pumps has already demonstrated some enhancements towards entangled photon pair generation [103], with further study in progress.

for several applications in telecom. However, these enhancements typically come at the expense of reduced stability in the pulse train, and consequently, the design of such lasers typically necessitates the incorporation of stabilization techniques [104, 105, 106, 107, 108]. Harmonic mode-locking is explored as a means to break the trade-off between generation rate and quantum signal to noise ratio in Chapter 3.

Finally, returning to the subject of frequency combs (Figure 2.4), their temporal and spectral domains resemble very much that in the previous figure - phase locking of spectral modes results in stable pulses in the temporal domain. However, where frequency combs differ from typical mode-locked lasers is in the active stabilization of their carrier-envelope offset and repetition frequencies. In the majority of commercial models, these optical frequencies are mapped to radiofrequencies, stabilized with respect to atomic standard reference frequencies, enabling a level of stability that makes frequency combs an important technology for the derivation and dissemination of timing signals[4] [109]. The direct use of such radiofrequencies is investigated for quantum signal characterization in Section 5.2.

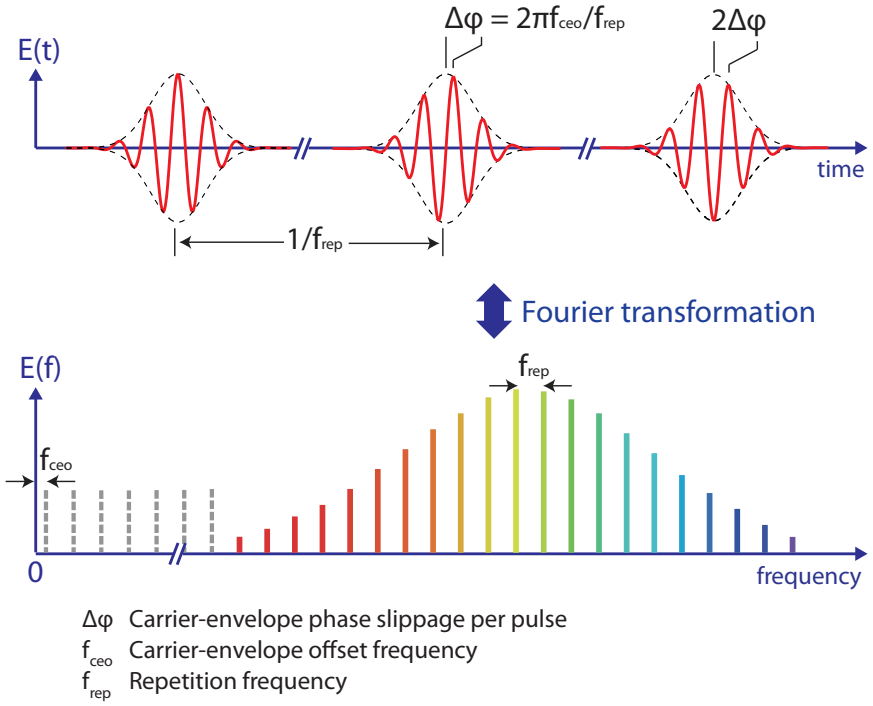

Figure 2.4: Temporal and spectral domain visualization of a frequency comb signal. Reproduced from Ref. [111], used with permission.

[4]Note these statements pertain to classical frequency combs; the stabilization of quantum frequency combs to this extent has not yet been explored in the literature.

2.3 Interferometry

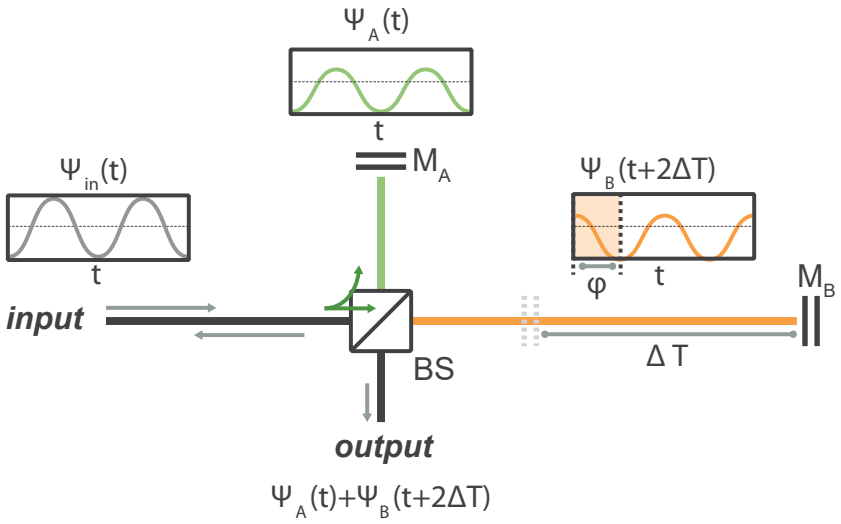

Figure 2.5: Schematic of a Michelson interferometer. An electromagnetic wave, $\psi_{in}(t)$ (grey), enters the input-port of a beam-splitter (BS), where it is reflected/transmitted into two, length-unbalanced arms (spatial modes). Here, the resulting fields are described by ψ_A (solid green line) and ψ_B (solid orange line), respectively. Following reflection at the terminating mirrors (M_A, M_B) and recombination on the beam-splitter, a summed wave, $\psi_{out}(t)$, is emitted from the two beam-splitter output ports (here, only one is shown for simplicity). As the relative phase difference between the two arms varies, the intensity of $\psi_{out}(t)$ oscillates sinusoidally – the signature effect of interferometers. Note that for clarity, constant phase shifts arising from e.g., the beam-splitter, are not depicted.

The superposition of electromagnetic waves, which enables interference, is one of the most fundamental phenomena in nature and finds ubiquitous use across foundational physics and interdisciplinary applications of photonics. Interferometers are devices that mediate this superposition to produce interference patterns. In one of the most common configurations used – known as the Michelson scheme, Figure 2.5 – light is split into two equal-energy beams by a beam-splitter. Following propagation in the two interferometer arms and reflection at their ends, the spatial modes recombine and interfere on the beam-splitter. Here, the light intensity at each of the splitter outputs is dependent on the optical path length difference travelled by the two beams (i.e., the relative optical phase). Specifically, for the injection of a single-frequency CW signal with optical frequency f, the intensity at the outputs of port 1 and 2 can be expressed as:

$$I_{out1}(\phi) = I_{mid}[1 + Vcos(\phi)]$$
$$I_{out2}(\phi) = I_{mid}[1 - Vcos(\phi)]$$

where the intensity I_{mid} relates to the interference extrema as $I_{mid} = (I_{max} + I_{min})/2$, $V = \frac{I_{max} - I_{min}}{I_{max} + I_{min}}$ is the interference visibility, and $\phi = \frac{2\pi n_g \cdot \Delta L \cdot f}{c}$ is the relative phase shift experienced in the two arms (where n_g is the effective group index of refraction, ΔL is the total length imbalance between the two interferometer paths, and c is the speed of light in vacuum).

Thus, length differences smaller than optical wavelengths (e.g., <2,000 nanometers for the infrared wavelengths used in telecommunications) have perceivable impacts on the recombined light's output intensity, meaning also that the coherent mixing of beams has strict stability requirements. Accordingly, various strategies for phase retrieval and stabilization in the fiber interferometer platform are investigated within Chapter 4. Optical beam-mixing operations enabled by interferometers hold relevance in both the history and the cutting edge of physics, e.g., in fundamental studies of light transport [112], the sensing of extremely faint signals [113], the characterization of optical coherence properties of light sources [114, 115, 116], scaling laser power [117], as well as classical and quantum signal-processing and communications [118, 119, 120, 73]; interferometric systems are without a doubt, critical, ubiquitous tools to modern science.

2.4 Photon detection and cross-correlation measurements

The infrastructure for measuring single-photon level signals is imperative for approaches making use of correlated and entangled photons. Various single-photon detector technologies exist, although the two types of infrastructures most widespread in fiber-based research settings are avalanche photodiode and superconducting nanowire single-photon detectors. Avalanche photodiode detectors are the older, more mature technology that already offers competitive footprints. However, such detectors support low probabilities of photon detection, typically <30%, limiting signal-to-noise ratios, extending integration times for measurements, and making some low-signal experiments effectively inaccessible. In turn, superconducting nanowire single-photon detectors offer excellent detection probabilities exceeding >85% and can even offer photon-number resolving capabilities in customized models [47]. However, their extremely low operating temperatures (< 3 Kelvin) make cryogenic infrastructures prerequisite to their operation, corresponding to significant energy and spatial footprints. Both detector types are used in the work presented in this thesis, with superconducting nanowire single-photon detectors (Quantum Opus; 85% photon efficiency, 1-10 Hz dark count rate, 100 ns dead time, 350 ps timing jitter) being the default. The few instances in

which we use avalanche photodetectors (ID Quantique ID210; 5% quantum efficiency, 1.3 kHz dark count rate, 10 μs dead time, 500 ps timing jitter) are explicitly noted in-text.

Detection infrastructures typically transduce photon detection events into electrical pulses, which go on to devices dubbed time-to-digital converters. Here, the arrival time of the pulse $T_{arrival}$ is digitally noted relative to some initial time T_0. For absolute timing modes, T_0 can correspond to the start time of the measurement, with all $T_{arrival}$ values essentially representing a stopwatch reading as photon events arrive relative to T_0. Alternatively, for so-called periodic 'sync/clock/trigger' signals, the T_0 is periodically reset (the number of resets is still typically noted) and the $T_{arrival}$ times are noted relative to this updating synchronization signal. Generally, the first operational mode is the default when no clock signals are present in the setup design. The second operational mode, which can generally be translated into the format of the former if needed, holds more information about the time scales addressed by the experiment. In particular, it is typically ideal for use with pulsed pumps where the laser repetition rate is used as a clock signal to help guide analysis. For example, with such a sync signal, post-processing can be used to consider only detection events within a small time window known to correspond with the pump's excitation, thus filtering out a portion of dark counts and noise from analysis (an approach known as time gating). In some cases, however, e.g., when the pump is CW or lacks a clear sync rate, the first operational mode must be employed.

With the detection events finally noted in the digital domain, analysis can be undertaken. The counts for each detector are first noted separately, even if the experimental setup involves multiple detectors (see Figure 2.6). The individual channels are post-processed, applying time-gating if desired or possible. From here, the average count rates on each channel can be determined by integrating them and then dividing the value obtained by the total measurement time. Moving average approaches can also be applied (as used in Section 4.3).

The primary tools in the arsenal of photon pair analysis are, however, two-detector measurements. Two channels, such as a signal and an idler photon channel, can have their signals cross-correlated (Figure 2.7 a) to determine a second-order correlation function (i.e., $g^2_{si}(\tau)$, τ being the signal-idler time delay) [2]. For the detection of correlated photon pairs, this function features a prominent peak for $\tau = 0$ ns, as there exists a higher probability *that the two channels will simultaneously witness detection events, as the correlated photons were generated simultaneously.* The

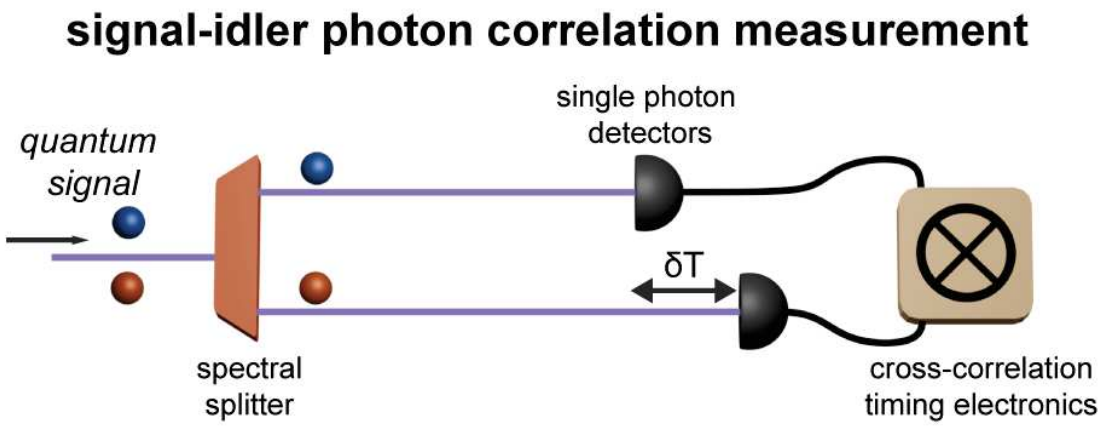

Figure 2.6: Cross-correlation measurement between a signal (blue) and idler (red) photon.

coincidence-to-accidental ratio (CAR) of quantum systems is a key operational metric that compares the probability of obtaining a coincidence detection from photon pairs generated during the same excitation event (coincidence rate), with the probability of measuring a coincidence detection event originating from two different excitation events, e.g., from dark counts, two different SFWM processes, unwanted noise processes like Raman scattering[5], etc. (accidental rate). In this sense, the CAR plays a similar role in quantum photonics to that of the signal-to-noise ratio in classical optics (see Section 3.1 for further discussion).

In practice, methods of measuring the CAR are unfortunately not standardized across the literature[6]. For CAR determination in this thesis, where only pulsed pumps were used, the analysis comprised fitting the raw second-order correlation trace with functions reflecting the signal and background count contributions. The signal fit corresponds to a Glauber function of the form $A \cdot exp(-B \cdot |\tau|)$ where A and B are fit parameters and τ is the signal-idler time delay with the peak at $\tau = 0$ (if the peak is off-center due to a length mismatch in the signal and idler propagation lengths, the expression may be amended to $A \cdot exp(-B \cdot |\tau - C|)$ with an additional fit parameter C, see Figure 2.7 b). This fitting function is based on the expression that the signal-idler cross-correlation takes on in a cavity [123]. Note that the measured signal will be a convolution of the true

[5]Raman scattering is an inelastic scattering process in which the optical signal exchanges energy with the material, resulting in the scattering of lower (Stokes) or higher (anti-Stokes) energy photons [88]. Raman processes are the main cause of noise background in fiber-based photon pair sources. While integrated platforms and careful design have aided in making this contribution narrower spectrally and thus easier to filter out [121], Raman scattering can still be a broadband noise source in many on-chip platforms, see, e.g., Ref. [122] and Figure 5.4.

[6]This can be a serious issue as it prevents comparing metrics between the works of different groups or even two different papers from the same group. As the quantum supply chain looks to be strengthened, metric standardization may turn out to be a recurring theme, following in the footsteps of other industries (e.g., telecommunications, electronics).

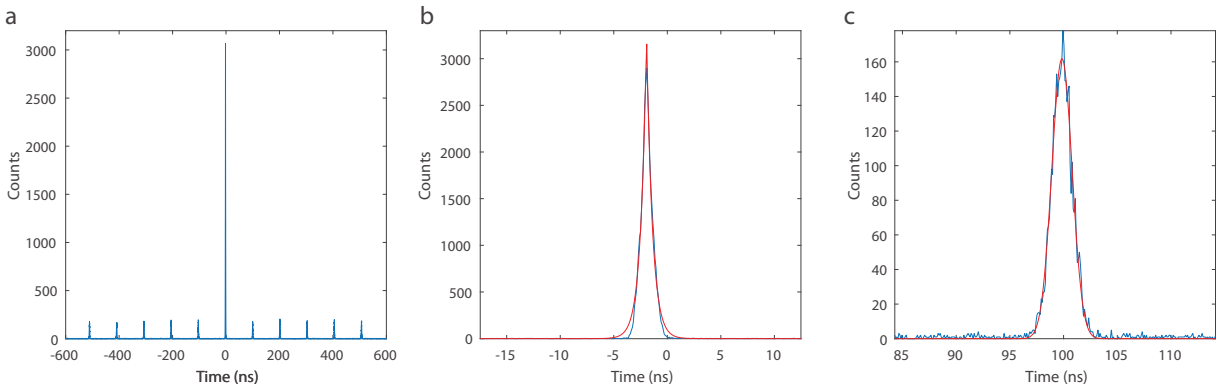

Figure 2.7: Determining the coincidence-to-accidental ratio from a signal-idler cross-correlation measurement. a) Raw signal-idler cross-correlation result following 60 seconds of measurement using the setup presented in Chapter 3. The most prominent peak, corresponding to the coincidences from signal and idler photons generated via the same SFWM process, is near the function center. The smaller peaks neighbouring the center are background counts, corresponding to coincidences from different SFWM processes (note the peaks are spaced by the pump repetition rate). The raw correlation function presented here is not normalized to its background level, as the background level must first be determined via analysis. b) Following subtraction of the average background level from the center peak (blue), the trace is fitted with a Glauber function (red). Note that the experiment here features a mismatch between the signal and idler propagation lengths (which is why the peak is not centred at $\tau = 0$) that must be accounted for when fitting is performed. c) One of the background peaks from the raw cross-correlation (blue) is fitted with a Gaussian function (red).

curve with the detector response, softening the peak shape and also motivating the use of detectors with high temporal resolution relative to the peak width (which is related to the coherence time of the source) [123]. In turn, the background fit follows the pump shape, for which a Gaussian function is typically appropriate (Figure 2.7 c). The CAR is then computed as the ratio of the signal and background fit maxima. In order to determine the coincidence rate (as also required by quantum interference measurements, where quantum projection bases are swept while the coincidence rate is tracked [124, 73]), this metric was determined by integrating raw counts over a consistent window spanning the coincidence peak. Note again that approaches in the literature vary [89].

2.5 Photon purity and degree of entanglement

Photons generated via spontaneous parametric processes like SFWM are typically entangled in frequency unless special care is taken in the source and pump design [38]. This can be highly detrimental for applications that demand pure, single-frequency mode photons: it means that heralding one photon of a pair through the detection of the other will bring about a mixed state of inconsistent photon frequency, which can degrade measurements like Hong-Ou-Mandel dips [38]. The effective number of spectral modes in a photon and the degree of entanglement in a photon pair are

thus key metrics in the context of quantum technologies. High photon purity in a single micro-ring resonance has also been previously investigated as a means of controlled entanglement scaling for high-dimensional states [55].

A frequency-entangled two-photon state can be described using its joint spectral amplitude [125] $F(\omega_{signal}, \omega_{idler})$ (where ω corresponds to optical frequency) and its degree of entanglement can be estimated by performing a Schmidt mode decomposition. In particular, the Schmidt number K represents the lowest amount of relevant orthogonal modes in the system [126] (defined as $K \equiv \sum_i \frac{1}{\lambda_i^2}$, where λ_i are the Schmidt eigenvalues with $\sum_i \lambda_i = 1$). Thus, a fully separable state has $\lambda_1 = 1$ and $K = 1$, while for an entangled state $K > 1$. It is, however, experimentally challenging to extract the joint spectral amplitude of a state, as such a measurement requires the reconstruction of the state's full phase information. A commonly employed alternative is to determine the lower bound for the Schmidt number from the joint spectral intensity $|F(\omega_{signal}, \omega_{idler})|^2$ of the state. This can be measured by performing spectrally-resolved coincidence measurements scanning across ω_{signal} and ω_{idler} (note that techniques for extracting such spectral state information using classical measurements have also been developed [127, 128]). Following this, the lower bound for the Schmidt number can be determined by extracting the eigenvalues λ_i using the singular value decomposition of $\sqrt{|F(\omega_{signal}, \omega_{idler})|^2}$. For more details about this approach, please refer to Ref. [55] or a recent thesis related to the subject in Ref. [77].

Alternative approaches are required for when the joint spectral intensity cannot be measured easily, e.g., for narrowband photon modes (100's of MHz) that cannot be swept across with a filter in the spectral domain, as is the case with photons from the single resonances of many QFCs (Section 2.1). For such cases, time-domain measurements of the second-order correlation function can be related to the effective mode number N_{eff} of the state [129] ($N_{eff} = 1$ for the case of a pure state). Specifically, N_{eff} can be retrieved from the second-order correlation value at zero-delay, following the relation $g^{(2)}(0) = 1 + \frac{1}{N_{eff}}$ [129, 130]. Towards this end, performing this characterization as part of the work presented in this thesis (Chapter 3), we select a single QFC resonance with a filter and input it into a 50/50 fiber beam-splitter. Each of the two splitter outputs is then fed to a single-photon detector, after which the second-order correlation function is computed. Given the narrow linewidth of the signal and idler resonances, corresponding to a long coherence time (>0.5 ns), the resolution of our detection system (100 ps) was sufficient to characterize the N_{eff} of the photons generated.

3 | Sources for Quantum Photonics

Chapter Abstract:

The compact and efficient generation of optical quantum states will enable low-cost and accessible advances for quantum technologies. A solution for scalable and multi-mode quantum light sources has recently been demonstrated in the use of integrated frequency combs, i.e. on-chip light sources with a broad spectrum of evenly-spaced frequency modes, towards quantum state generation. Advances in the emission of pulsed quantum frequency combs are of particular interest, as their photon properties and discrete emission times are well-suited for several applications in quantum information. However, generation schemes for such pulsed combs have so far relied on bulk lasers external to the sources, impractical due to footprint and versatility considerations. In this chapter, we introduce a novel architecture for pulsed quantum comb generation, which hybridizes fiber lasers and integrated non-classical optical sources. We go on to characterize the new architecture's performance, finding that it allows for the scaling of photon generation rates while maintaining quantum signal quality.

My contributions to this work include: the experimental realization and design of the source, the characterization of its performance, and the analysis of acquired data. The setups presented in this chapter were built using procured, off-the-shelf telecom components, with the exception of the integrated samples, obtained via collaboration with Profs. Brent Little (Chinese Academy of Science) and Sai T. Chu (City University of Hong Kong). The work resulted in one journal publication and one patent ([J.7] and [P.1] respectively, see Appendix B).

3.1 Motivation

Driven by the needs of emerging quantum photonics applications, a priority for present research efforts is to develop sources of correlated and entangled photon pairs. These must be optimized with respect to several criteria, including:

(i) **photon generation rate**, which inversely affects the integration time that is required to reconstruct specific signal statistics

(ii) **coincidence-to-accidental ratio (CAR)**, a photon signal-to-noise metric, high values of which are related to strong quantum interference fringes, enhancements for quantum illumination applications [131], and higher efficiencies for the heralding of single photons[1] [38]

(iii) **photon purity**, which quantifies the output's closeness to an ideal single-mode state (important for schemes, e.g., in quantum information processing [36, 38]) and which, alongside metrics like quantum fringe visibility and state fidelity, characterizes pair entanglement [38, 126]

(iv) **considerations of out-of-lab deployability**, including source portability, spatial/energy footprint, mass producibility, and compatibility with mature telecommunications, detection, and optical infrastructures

The recent use of integrated frequency combs for quantum state generation has suggested a solution for scalable and multi-mode quantum light sources, towards the simultaneous satisfaction of the criteria above. In particular, integrated frequency combs are on-chip light sources with a broad spectrum of evenly-spaced frequency modes, commonly generated by spontaneous four-wave mixing in optically-excited nonlinear micro-cavities. The principle and milestones for this source type, dubbed quantum frequency combs (QFCs), were summarized in Section 2.1 and Refs. [76, 75, 72].

However, in contrast to the excitation of these QFCs using a continuous-wave (CW) pump laser, their excitation using a *pulsed* pump laser (i.e., such that the photon pair generation still occurs probabilistically, but in discrete time windows) is especially suitable for quantum technologies and

[1] As well, for two equal detection rates (Coincidence+Accidental), a higher CAR allows the location of the coincidence peak to be determined within a smaller integration time, as a greater portion of the detection events are coincident.

the fulfilment of the four criteria presented above. Such pulsed sources significantly simplify the synchronization between photon sender and receiver stations, allow for the reduction of detector noise counts through the use of temporal gating or post-selection, and can be used in future systems that feature quantum repeaters or relays where accurate knowledge of photon timing is required for two-photon interference [132]. Additionally, pulsed pump approaches are the basis for time-bin entanglement schemes, a framework which is very well-suited for existing fiber and electronics infrastructures [133, 134]. Moreover, pulsed excitation is necessary for the generation of fully separable two-photon states (i.e., exhibiting no spectral entanglement, see Section 2.5) [38], enabling the heralding of pure, single frequency-mode photons[2] [135].

However, to date, pulsed generation schemes for micro-cavity excitation have relied on lasers external to the source, a far from ideal solution for the realization of efficient and low-footprint quantum light sources (criterion *iv* in the list above). First, such excitation schemes reduce the overall source scalability, and are incompatible with the ultimate vision of a truly compact system. Second, the stability of QFC sources relies on the continuous excitation of a micro-cavity resonance, but laser light absorption causes thermal frequency-shifts of the resonance frequencies [96]. For stable long-term operation, this necessitates active compensation of the thermal shift via complex schemes for cavity and/or excitation-wavelength tuning. New methods for micro-cavity excitation without active feedback have been demonstrated [136, 137, 138], but lead to turbulent pulse dynamics below the optical parametric threshold, or offer very limited coincidence rates due to multi-stable dynamics at higher pulse powers [139]. Alternatively, pulses with a broad spectral width encompassing the thermal shift range can be used to achieve stable excitation with less complexity; this approach, however, has stricter requirements on the filter isolation and bandwidth necessary to separate the quantum signal from the classical excitation field, and reduces the energy efficiency of the system, in turn increasing the total energy consumption (i.e., most of the laser bandwidth is not used to excite the narrow resonance, corresponding to 100's MHz, and is thus wasted). Finally, external pulsed lasers are largely limited in terms of flexible control of their output, e.g., repetition rate modification, reducing the overall versatility of QFC generation.

As pulsed QFCs are among the most promising approaches for on-chip quantum state generation, the resolution of these issues through the development of a scalable, stable, low-power, and versatile

[2]This is of particular importance as pure single photon states are among the most fundamental entities in quantum optics and are required for high-visibility multi-source quantum interference (a basis for e.g. linear quantum optical computing) [36] and for scaling state complexity (towards, e.g., multi-photon states) [73].

pulsed QFC excitation scheme is central to the advancement of sources for quantum science and technologies. Here, we present **a novel QFC generation architecture**, based on an actively mode-locked nested cavity, combining concepts from fiber lasers and integrated quantum optics. The methodology related to this architecture is explored in Section 3.2.1 and the results achieved with its use are outlined in Section 3.2.2.

3.2 Actively mode-locked nested cavities for photon pair generation

3.2.1 Technical Approach

In this Section, we will discuss a new intra-cavity mode-locked excitation scheme that enables the generation of high-quality pulsed quantum frequency combs in a flexible and efficient manner. Specifically, we excite a nonlinear micro-cavity using a self-locked, nested-cavity configuration with an active modulation and verify the emission of high-purity photon states. This is, to the best of our knowledge, the first scheme to generate pulsed integrated quantum frequency combs without the need for an external laser. The scheme's versatility and its use of chip-compatible components make it a significant step towards a truly compact pulsed quantum comb source.

The generation scheme for pulsed QFCs consists of a nonlinear micro-cavity embedded in an input-drop configuration inside a longer, external laser cavity (Figure 3.1). The external cavity incorporates an active electro-optic amplitude modulator, an optical gain component, and a narrow band-pass filter, with the latter limiting the cavity lasing to a pass-band corresponding to a single micro-cavity resonance. In our experimental realization, the nonlinear micro-cavity is a four-port integrated micro-ring resonator with a free spectral range of 200 GHz and Q-factors of 235,000 ($\approx$800 MHz resonance bandwidth), fabricated in the silicon oxynitride platform [81]. However, the scheme is compatible with a wide range of resonant structures, e.g., with photonic crystal waveguides [140] and resonators [141], as well as micro-disks [142], coupled resonator optical waveguides (CROWs) [143], and second-order nonlinear micro-cavities [144] (as long as an input-drop configuration is accessible). The amplification element in my realization is an erbium-doped fiber amplifier (EDFA), and the mode-locking element is a radiofrequency (RF) signal-driven amplitude modulator. An isolator in the cavity ensures uni-directional pulse propagation, and all components are connected with polarization-maintaining fibers for added environmental stability. The narrow band-pass filter

(corresponding to the H34 telecommunications band) limits the cavity lasing to a single micro-ring resonance that is centered at 1550 nm.

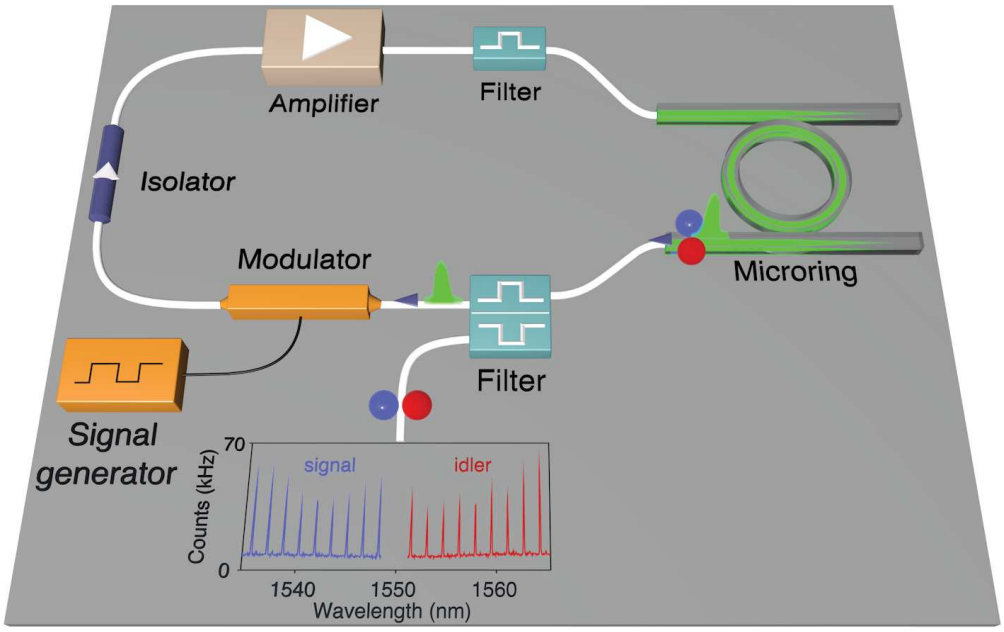

Figure 3.1: Experimental setup for pulsed quantum frequency comb generation. The scheme consists of a nonlinear micro-cavity embedded in a larger, external cavity. The external cavity incorporates an active electro-optic amplitude modulator, an optical gain component, and a narrow band-pass filter, with the latter limiting the scheme's lasing to a pass-band corresponding to a single micro-cavity resonance. The external cavity length was chosen such that several external cavity modes oscillate within the bandwidth of this single resonance. With the introduction of the amplitude-modulation (at a frequency equal to the external mode spacing or a multiple of this quantity, i.e., a harmonic frequency), these mode oscillations are phase-locked. This gives rise to a pulsed excitation that is limited to the resonance bandwidth, with a repetition rate corresponding to the modulation frequency. In turn, this pulsed excitation leads to the generation of a pulsed quantum frequency comb, which can then be separated from the excitation field via a high-isolation notch filter. *Figure inset:* Spectrally-resolved measurement of the emitted single-photon counts measured after the excitation field is filtered out, acquired using a 12.5 GHz tunable band-pass filter and a single-photon detector. See Section 5.3 for more details on few-photon spectral characterization.

The external cavity length was chosen such that several (approximately 84) external cavity frequency modes oscillate within the 3 dB bandwidth of this single micro-cavity resonance (800 MHz). The relative phases of the cavity modes are typically random, giving rise to turbulent pulse trains [103], but the introduction of the amplitude-modulation (at a frequency equal to the external mode spacing, here 9.8 MHz, or its harmonics), drives these mode oscillations to become phase-locked (see Section 2.2). This gives rise to a pulse train with a repetition rate corresponding to the modulation frequency. As well, the pulses have an optical bandwidth and center frequency that are intrinsically matched to those of the micro-cavity resonance, enabling low-power, stable, and low-complexity micro-cavity excitation even if the resonance frequency were to slightly shift due to, e.g., thermal instabilities.

3.2.2 Results

Once the correct modulation frequency (corresponding to the cavity mode spacing) was identified by frequency sweeps or radiofrequency analysis of the mode-unlocked operation, the mode-locked pulsing is found to start immediately once the amplitude-modulation signal is provided[3]. This corresponds to a stable pulse train with low root mean square (RMS) noise (0.42%, Figure 3.2) that is able to operate without interruption for days. Most types of modulation signal can be used here for mode-locking (e.g., sine, square, etc.) if they redistribute energy to harmonics of the cavity mode spacing frequency [102]. Here, we specifically make use of a rectangular modulation signal, having observed that it forces a low-jitter timing on the pulse and is very robust over days of operation. Changing the modulation frequency within ±0.001 MHz of the repetition rate does not affect the mode-locked operation, enabling a range of accessible values for the repetition rate, and also demonstrating the scheme's overall relaxed driving signal requirements.

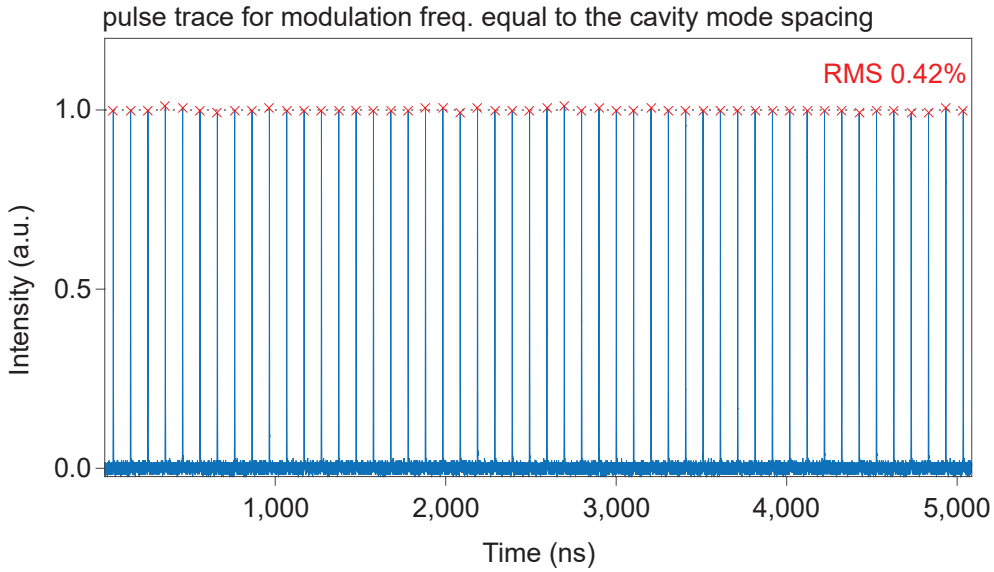

Figure 3.2: Characterization of the actively mode-locked pulsed pump. Real-time intensity trace of the pulse output, showing 50 pulses with very low 0.42% RMS noise. The trace is captured using a fast detection system (photodiode and oscilloscope with 25 GHz bandwidth). The pulse train corresponds to a mode-locked operation of the setup in Figure 3.1, with an amplitude-modulation signal at a frequency corresponding to the external cavity mode spacing (here 9.8 MHz).

By changing the net cavity gain (via the amplifier gain and/or cavity loss), the optical power of the excitation pulse train can be adjusted, which in turn changes the characteristics of the emitted

[3]I would recommend starting the optical amplification either following the modulation and at a characterized gain value, or before the modulation and with a low gain that is adjusted upwards to the desired pump power. Starting the amplifier at a high, uncharacterized gain can lead to high pulse powers that can even destroy power-limited cavity components.

QFC. A high-isolation notch filter is used to separate the excitation field from the QFC for its characterization. Signal and idler photons (here, from the second resonance pair away from the excitation field) are routed to separate detectors, where a cross-correlation function $g_{si}^{(2)}(\tau)$ (see Section 2.4) of their coincident detections is measured (Figure 3.3 a).

As previously mentioned, the coincidence-to-accidental ratio (CAR) of quantum systems is a key operational metric akin to the signal-to-noise ratio of classical systems [42] (see Section 2.4 for more discussion on CAR and its calculation). We extract the CAR from the correlation functions we obtained, and measure it in our system realization as a function of the peak excitation power coupled into the micro-ring (Figure 3.3 b). The mode-locking operation persisted through the entire power range tested. The system achieves a maximum CAR of 110 and shows the expected CAR decrease with increasing laser powers (caused by a higher probability of generating multiple photon pairs at stronger excitation energies) [42]. The coincidence rate exhibits the predicted increase with growing excitation powers and, at a CAR of 11 (sufficient for, e.g., qubit entanglement verification experiments), we demonstrate coincidence rates of 1.95 kHz. Taking into account the losses after the micro-ring output (11.4 dB per signal/idler photon), this corresponds to a pair generation rate of 363 kHz (0.04 pairs per pulse) for this channel couple. By reducing optical losses and using micro-cavities with higher nonlinearity, the scheme can be applied to demonstrate higher coincidence rates.

In this source design, which has a resonance-matched pump bandwidth, the majority of the pulse energy can couple to the resonance for excitation. In turn, for external lasing schemes (where pulses are typically much broader spectrally than the very narrow, 100's MHz resonance), much less of the total pulse energy couples into the resonance. For these external schemes, both the CAR and coincidence curves (Figure 3.3 b) would thus shift towards higher excitation powers (stretched to an extent determined by the ratio of the pulse to resonance coupling). This would in turn lead to a corresponding drop in the source's power efficiency, which the scheme presented here manages to avoid.

Finally, a central feature of this scheme is the flexible control of the QFC generation rate. This can be accomplished without changing any components within the cavity, solely by modifying the RF amplitude-modulation signal frequency. In particular, by driving the amplitude modulator with frequencies at integer multiples of the external cavity mode spacing, we attain stable harmonic

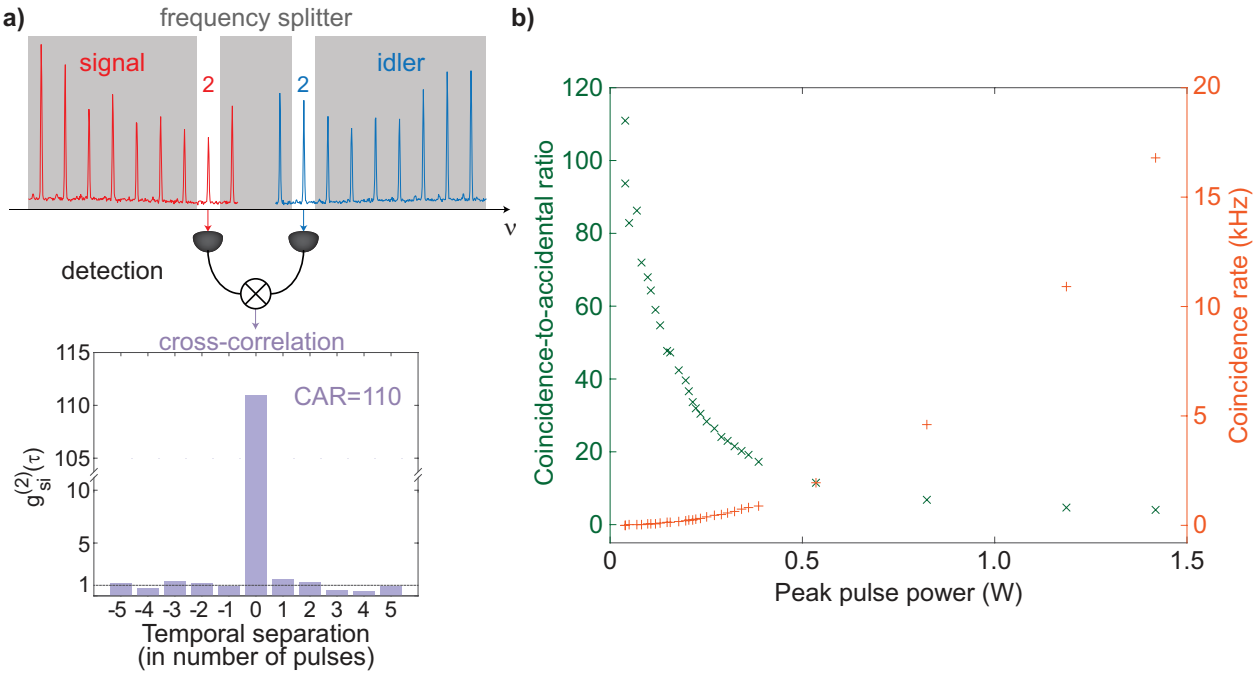

Figure 3.3: Characterization of the photon pair coincidence-to-accidental ratio. (a) The signal and idler photons (signal-2, idler-2) are routed to two separate detectors, where a correlation function of their coincident detections is measured. (b). The coincidence-to-accidental ratio shows the expected decrease with increasing laser powers, while the coincidence rate shows the predicted increase, as caused by an increased probability of generating multiple photon pairs at stronger excitation energies.

mode-locking (see Section 2.2) at different harmonic repetition rates (see, e.g., Figure 3.4 with modulation at 19.5 MHz, resulting in a pulse train with 0.95% RMS noise).

Interestingly, this repetition rate control enables preserving a high CAR while increasing the coincidence rate. By using higher pulse repetition rates, yet maintaining a constant excitation-pulse peak power, the coincidence rate can be scaled up linearly without changing the setup geometry (Figure 3.5 top and middle). Moreover, characterizing the purity of the emitted photons from a single resonance as a function of the system's repetition rate (Figure 3.5 bottom) by using a Hanbury Brown and Twiss detection configuration (see Section 2.5 and Refs. [145, 129, 130]), we found, on average, an effective mode number of 1.00±0.11 for the various repetition rate harmonics. This corresponds to a high-purity, separable two-photon state, and also confirming that the scheme excites the micro-ring resonance over its entire bandwidth [135]. This measurement result is also of fundamental interest, as at higher repetition rates fewer cavity modes are excited within the resonance. The limiting case of this, not found to be accessible in this setup, would potentially be single-mode excitation (continuous-wave), commonly associated with multi-frequency-mode daughter photons

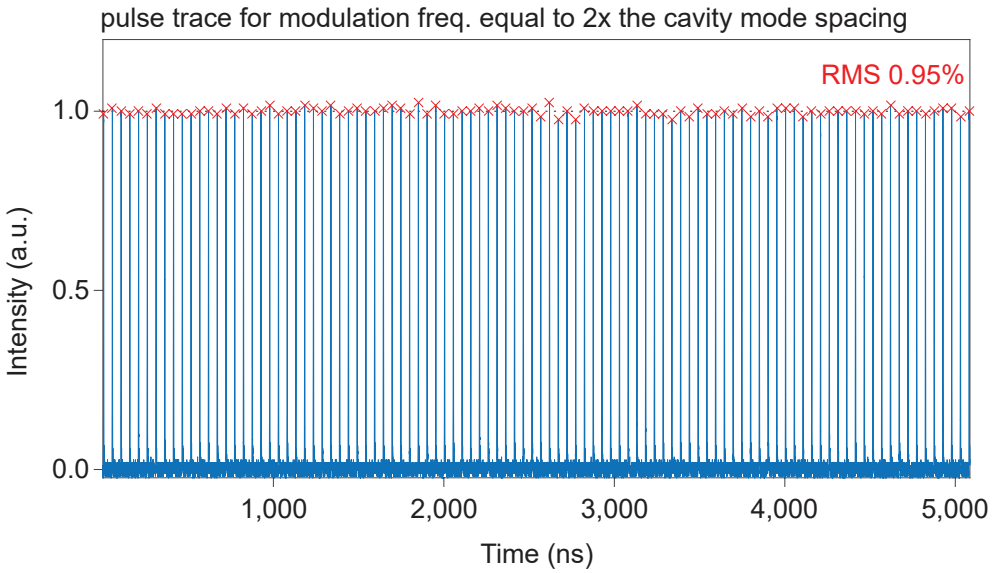

Figure 3.4: Characterization of the harmonically mode-locked pulsed pump. Real-time intensity trace, showing 100 pulses with 0.95% RMS noise, recorded when the amplitude-modulation is driven at double the cavity mode spacing frequency, i.e., 19.5 MHz.

(i.e., frequency entanglement) [135]. Nevertheless, the spectral purity was not found to diminish in the harmonics studied here.

The results in Figure 3.5 are, overall, remarkable with respect to pulsed QFC generation, as repetition rate tunability is a central feature that is almost always inaccessible when using external excitation lasers. At higher repetition rate harmonics (above the fourth harmonic) we observe increasing pulse power fluctuations, a common challenge for harmonic mode-locked lasers [146]. Access to these higher repetition rate regimes could be enabled via the implementation of harmonic-mode-locking advances developed to mitigate instability and noise, including, e.g., cavity length modulation [104, 105], nonlinear compensation [106], and high-finesse filtering techniques [107, 108].

Furthermore, while we observe mode-locking when the amplitude modulator is replaced with a phase modulator, this setup shows a higher sensitivity to the RF driving frequency and occasional operational instabilities. We thus employ a more robust amplitude-modulated setup; however, the scheme can likely make use of phase modulators if coupled with active synchronization methods, e.g., regenerative feedback circuits [147]. Since mode-locking is also observed when the fiber amplifier is replaced by a semiconductor optical amplifier (which is chip-compatible, like all the other components), this demonstration represents a significant step towards the realization of compact, versatile, and scalable sources of pulsed quantum frequency comb states.

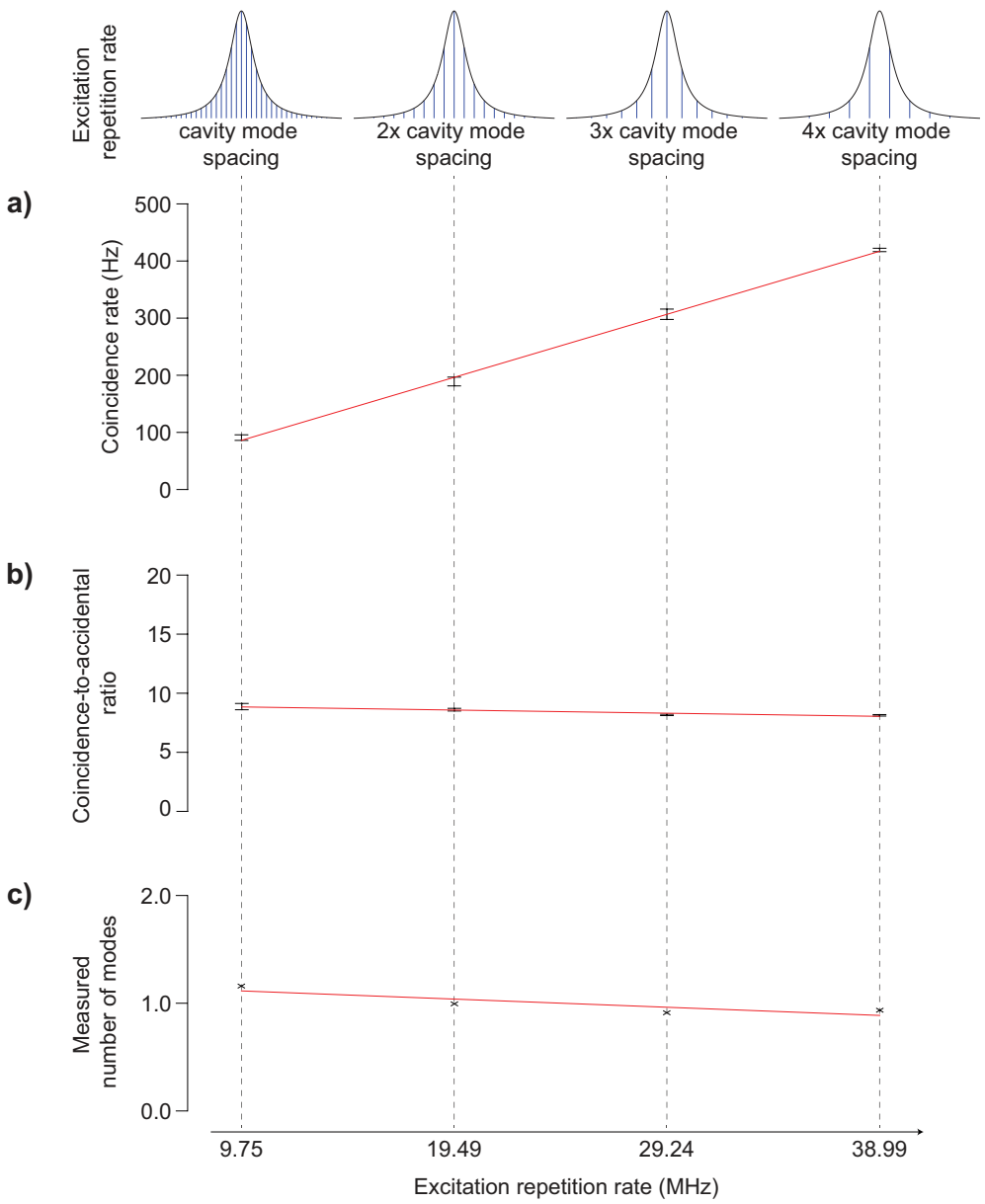

Figure 3.5: Properties of generated photons as a function of varying pump repetition rate (x-axis on top and bottom, in increments of the fundamental cavity mode spacing). (a) The coincidence rate is measured for photon pairs (produced in the second signal and idler resonances away from the pump) as a function of the repetition rate of the harmonically mode-locked laser. The coincidence rate was found to grow linearly with the pump harmonic. (b) The coincidence-to-accidental ratio is found to be preserved with increasing repetition rate of the harmonically mode-locked pump (as the pulse shape and peak power were maintained between the different repetition rates). (c) Second-order coherence function measurements were used to determine the effective number of spectral modes in the signal resonance (see Section 2.5 for details). We find an effective mode number of 1.00±0.11 as the mean across the repetition rates tested, corresponding to a pure single-frequency-mode photon state. Red lines in the figure (superposed) correspond to linear fit functions.

4 | Quantum Signal Processing

Chapter Abstract:

First, targeting the retrieval of phase values in fiber interferometric systems for quantum technologies, we characterize a phase-recovery method (based on both bright and dim/photon-level beams) that makes use of quadrature encoding in degrees of freedom well-suited for inexpensive manipulation and propagation in optical fiber. We study the use of continuous-wave and pulsed reference signals, showing that the latter has the potential to enable increased quantum signal-to-noise ratios via the temporal multiplexing of the signal and reference. Second, we present a scheme for the coherent control of time-frequency hyper-entangled states (i.e., states that are simultaneously time-bin and frequency-bin entangled) that is based on a fiber Bragg grating array alongside phase and amplitude modulation components in a self-referenced fiber loop.

My contributions to this work include: the experimental realization and design of the interferometer schemes, the characterization of their performance, and the idea for the coherent control scheme design. The setups presented in this chapter were built using procured, off-the-shelf telecom components, with the exception of the fiber Bragg grating array, obtained via collaboration with Prof. Raman Kashyap (Polytechnique Montreal). The work resulted in three journal publications and two patents ([J.2], [J.14], [J.20], as well as [P.4] and [P.5] respectively, see Appendix B).

4.1 Motivation

Wave functions are among the most common representations of quantum state and comprise a complex valued function, i.e., featuring amplitude and phase profiles. As quantum states are processed, it is important to bear both of these profiles in mind, modifying them intentionally and minimizing unwanted transformations. In particular, the processing of quantum photonic signals may involve the tuning of their amplitude and phase components, as well as the implementation of mode-mixing operations as part of projection measurements. Unfortunately, imperfections in system components may have detrimental impacts on the precision, reproducibility, and quality of processing operations. For example:

(i) The **amplitude profile/coefficients** of a wavefunction may be negatively affected by optical losses in the propagation medium or the losses induced from coupling between different optical platforms[1]; real-life mode-splitting components may also exhibit deviation from ideal transfer function coefficients, resulting in a perturbation from the intended operation at best and complete breakdown of the processing step at worst.

(ii) The **phase profile/coefficients** of a wavefunction are generally robust during propagation, but may be negatively affected by unwanted deterministic or stochastic phase changes in the state's encoding degree of freedom (e.g. dispersion for frequency, polarization mode dispersion for polarization, temporal phase drifts for time[2]). In particular, quantum states are most susceptible to stochastic phase contributions when different parts of the state occupy different, uncoupled spatial modes (e.g., different optical fibers).

As part of this Chapter, we will investigate techniques to enact quantum photonic signal processing operations in schemes that target precision, reproducibility, and quality of processing operations and manage the above-listed complications. The first component we target to advance is a **fiber-based optical interferometer**, where the state must be split into different spatial modes. Second, we will target the development of a scheme for the **coherent control of quantum states hyper-entangled** (i.e., simultaneously entangled in two different degrees of freedom [56]) **in both frequency and time**.

[1]Note that while constant loss over the wavefunction profile might not warp the wavefunction's normalized amplitude coefficients, it will decrease signal rates.

[2]Note that many of these can be compensated for if their impact is known; stochastic phase drifts may be more difficult to compensate for, but this is not impossible with feedback or post-compensation as in Secs. 4.2 - 4.4.

In particular, with respect to the first goal, interferometers are devices that mediate the superposition of electromagnetic fields to produce interference patterns (see Section 2.3 for further background). While the sensitivity of interferometers to small perturbations predicates their widespread use for metrology, it is a detriment when used for coherent signal processing: unintentional perturbations (e.g., mechanical, seismic, thermal effects) easily couple to the interferometer and, thus, to the beam-mixing procedure (Figure 4.1 a). Without proper treatment, these errors can reduce interference contrasts and in extreme cases, render interferometers inoperable (Figure 4.1 b), effectively increasing the decoupling of the two spatial modes that the quantum state is split into. This can in turn lead to the destruction of the state's phase profile/coefficients due to stochastic phase contributions. This issue is further exasperated when several interferometers/operations are concatenated, which limits the complexity/scalability of quantum signal processing.

Being able to distinguish a signal from such perturbations, accurately reconstruct the interferometer phase, and/or actively stabilize this phase (in real-time or in post-compensation) is the basis of most quantum interferometer applications, amounting to the establishment of a known and coherent relation between the spatial modes that the quantum state is split into. In free-space interferometers, where the beams propagate through air or vacuum, over a century of development has produced numerous solutions for the reconstruction of phase. These include: arm dithering [148, 149], adding auxiliary active and passive optical elements into the arms [150], using multiple spatial paths per arm [151, 152], as well as complex and expensive isolation infrastructure and light sources [113]. The basis of many of these methods is the so-called 'quadrature condition', which refers to the use of two reference signals whose interference responses are offset from one another by $\frac{\pi}{2}$ (e.g., a sine and a cosine response). Thus, when one signal is at a minimum in sensitivity to perturbation, the other signal is at a maximum. This enables a linear, phase-independent response to perturbations [150, 151, 153, 154]. However, free-space interferometers are generally neither durable, compact, nor mass-producible – characteristics required by the demanding frontiers of established and emerging quantum applications (e.g., technologies deployed as part of telecommunications grids [64, 65] and space-borne instrumentation [66, 67]). The technological maturity of fiber optics should allow to address these requirements, to access large length scales (inaccessible to integrated photonics [155]) in a compact footprint, and to enable practical, widespread interferometry. Moreover, fiber plays a central role in the quantum telecommunications infrastructure. Fiber interferometric systems are particularly critical for time-based data manipulation (e.g., executing projection measurements on

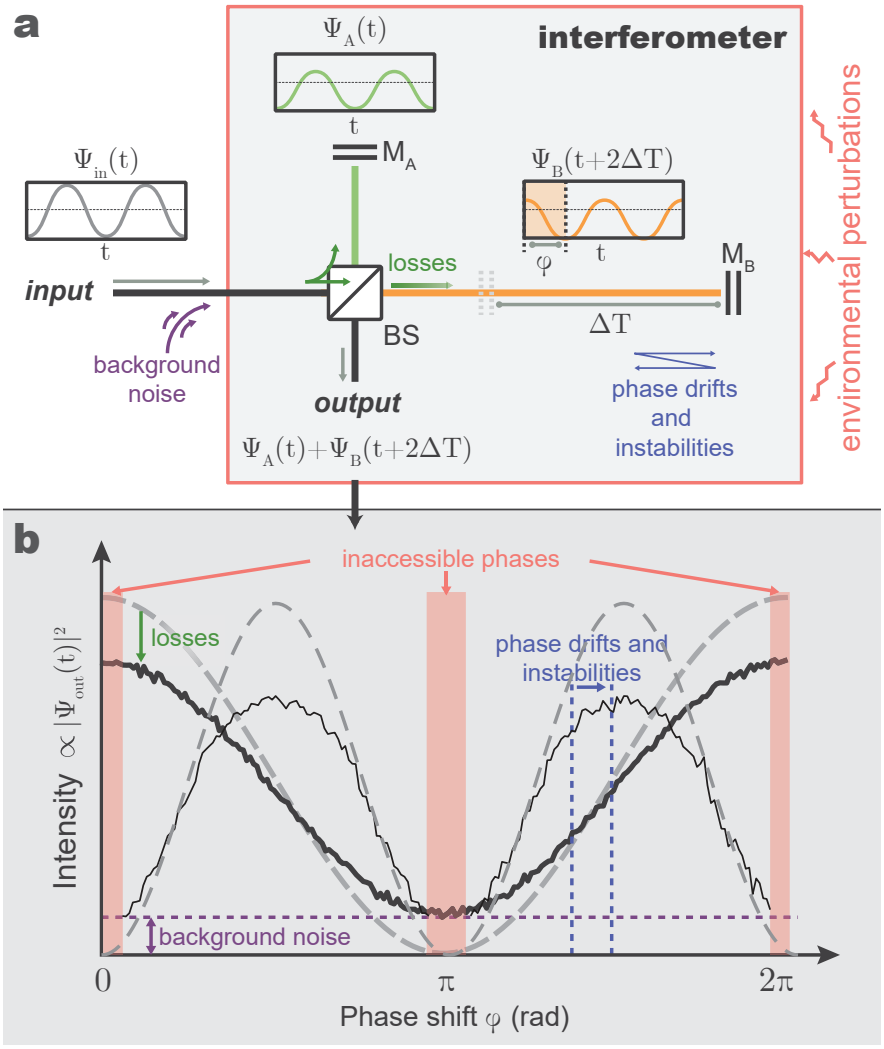

Figure 4.1: Role of optical phase on the operation of an interferometer. a) Schematic of a standard unbalanced interferometer, here a Michelson-type commonly used in coherent signal-processing (see Section 2.3). An electromagnetic wave, $\psi_{in}(t)$ (grey), enters the input-port of a beam-splitter (BS). Following reflection at the terminating mirrors (M_A, M_B) and recombination on the beam-splitter, a summed wave, $\psi_{out}(t)$, is emitted from the two beam-splitter output ports (here, only one is shown for simplicity). Note that constant phase shifts arising from, e.g., the beam-splitter, are not depicted. b) Environmental perturbations and non-idealities couple to the operation of the interferometer and degrade the ideal high-contrast interference (dashed gray line). In practice (solid black line): i) optical losses and background events reduce interference contrast (i.e., visibility), ii) interferometer phase drifts and instabilities may distort the fringes, and iii) not all interferometric phases may be accessible/resolvable (depending on the interferometer phase-reconstruction method used). Here, phases inaccessible for stabilization using single-color reference-based schemes are illustrated.

time-bin encoded quantum states using imbalanced interferometers [41, 156, 157, 158]) with reduced coupling losses versus, e.g., fiber-to-chip coupling. However, stability and full phase control are not easily achievable in fiber interferometric systems, currently limiting their potential use.

In particular, many free-space components or already-developed interferometer designs do not have accessible counterparts in fiber and generally, deployed optical fiber systems suffer from larger

phase drifts. Several works towards reconstructing and stabilizing phase in fiber interferometers have thus been introduced [159, 160, 161, 162, 163, 164, 165], featuring impressive milestones accomplished through diverse experimental approaches. These include, for example, the injection of single-frequency reference lasers [159], variants of the Pound-Drever-Hall method [164], modulation of an interferometer arm [161, 162, 163, 165], and explorations of weak references for phase-reconstruction [160, 166].

However, present phase-retrieval schemes address some interferometer requirements while compromising others. These include:

(i) introducing ambiguities in the reconstructed phase (due to phase-to-feedback mappings that are not one-to-one [159, 160])

(ii) making certain interferometer phases inaccessible for stabilization, or accessible but at the cost of limited resolution or robustness [159, 160, 161] (e.g., by sweeping the interferometer delay or optical reference frequency to follow high-derivative interference points)

(iii) demanding increased setup complexities, footprints, and costs (requiring, e.g., additional radiofrequency routing [161, 164], intricate vibration isolation and temperature controls [167], dithering of an interferometer arm [148, 161, 163, 165]

(iv) introducing noise background photons [148, 159, 161, 163, 164] (originating from bright stabilization lasers or their nonlinear/Rayleigh scattering)

In a recent, impressive demonstration in the context of quantum telecommunications [166], a phase drift of 19.63 rad/ms was post-compensated by probing the interferometric system phase at μs rates by means of weak pulse trains with alternating, orthogonal (0 or $\frac{\pi}{2}$) phase encodings. It is however expected that in deployed conditions, much faster phase drifts will have to be tracked, demanding further investigation into the constraints of such coherent-state-based recovery schemes.

Towards addressing these issues and developing practical fiber-interferometry for quantum photonic signal processing, we undertake the development of novel schemes for phase retrieval in such devices. First, we pursue the development of phase retrieval using bright continuous-wave reference signals. The methodology and results related to this architecture are explored in Section 4.2.1 and Section 4.2.2 respectively. Second, we pursue the development of attenuated coherent state references for probing such devices with minimal signal cross-talk for quantum users. The methodology

and results related to this architecture are explored in Section 4.3.1 and Section 4.3.2 respectively. Finally, we pursue the development of bright and dim pulsed reference signals, for phase retrieval in quantum experiments particularly sensitive to background noise. The methodology and results related to this approach are explored in Section 4.4.1 and Section 4.4.2 respectively.

As the second main focus of this Chapter, we pursue the development of coherent control techniques for time-frequency hyper-entangled states. Hyper-entanglement refers to the simultaneous entanglement of states in multiple different degrees of freedom, which can be treated as independent parties of the state. States of this type have been realized using combinations of, e.g., polarization, optical paths, and temporal modes [56, 168, 169, 170]. Recently, we undertook the demonstration of high-dimensional hyper-entangled states, using two intrinsically linked and non-commuting observables, i.e., two discrete forms of energy-time entanglement, namely time-bin [134, 73] and frequency-bin [91, 93, 55]. Both time and frequency are degrees of freedom particularly well-suited for propagation and manipulation using fiber optics infrastructures, as these degrees of freedom are commonly used in classical telecommunications.

Time-bin entanglement can be generated by exciting a spontaneous parametric process in an optical nonlinear medium with multiple pulses that are phase-locked [73], see Figure 4.2 a. On the other hand, frequency-bin entanglement can be realized when the nonlinear medium is placed within an optical resonator, where the emission bandwidth covers multiple resonances [55], see Figure 4.2 b. In recent work, we demonstrated that, remarkably, if the time-frequency product corresponding to the individual modes is well above the quantum limit, frequency-bin and time-bin entanglement will become independently controllable [41]. In particular, this will allow for the preparation of hyper-entangled, multipartite states, which can be produced by exciting the nonlinear element, placed inside the resonator, with a coherent set of multiple pulses, see Figure 4.2 c. The pulse separation for this scheme must be much larger than the photon lifetime inside the resonator, which enables the time-bin component to be fully controlled in the temporal domain, and the frequency-bin component to be completely and independently controlled in the frequency domain.

Time-frequency hyper-entangled states are thus attractive resources for quantum technologies, scalable in dimensionality and Hilbert space size [41]. We go on to transform them via quantum signal processing into so-called cluster states, a family of states central to quantum repeater and quantum information processing applications, as further discussed in Refs. [57, 37, 77]. In this

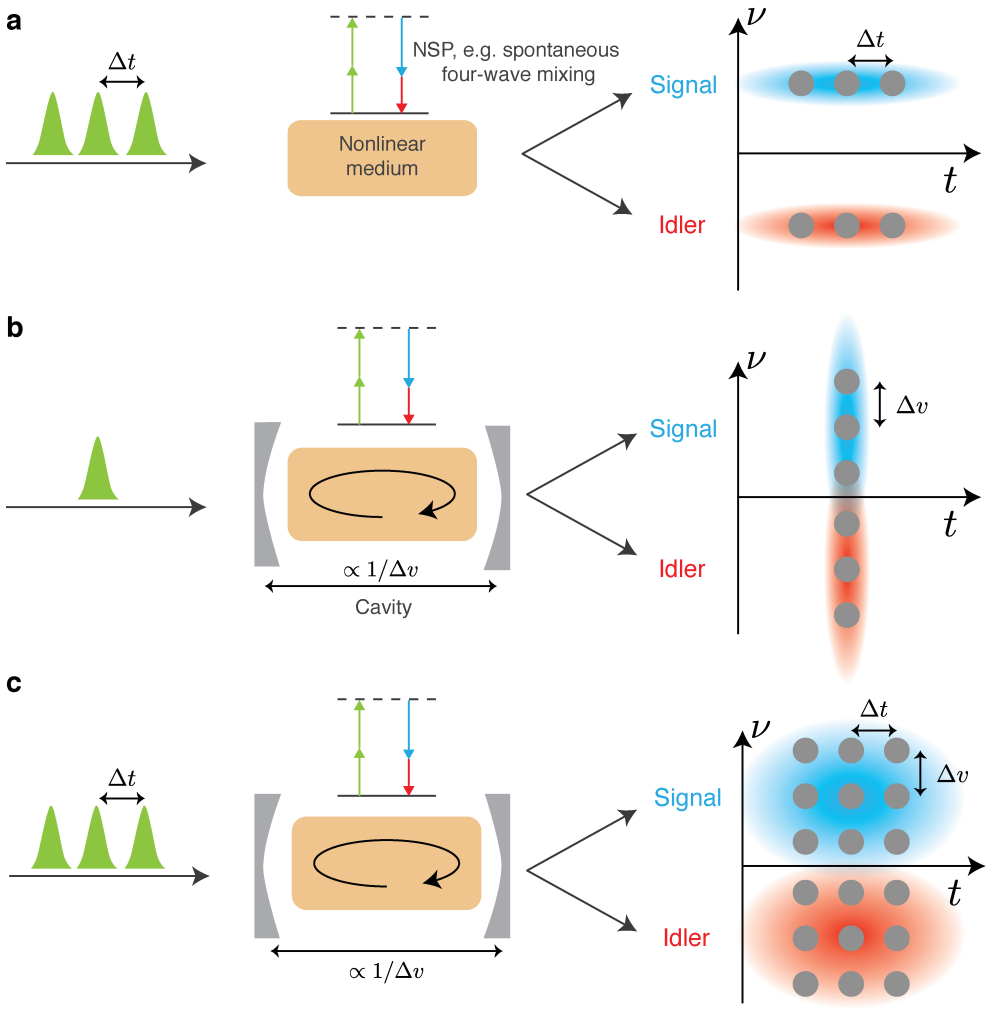

Figure 4.2: Time-frequency hyper-entanglement. a) An optical pulse train (composed of three pulses in this example) excites a nonlinear medium where photon pairs (signal and idler) are simultaneously generated via a nonlinear spontaneous process, in a superposition of several time modes (here d = 3, given by the number of pulses) generating a d-level time-bin entangled two-photon state. b) A single pulse excites a nonlinear medium placed inside a cavity (composed of two semi-reflective mirrors), where photon pairs are created over a broad bandwidth in a superposition of several spectral modes (here d = 3, given by the number of selected cavity resonances per photon), leading to a d-level frequency-bin entangled state. c) An optical pulse train excites a nonlinear cavity (merging the concepts of a and b) generating a simultaneously time- and frequency-bin entangled photon pair, i.e., a d-level hyper-entangled state.

Chapter, we focus on the candidate's contribution to this work, which is the design of a coherent control platform for time-frequency hyper-entangled states. While it is used to enact an operation modifying the initial hyper-entangled states into cluster states, the scope of this technique is much broader and enables fine and versatile coherent control. The methodology and results related to this approach are explored in Section 4.5.1 and Section 4.5.2 respectively.

4.2 Fiber-based interferometry with bright continuous-wave reference signals

4.2.1 Technical Approach

Presently, a common inexpensive stabilization technique relies on coupling a reference continuous-wave laser into the interferometer and measuring the interfered signal (I_x, Figure 4.1 a). This signal varies as a cosine ($I_x(\phi) = I_{mid}[1 + Vcos(\phi)]$, where the intensity $I_{mid} = (I_{max} + I_{min})/2$ and V is the interference visibility) and is used to extract the interferometer phase ϕ [159]. While experimentally straightforward relative to the current state-of-the-art, such a single-color approach is limited since several phases between 0 and 2π correspond to the same intensity (that is, the map from intensity to phase is not one-to-one in this range, e.g., $\phi = \frac{\pi}{2}, \frac{3\pi}{2}$ both map to I_{mid}). This leads to ambiguities in phase retrieval, typically requiring the active sweeping of the laser wavelength or the interferometer delay [159, 161], making it difficult to reproduce phase settings, or to lock multiple interferometers to different phases with a single source.

However, as the optical frequency of such an injected signal is changed (e.g., via an acousto-optic modulator), its cosine response is shifted in phase[3]. This means that a slightly-offset optical frequency component is sufficient to output a $\pi/2$-shifted, sine response relative to I_x (i.e., the quadrature signal, I_y, Figure 4.1 a). Phase ambiguity is present when only I_x is acquired, but can be eliminated by simultaneously measuring the orthogonal signals I_x and I_y. When acquired together, I_x and I_y map one-to-one to a phase between 0 and 2π (Figure 4.1 b), allowing for the unambiguous retrieval of the interferometer phase. Specifically, the cosine-sine relationship of I_x and I_y allows for straightforward reconstruction of the interferometer phase (relative to the optical reference) using:

$$\phi = arctan2\left(\frac{2I_y - I_y^{max} - I_y^{min}}{I_y^{max} - I_y^{min}}, \frac{2I_x - I_x^{max} - I_x^{min}}{I_x^{max} - I_x^{min}}\right) \tag{4.1}$$

where arctan2 is the two-argument arctangent function, while I^{max} and I^{min} correspond to the interference maxima and minima, respectively.

[3]Note that this arises due to the proportionality of the interferometer phase ϕ with the optical frequency, as covered in Section 2.3. Note also that this is only true for unbalanced interferometers (where $\Delta L \neq 0$), and all techniques covered in this Chapter are only pertinent to such interferometers.

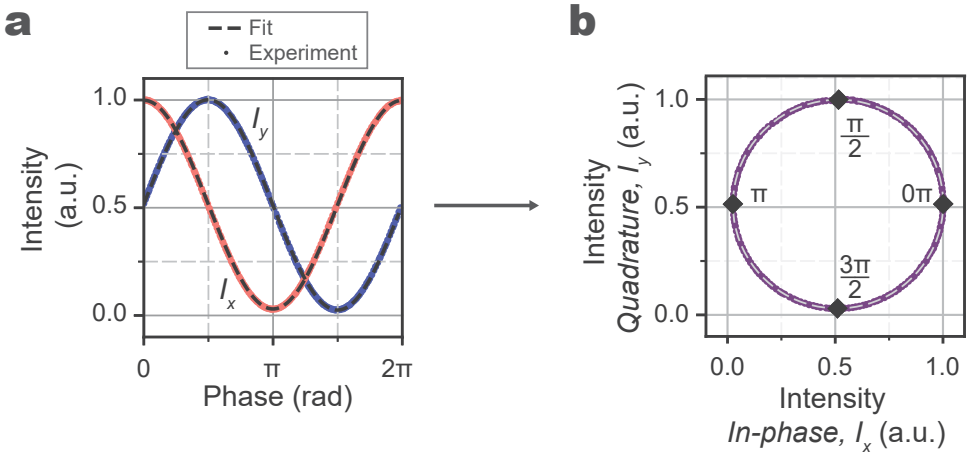

Figure 4.3: Retrieving fiber interferometer phase using a two-color reference signal. a) A two-color (ω_x and ω_y) optical signal, created from a single source, is injected into an interferometer, with the ideal (dashed line) and experimental (acquired with photodiodes, red and blue markers) interference outputs I_x and I_y shown as a function of the interferometer phase (referenced at ω_x, see Experimental Section). ω_y was chosen such that I_x and I_y are out of phase by $\pi/2$. The use of such a reference signal enables an unambiguous, one-to-one map between the experimental coordinate pair $\{I_x, I_y\}$ and the interferometer phase ϕ in the range $[0, 2\pi)$. This is evidenced in (b) depicting the relation of I_x and I_y (Lissajous pattern, with ellipse fit overlaid).

A very small optical frequency offset between the two injected signals is required to maintain a similar period of I_x and I_y. For example, for a portable interferometer with a 4 ns imbalance in the telecom band at 1,550 nm [73, 134], a frequency offset of 188 MHz can be used. However, most off-the-shelf filters cannot separate such finely-spaced frequencies for the simultaneous measurement of the two interferences. Towards this end, we exploit the polarization degree of freedom – easily controlled and propagated with minimal cross-talk in fiber optics – to prepare a reference signal where I_x and I_y travel in orthogonal polarization modes of the fiber (Figure 4.4). The two-color reference signal is prepared from one source, which is split into a passive and an acousto-optic modulated (AOM) arm to create the frequency-shifted, orthogonally-polarized, I_x and I_y components. This reference signal is fed into the interferometer[4]. Once it is interfered and output, an off-the-shelf fiber polarization beam-splitter (rather than an expensive, custom-made filter) is used to split the two frequencies for detection of the intensities I_x and I_y. Note also that this signal can be prepared once and distributed among several interferometers, providing a common reference.

[4]Note that in a fiber interferometer of this type, there is also the issue of imperfectly balanced splitting, as mentioned in Section 4.1. Imperfect splitting here, causing a subsequent drop in interference visibility, can be caused by an imperfect beam-splitter ratio and/or unequal losses in both arms of the interferometer. Such issues are almost always present in these devices, especially as the interferometer arm lengths in the scheme are unequal and have different components. Unfortunately, to increase visibility for this case, additional losses must be introduced to equalize the response.

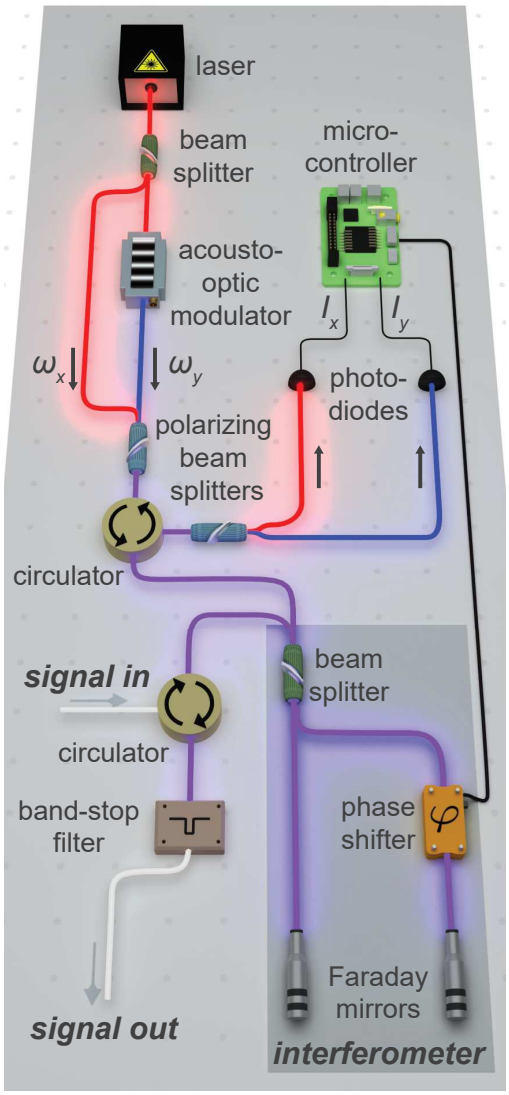

Figure 4.4: Setup for interferometer phase extraction using a two-color reference, experimentally realized using off-the-shelf telecommunications components, with the two parts of the reference prepared to propagate on orthogonal fiber polarizations. This enabled straightforward separation of the two finely-spaced reference frequencies ω_x and ω_y at the detection stage (using only a polarizing beam-splitter rather than expensive filters) for phase extraction and stabilization. In parallel, an input signal-under-test co-propagates in the unbalanced interferometer (built to provide a 11.5 ns imbalance). As the frequency difference between the signal-under-test and the reference signal can be chosen to be on the order of hundreds of GHz, they can be easily separated by using off-the-shelf filters.

For these experiments, the reference signal used is a low frequency-jitter CW source (NKT Koheras BasiK E15, 1,550 nm central wavelength, 40 mW optical power, <2 kHz bandwidth, coherence length above 47.7 km $\gg$ the maximum 2.3 m interferometer imbalance used in the measurements). The acousto-optic modulator (Brimrose TEMF-200-40-30-1500-2FP) is driven by an RF synthesizer (Tektronix AWG701B) and RF amplifier (Kune Electronic Microwave Components KU-PA-BB-005250-2A). In order to satisfy the orthogonality criterion for the two components, the

RF signal amplitude is adjusted to provide near-equal interference amplitudes for I_x and I_y, and δf is made equal to $\frac{c}{(4n_g \cdot \Delta L)}(2n+1)$, where c is the speed of light in vacuum, n_g is the effective group index of refraction, ΔL is the total length imbalance between the two interferometer paths, and n is an integer (kept as small as possible to ensure comparable periodicity between I_x and I_y).

For the stability analysis in Figure 4.6, the reconstructed phase is evaluated using the Allan deviation, a metric first introduced in the context of clocks/frequency references and that describes the stability of the interferometric phase over different time scales (with lower deviation values being preferable) [171, 172]. Here, we used the Allan deviation expression given by:

$$\sigma(\tau) = \sqrt{\frac{1}{2M}\sum_{m=1}^{M-1}(\overline{\phi}_{m+1} - \overline{\phi}_m)^2} \tag{4.2}$$

where $\overline{\phi}$ is the average of $\phi(t)$ over an integration time τ, with m being an index of consecutive averages, and $M = m\tau$.

4.2.2 Results

With the additional use of passive stabilization methods (mechanical damping), perturbations are limited to frequencies below tens of kHz. Consumer-grade, portable digital electronics are then easily integrated into the system for phase retrieval and real-time correction (similarly, low-footprint electronics can also provide the AOM driving signal), with on-the-fly phase tunability via a fiber stretcher in one of the arms. Tracking and compensating for fluctuations enables long-term phase stability (relative to our reference, i.e., measured in-loop, Figure 4.5), as required for many measurements with long integration times and common optical references (e.g., quantum state characterization). Alternatively, without real-time stabilization, if our reference signal was to be tracked through the duration of a measurement, the phase could be post-compensated/post-selected. Such interferometric phase-tracking schemes for post-compensation are already used in several application domains [173, 174, 175].

An issue in phase-recovery schemes based on the use of a single interference signal (without sampling an orthogonal component) is that phase perturbations are not equally resolvable across all phases. This limits the range of accessible interferometric phase values, unless, e.g., the reference laser frequency or interferometer delay is actively tuned to follow sensitivity maxima [159, 161],

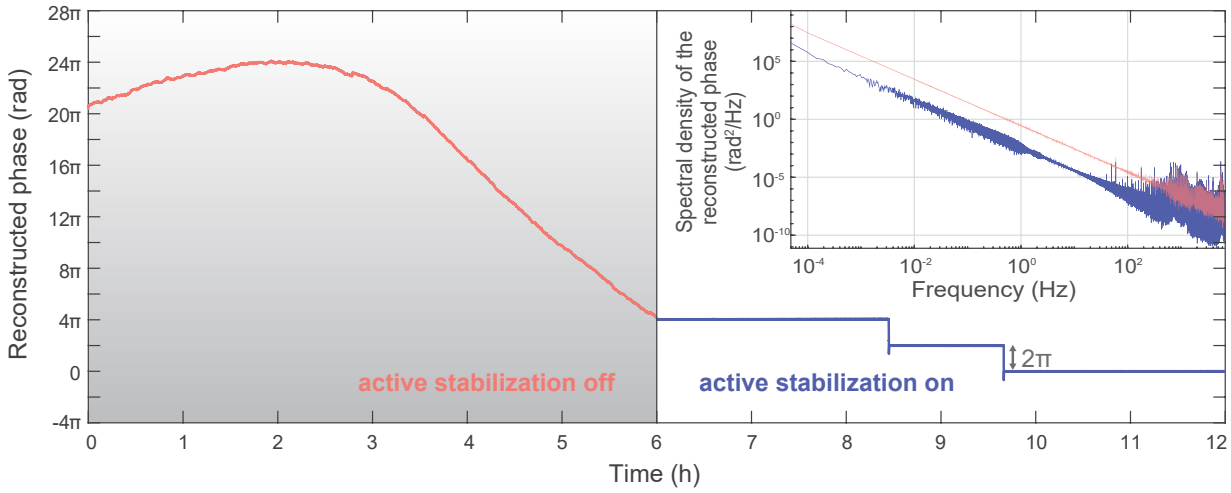

Figure 4.5: Long-term interferometric phase stability. Phase drift in a fiber interferometer reconstructed in-loop from our error signal without (left) and with (right) active phase recovery-and-feedback. When the fiber-stretcher/digital-to-analog converter voltage limits are reached, the target phase is preserved by the stabilization algorithm enacting a fast, cyclic shift of 2π (see step-like transitions on right). Such long-term stability is particularly important for long measurements, e.g., those related to quantum state tomography. Inset: Spectral density of the reconstructed phase in the presence (blue) and absence (red) of active stabilization, demonstrating an order of magnitude reduction in phase change for most spectral components, particularly the low and intermediate frequencies currently accessible with the speed of our feedback loop.

which unfortunately introduces issues in terms of setup complexity and setpoint reproducibility. Looking at the example of a single-color reference signal (which, while not the most advanced, has a low experimental complexity that is comparable to the presented method), the response of the feedback signal to phase changes (the so-called system 'sensitivity') is described by $S \propto \left|\frac{dI_x}{d\phi}\right| = |VI_{mid}sin(\phi)|$. The sensitivity, and by proxy the accuracy of phase retrieval (relative to the optical reference), can be seen to be extremely phase dependent, with minima at the 0 and π phases. This restricts the range of phases accessible using such a feedback signal (Figure 4.6 a).

Instead, using our two-colored feedback signal, comprised of the in-phase and quadrature components, makes the sensitivity constant for all phases, as:

$$S \propto \left|\frac{d(I_x + iI_y)}{d\phi}\right| = |-VI_{mid}sin(\phi) + iVI_{mid}cos(\phi)| = VI_{mid}$$

As a result, all phases $[0, 2\pi)$ are individually accessible (Figure 4.6 a) with a phase-independent stabilization performance (Figure 4.6 b). This is demonstrated even more directly via Allan error signal deviation analysis for different integration times (Figure 4.6 c). Moreover, we observe an Allan deviation of $5.89 \times 10^{-5}\pi$ rad (in-loop, equivalent to 0.04 nm at 1,550 nm optical wavelength) for an integration time of 2:11 minutes (and even for integration times of 1h09m, this value remains

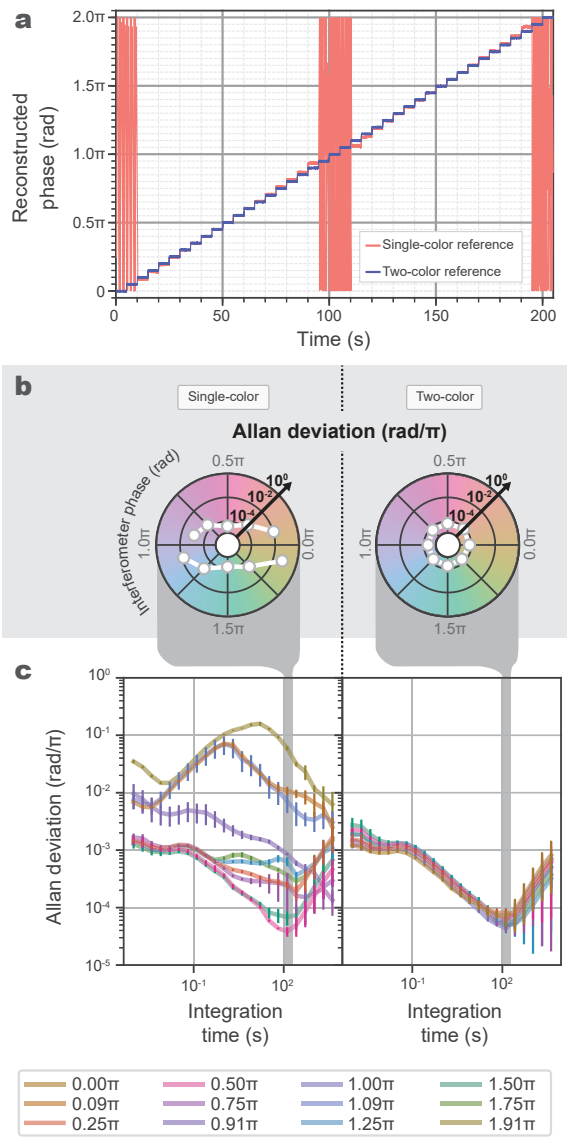

Figure 4.6: Use of the two-color reference signal for phase-independent interferometer stability. a) The interferometric phase is stabilized from 0 to 2π in steps of 0.05π, using both single-color (red) and two-color (blue) phase-stabilization algorithms in the feedback loop. The single-color feedback system is unable to stabilize at the minima points of its sensitivity (0 and π) and has an increasing error when approaching these points. In contrast, the two-color feedback system has stable access to all phases in the range [0,2π) while maintaining a comparably low setup complexity. b) System phase stabilization as a function of the target interferometer phase (plotted in polar coordinates, with a logarithmic radial axis). The points correspond to the Allan error signal deviation value at an integration time of 131 s (vertical grey bar in c). The single-color method (left) demonstrates a decrease in stability approaching its sensitivity minima at 0 and π, while the two-color method (right) has a largely uniform stability across all phases in the [0,2π) range. c) Allan deviation analysis of the phase error signal over a range of integration times. While the two-color stabilization (right) shows near-identical in-loop stability between all target phases, the single-color Allan deviation magnitudes vary greatly between phases. As the single-color retrieval could not be stabilized at 0 and π, measurements were instead performed at $\pm 0.09\pi$ of these points. Error bars correspond to the standard deviation calculated from three measurements.

below $1 \times 10^{-3}\pi$ rad). This value outperforms most other implementations in the state of the art (see Appendix A), and is also unique in its practical, inexpensive, real-time stabilization.

Several fields that require coherent optical processing can benefit from our scheme: quantum optical state processing and characterization constitute applications with some of the most strict and demanding requirements. Specifically, our scheme gives access to long integration times for photon signals, and unambiguous, uniform-stability across all phase projection measurements. These are required for complete quantum state characterization (tomography), high-visibility quantum interference, and repeatable quantum operations – measurements demonstrated (using the presented scheme for real-time stabilization) in the context of recent two- and high-dimensional time-bin entanglement works [73, 55, 72].

4.3 Fiber-based interferometry with an attenuated coherent state reference

4.3.1 Technical Approach

A number of quantum photonics experiments and technologies demand minimal background photon counts, which bright stabilization lasers (in wavelength regions near the quantum signal bands) and limited filtering cannot always provide, bringing about non-negligible cross-talk. Towards resolving this issue for such delicate application cases, we investigate the implementation of a heavy attenuation of the bi-chromatic CW reference signal (prior to injection into the interferometer) to produce a few-photon interference response (measured using single-photon detectors).

For this, a polarization-maintaining variable optical attenuator is inserted immediately before the two-color reference signal is injected into the interferometer. The rest of the setup is kept the same as in Figure 4.4, with the exception of the photodiodes replaced with two superconducting nanowire single-photon detectors (Quantum Opus, one for I_x and one for I_y), connected to time-to-digital conversion electronics (Picoquant Hydraharp). For Figure 4.7, the fiber stretcher in the interferometer arm is then swept, and the photon arrival times at each channel collected. A moving integration window is then implemented in post-selection to determine both the count rates and the integration-time response of the system.

This is an attractive solution, as the low-power probe signal no longer requires high rejection filters, meaning that even off-the-shelf DWDM (dense wavelength division multiplexing) filters can

reduce cross-talk. Such attenuated coherent states have been investigated for interferometer phase reconstruction [176] and experimentally demonstrated in a single-color stabilization scheme to lock on one phase [160]. Here we extend these efforts and investigate the use of two attenuated coherent states in quadrature for phase-retrieval.

4.3.2 Results

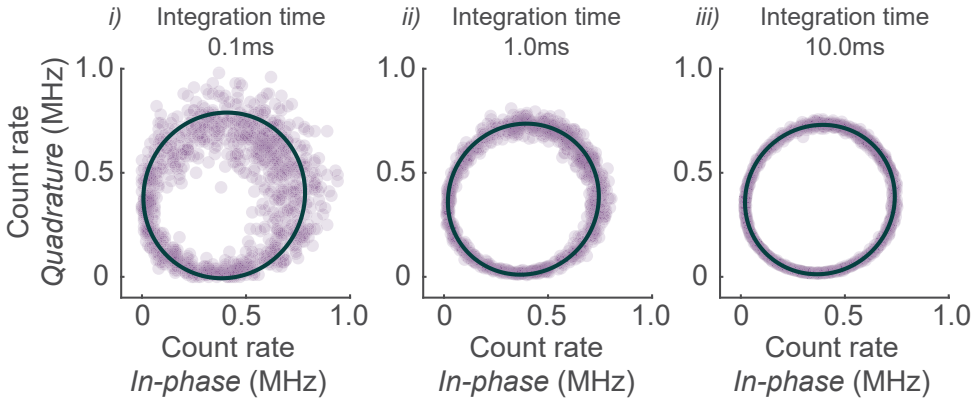

Figure 4.7: Interferometer phase estimation using attenuated coherent states in quadrature. Photon count rates for the in-phase and quadrature channels, measured with two single-photon detectors as the interferometer phase is swept. Increasing the signal integration time shows an increase in phase estimation accuracy.

By measuring the in-phase and quadrature signal outputs at one interferometer port (Figure 4.7), we illustrate the trade-off, brought about by the Poissonian statistics governing coherent states, between the phase estimation error and the signal integration time (i.e., better phase estimation for longer integration times and higher reference signal powers). These statistics give rise to a phase-dependence in the phase estimation error (Figure 4.8, a dependence removed when both output ports are used). Here, the mean photon number of each quadrature channel is $\overline{n}_x = \frac{\overline{n}}{2}(1+Vcos(\phi))$ and $\overline{n}_y = \frac{\overline{n}}{2}(1+Vsin(\phi))$, where V is the interference visibility, $\overline{n}$ is the input mean photon number, and each channel has variance $\Delta n^2_{x,y} = \overline{n}_{x,y}$. Propagating this variance through Equation 4.1, the mean squared phase error is (Figure 4.8, solid red line):

$$\Delta\phi^2_{est} = \frac{2}{V^2\overline{n}}(1 + Vsin(\phi)cos^2(\phi) + Vsin^2(\phi)cos(\phi)) \tag{4.3}$$

which scales in agreement with the standard quantum limit [160, 176]. If, instead, both output arms of the interferometer were monitored using a difference detection scheme (i.e., the corresponding reference signals at each output arm are subtracted from one another), this phase-dependent error

is removed and $\Delta\phi_{est}^2 = \frac{1}{V^2\overline{n}}$ (Figure 4.8, solid purple line). However, such monitoring requires increased costs and complexity as two additional single-photon detectors are needed.

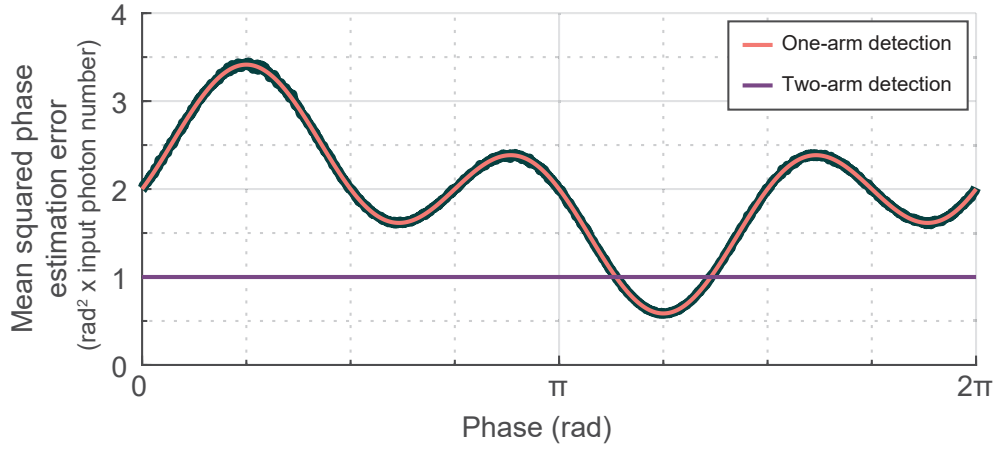

Figure 4.8: The phase dependence of the estimation error for the attenuated coherent reference method presented in Figure 4.7. The error arises from the Poissonian statistics governing coherent states, determined analytically (red curve) and from the average of 10,000 Monte Carlo simulations (black curve).

For experiments where these detriments can be tolerated in exchange for reduced cross-talk, we append a heat map illustrating the trade-off between these parameters (Figure 4.9). Experimentally, the mean photon number is the product of the detector integration time, τ, and the photon flux rate, Θ, both of which may be bounded by implementation considerations such as the maximum phase drift velocity present (v), detector saturation rate, or maximum permissible phase estimation error ($\Delta\phi_{max}$). For the bounds on integration time in Figure 4.9, the definition that we make use of is $\tau \leq \Delta\phi_{max}/v$. Bound 1 is based on data from the system presented in this work, i.e., $\Delta\phi_{max} = \pi \times 10^{-3}$ rad (from Figure 4.6) and v=0.071 rad/s (identified as the fastest phase drift in the unstabilized trace of Figure 4.5). Bound 2 is based on data from Ref. [64] for an interferometric system with arm lengths of 275 km, with v=1.0 rad/ms and assuming $\Delta\phi_{max} = \pi/16$ (corresponding to half the phase slice size employed in Ref. [64]). In practice, the integration time should be chosen so that the fastest phase drifts can be resolved, while the count rate will be limited by the saturation point of the detectors used, the maximum power available from the optical reference, or the maximum power allowed that still minimizes cross-talk to acceptable boundaries.

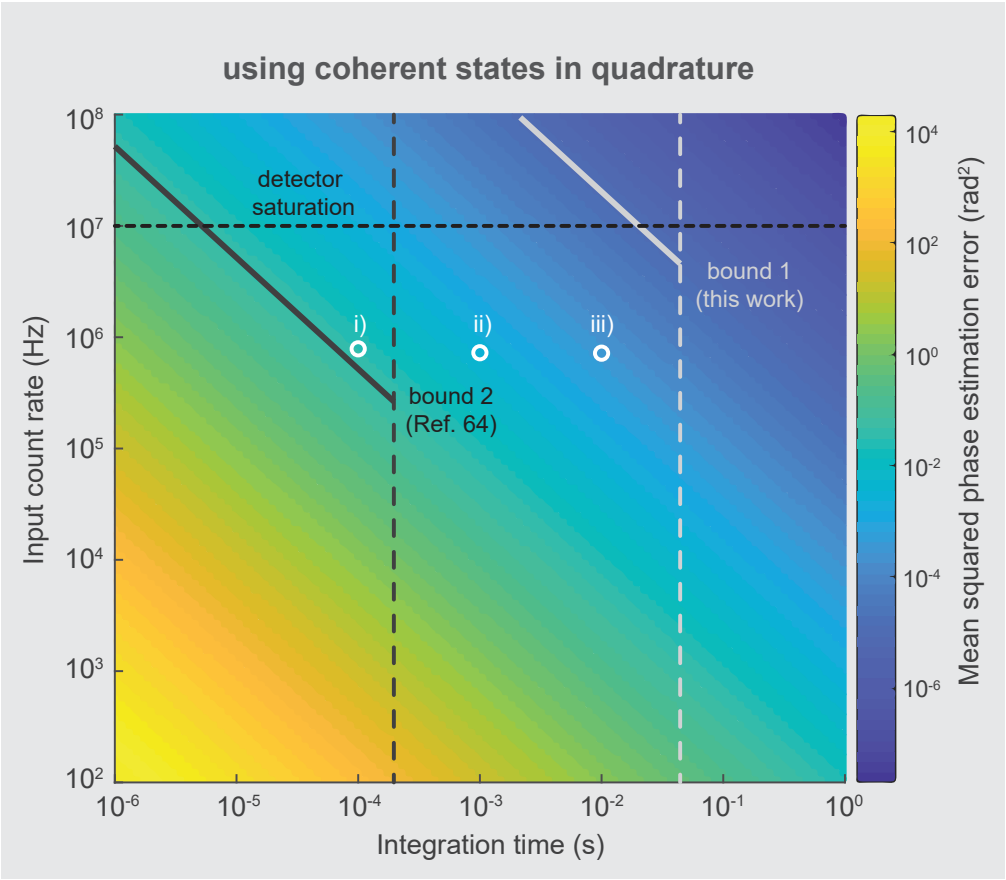

Figure 4.9: Average phase estimation error as a function of photon flux and integration time. The maximum phase drift rate, maximum allowable phase error, and single-photon detector saturation rate are the key parameters for deciding the experimental values of count rate and integration time to be used. We denote two example bounds: bound 1, based on the data corresponding to our interferometer system (our system's detector saturation rate is also illustrated), and bound 2, based on data from a recent work making use of a 275 km fiber interferometric system [64]. White markers indicate our expected performance with the three integration times demonstrated in Figure 4.7.

4.4 Fiber-based interferometry with bright and dim pulsed references

4.4.1 Technical Approach

As mentioned in Section 4.3.1, a number of quantum photonics experiments and technologies demand minimal background photon counts that the use of a bright CW reference as in Section 4.2 can be insufficient to provide. In Section 4.3, an attenuated CW reference approach was pursued. However, the reference laser used in the phase-retrieval scheme does not have to be continuous-wave (after all, CW references produce background noise photons over all detection time windows). Mode-locked sources (and especially stabilized frequency combs) have sufficient coherence lengths to produce interference signals (Figure 4.10), a characteristic already exploited in the context of

classical optics [177] as well as quantum communications [166], and here implemented with our I_x and I_y reference scheme.

For this investigation, the setup is identical to the one used with the CW reference (Figure 4.4), but with the original laser source replaced with a stabilized frequency comb output (Menlo FC1500-250-WG, 250 MHz repetition rate) filtered down to a 200 GHz optical bandwidth using band-pass filters and amplifiers (Santec and Lightwave 2020, Pritel SPFA). For Figure 4.10, the integrating photodiodes used (Thorlabs PDA50B, 2.1 kHz bandwidth, acquired with a National Instruments DAQ System PCI 6251 + BNC2090) are slow with respect to the signal repetition rate and act as a signal integrator. On the other hand, the fast photodiodes (Finisar XPDV, 50 GHz bandwidth) are connected to a high-bandwidth oscilloscope to reproduce the pulse train interference (Agilent DSO-X 92804A, 28 GHz bandwidth, 80 GSa/s).

In the reference signal preparation (Figure 4.4), the source is equally split into two different paths to introduce a frequency-shift with the AOM on one of them. In order to achieve the time multiplexing demonstration illustrated in Figure 4.11, before recombination, we add an optical delay line to implement a relative time difference between the pulses of I_x and I_y. The injection of this temporally-interleaved reference signal into the interferometer can then be adjusted with another delay line to enable time-multiplexing with the signal-under-test. The detector trigger signal is provided by the frequency comb pulse train. In post-processing, the different temporal channels (Figure 4.11) can then be easily separated to reconstruct the respective signals. The presented data are acquired for 120 s with an integration time of 100 ms (this corresponds to averaging over many sampling cycles).

4.4.2 Results

To visualize the interference of the bright pulsed reference, we use a fast photodiode to track the phase from pulse to pulse; alternatively, a slower photodiode can effectively integrate over the signal if simpler/cheaper electronics are required (Figure 4.10).

In the context of quantum optics, the use of such pulsed sources allows new functionalities for interferometric systems. In particular, when a pulsed laser is used within our scheme as a reference, its induced photon background becomes limited to distinct temporal modes that can be delayed

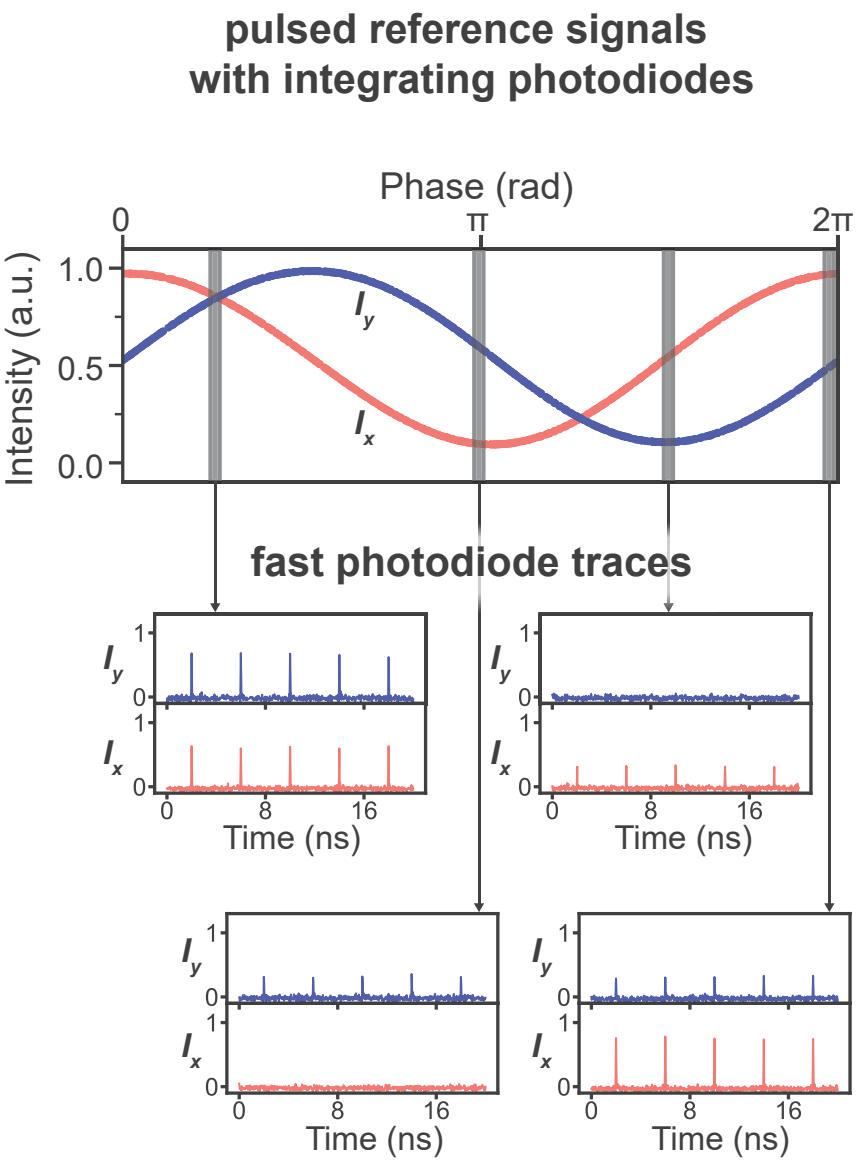

Figure 4.10: Interferometry with a pulsed optical reference in quadrature. Slow (2.1 kHz, top) and fast (50 GHz, bottom) photodiode traces of the interferometer output when a frequency comb laser is used in the scheme (Figure 4.4). Importantly, the interferometer arm difference is matched to the laser repetition rate (or its multiple). The signals I_x and I_y then maintain orthogonality and continue to allow unambiguous phase retrieval, while allowing to confine reference-induced background photon-counts to specific time windows.

with respect to the quantum input being interfered (i.e., the cross-talk between quantum signal and reference can now also be reduced even further by temporal filtering). This background can be then either suppressed via time-gating, or post-selected out in analysis.

Reducing resource requirements further, the pulsed reference can be attenuated to the few-photon level (alike to the approach in Section 4.3) and the in-phase and quadrature components of the feedback signal can be temporally-delayed with respect to one another (via a tunable fiber

imbalance on the AOM arm). Such an approach, which resembles temporally-interleaved quadrature sampling techniques from the field of digital signal processing [178, 179], allows us to retrieve the interferometer phase information using only one single-photon detector (Figure 4.11).

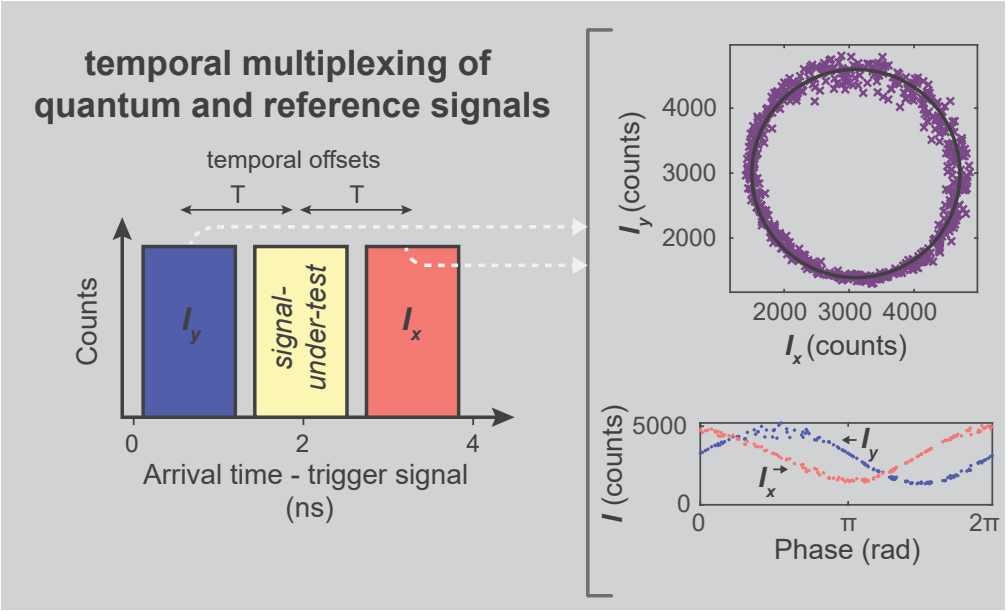

Figure 4.11: Use of an attenuated pulsed reference. The in-phase and quadrature signals can be offset by a time T (here with a delay line) with respect to processed quantum inputs to increase their signal-to-noise ratio. Here, we offset a signal-under-test with respect to the pulsed references, and feed it into a single, triggered photon-detector. We find that the reference maintains orthogonality, meaning a single detector can retrieve both a signal-under-test and its corresponding phase mapping.

While requiring less infrastructure as only one detector is used, the non-simultaneous measurement of the in-phase and quadrature signals will give rise to a phase-dependent error in the phase reconstruction, brought about by phase drifts between this sampling, on top of the aforementioned noise contributions arising from Poissonian photon statistics. Specifically, fast fluctuations in fiber length can impart different interferometric phases onto each of these sampled I_x and I_y components. To estimate the maximum error that could be introduced from such temporal interleaving, we assume a maximum phase drift rate of v that is changing linearly over the total reference time window. I_x and I_y are separated in time from the signal-under-test by +T and -T, respectively, with measured intensities $I_x(\phi + vT)$ and $I_y(\phi - vT)$. When comparing the phase estimated from these shifted reference signals and the interferometer phase at the signal-under-test (ϕ), a phase-dependent error arises (Figure 4.12). For small values of vT the maximum observed error is equal to vT – however, as this product increases the maximum error begins to scale non-linearly and the phase-dependent error plotted in Figure 4.12 becomes skewed. Note that such small errors are

negligible for most applications, e.g., the maximum phase drift vT is <10 mrad in a recent literature example [166].

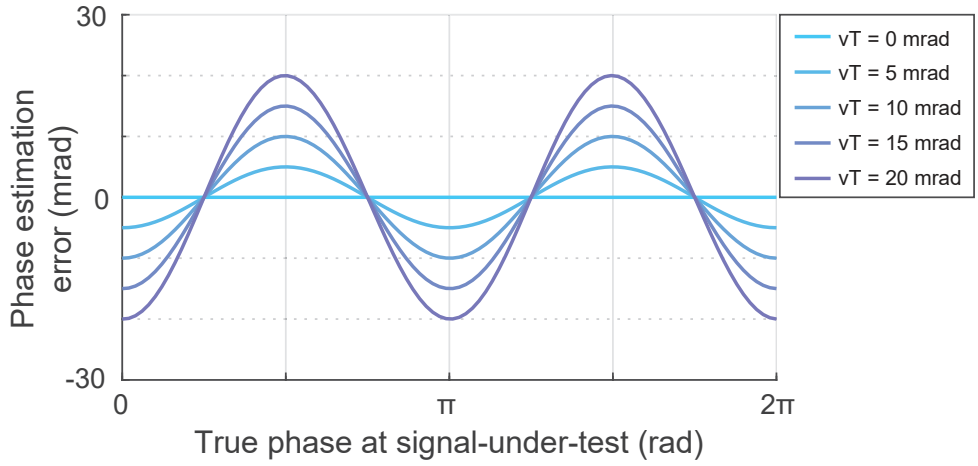

Figure 4.12: The error in the reconstructed phase induced when the in-phase and quadrature signals are measured at times +T and -T relative to the signal-under-test, respectively, and in the presence of a linear phase drift rate v.

These analyses can be generalized to any coherent states in quadrature used for phase reconstruction (i.e., also in degrees of freedom alternative to polarization). As coherent-state phase-retrieval techniques of this type have recently been introduced into the context of quantum communications [166], these considerations may be of use for extending such systems to realizations deployed out-of-lab (where faster phase drifts will have to be compensated).

4.5 Coherent control of hyper-entangled states

4.5.1 Technical Approach

As motivated in Section 4.1, we present a general approach to coherently manipulate discrete d-level multi-partite quantum systems based on the simultaneous entanglement of photons in time and frequency, by making use of fibre-optics telecommunications components [73, 55]. The states used here are generated in an integrated platform, produced using the nonlinear process of spontaneous four-wave mixing within a micro-ring resonator (the quantum frequency comb concept, see Section 2.1). The same micro-ring resonator is employed as in Section 3. By exciting the nonlinear resonator with three phase-locked pulses (from a carrier-envelope phase-stabilized mode-locked laser, Menlo Systems Inc.) and considering three frequency mode pairs in the emitted photons (see Figure 4.2

c), we generate states simultaneously entangled in time and frequency. These are described by the following expression:

$$\begin{aligned} |\Psi_H\rangle = & \quad (|1_s, 1_i\rangle + |2_s, 2_i\rangle + |3_s, 3_i\rangle) \otimes (|a_s, a_i\rangle + |b_s, b_i\rangle + |c_s, c_i\rangle) \\ = & \quad |1_s, 1_i, a_s, a_i\rangle + |1_s, 1_i, b_s, b_i\rangle + |1_s, 1_i, c_s, c_i\rangle \\ & + |2_s, 2_i, a_s, a_i\rangle + |2_s, 2_i, b_s, b_i\rangle + |2_s, 2_i, c_s, c_i\rangle \\ & + |3_s, 3_i, a_s, a_i\rangle + |3_s, 3_i, b_s, b_i\rangle + |3_s, 3_i, c_s, c_i\rangle, \end{aligned}$$

where numbers indicate the three time bins (1,2,3) and letters indicate the three frequency bins (a,b,c), with the indices s and i referring to the signal and idler photons, respectively (to keep the equation compact, the normalization is not shown here). This hyper-entangled state is bi-separable, since any projection measurement performed in, for example, the time-bin basis, does not affect the frequency-bin entangled sub-state and vice versa. As well, this corresponds to a four-partite (N=4), three-level (D=3) state with a large Hilbert space (D^N=81, corresponding to 6.34 qubits) in just two photons.

The coherent control of this particular state is accomplished in the context of its transformation into the first high-dimensional cluster state. For more details on this task, please consult Refs. [41, 180, 77], which describe the theoretical insights required to verify the success of the transformation. Here, we will focus solely on the candidate's contribution, which is the coherent control gate used to perform this transformation, an approach far from limited to the preparation of cluster states. In particular, to arbitrarily transform this hyper-entangled state into another state, experimental access to its individual terms is necessary while maintaining coherence. For multi-particle states, this is very challenging from the technical side, requiring two-party quantum gates, which are typically probabilistic [181].

However, making use of two different types of discrete energy–time entanglement (that is, time-bin and frequency-bin) associated with different timescales opens up the possibility of fully mapping the entangled state into the time domain to perform coherent state manipulations by using synchronized electro-optic modulation. Towards this end, our design makes use of frequency-to-time mapping (Figure 4.13) performed with a fiber Bragg grating array (where each grating reflects a specific optical frequency) placed in a self-referenced and phase-stable loop configuration. The array is comprised of six independent fiber Bragg gratings matched to the six photon wavelengths (1551.08,

1552.70, 1554.31, 1557.55, 1559.17 and 1560.80 nm), spatially separated in the fiber to achieve a 3.96 ns temporal delay between adjacent frequency modes (i.e., to introduce the frequency-to-time mapping).

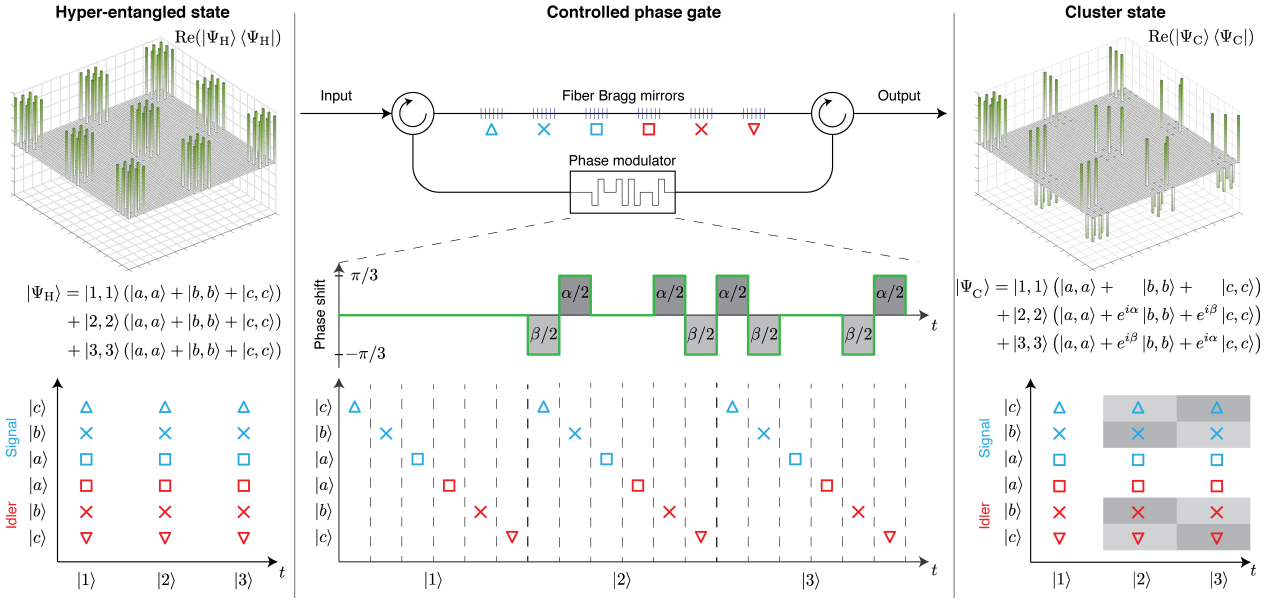

Figure 4.13: Coherent control of time-frequency hyper-entangled states. The two-photon d-level hyper-entangled state is simultaneously composed of three temporal modes $|1\rangle$, $|2\rangle$, and $|3\rangle$ and three frequency modes $|a\rangle$, $|b\rangle$ and $|c\rangle$ per signal and idler photon, given by the state wave function $|\Psi_H\rangle$ (the real part of the associated density matrix is depicted in the top left panel). The presented scheme gives access to the individual terms of the quantum state. This is realized by temporally dispersing the individual frequency modes into different time slots via a fiber Bragg grating array (i.e., by means of frequency-to-time mapping) such that each individual state term has its own time slot (see middle panel). An electro-optic modulator is used to change the phase of the individual state terms, here by $\alpha/2$ and $\beta/2$ (see middle panel). For the manipulation of the quantum state's amplitude coefficients, an intensity modulator could be installed in this loop as well. The photons then enter the fiber Bragg grating array from the opposite end, such that the frequency-to-time mapping is coherently reversed. In this example, by choosing the phases α=$2\pi/3$ and β=-$2\pi/3$, the hyper-entangled state is transformed into a d-level cluster state $|\Psi_C\rangle$, where the two gray shading tones indicate the two opposite phase changes (the real part of the associated density matrix is shown in the top right panel).

Following reflection on the custom fibre Bragg grating array, every part of the state is mapped to an individual temporal mode. Every amplitude and phase coefficient is thus experimentally accessible, as phase and amplitude modulation operations can be synchronized to the individual time bins, imparting changes onto the state coefficients. In our particular implementation, we only imparted phase modulation (using an electro-optic phase modulator (EOSpace), which was driven by an arbitrary waveform generator (Tektronix), synchronized to the 10 MHz reference clock of the mode-locked laser), but amplitude modulation is also possible simultaneously in this scheme.

Finally, the frequency-to-time mapping is reversed as the state is incident on the fiber Bragg grating array once more, from the other side. Any length shifts in the grating array fiber are thus automatically compensated without any active feedback required.

4.5.2 Results

For the realization of the scheme presented in the previous section, the full project's target was the transformation of the hyper-entangled state into a cluster state. State verification for such a complex state type is a field of physics onto itself, requiring the judicious design of so-called entanglement witnesses - these minimize the number of measurements needed to make the task of verification feasible. For our particular cluster state, the witness design and enactment is outside the scope of this thesis, in particular being the subject of a dedicated paper [180] and thesis [77]. To summarize, the witness detects the presence of a cluster state when its expectation value is negative (a minimum of -1 is reached by a theoretically optimal cluster state; that is, in the absence of imperfection or noise contributions). We measure a witness expectation value of $\langle W \rangle = -0.28 \pm 0.04$, confirming (within the range of 7 standard deviations) the presence of a cluster state exhibiting genuine three-level four-partite entanglement [41] and the corresponding success of the coherent control scheme outlined above.

5 | Characterizing Quantum Signals

Chapter Abstract:

The characterization of quantum signals is necessary at various stages of development and deployment of a quantum system. Many methods for quantum signal characterization already exist, including quantum state tomography, entanglement witnesses, and Bell tests. However, the development of new quantum photonics platforms opens up new characterization needs, as well as novel degrees of freedom that can be exploited towards such analyses. Here, we undertake quantum interference characterization of an entangled photon pair by making use of a radiofrequency-controlled setup (an atypical degree of freedom in quantum photonics). As well, we undertake the spectral characterization of a quantum frequency comb emitted from an on-chip source by making use of frequency- and time-gating methods realized using free-space and fiber-optics setups.

My contributions to this work include: the experimental realization of the quantum interference scheme, the experimental realization of the spectral characterization setups, and the analysis of the acquired data. The setups presented in this chapter were built using procured, off-the-shelf telecom and free-space components, with the exception of the integrated samples, obtained via collaboration with Profs. Brent Little (Chinese Academy of Science) and Sai T. Chu (City University of Hong Kong). The work resulted in two journal publications ([J.2] and [J.20], see Appendix B).

5.1 Motivation

The characterization of quantum signals is prerequisite to quality assessment and improvement processes for deployed technologies, to verification that desired signal processing steps are being enacted, and even to system design as the compatibility of components must be confirmed. Many characterization techniques for photonics exist and some of these, including correlation functions (see Section 2.4), are used for classical and quantum optics testing alike. Characterization techniques greatly differ in complexity, with some involving a great number of measurements to reconstruct all state details (e.g., state tomography [182, 183]), others reduce the measurement number but still return complex information regarding the state (e.g., state witnesses [77], state interference), while others target the measurement of a single metric and are simpler to acquire (e.g., photon generation rate).

Nevertheless, as new platforms in quantum photonics develop, so does the need for new characterization methods. These may make use of novel degrees of freedom opened up by such approaches or may, otherwise, be necessary to assess specific design features. Here, we undertake the demonstration of two such characterization techniques. First, while quantum interference measurements are usually accomplished by switching the projection measurements enacted onto the quantum states (e.g., rotating a polarizer, tuning the phase of an interferometer) in a mechanical or digital interface, we demonstrate a **quantum interference measurement enacted with an unusual control degree of freedom - the frequency of an RF signal**. The methodology related to this demonstration is explored in Section 5.2.1 and the results achieved with its use are outlined in Section 5.2.2. Second, the characterization of emission spectra from photon sources has gained increasing interest, especially as optical frequency has proven to be a robust encoding degree of freedom for fiber-based systems. While many advanced techniques for visualizing such spectra already exist [127, 128, 184, 185], we present work **making use of accessible fiber and free-space components towards resolving such spectra**, which alongside time-gating techniques can be used to thoroughly characterize signals. The methodology related to this work is explored in Section 5.3.1 and the results achieved with its use are outlined in Section 5.3.2.

5.2 Radiofrequency-controlled quantum interference

5.2.1 Technical Approach

Here, we demonstrate the radiofrequency-controlled quantum interference of high-dimensional time-bin entangled states, see setup in Figure 5.1. A stabilized frequency comb source (Menlo FC1500-250-WG, 250 MHz repetition rate) is used to excite a single resonance of a nonlinear microcavity to generate time-bin entangled photon pairs (via SFWM, see Section 2.1) described by the quantum state:

$$|1\rangle_s|1\rangle_i + e^{i\theta_{CEO}}|2\rangle_s|2\rangle_i + e^{i2\theta_{CEO}}|3\rangle_s|3\rangle_i$$

where $|k\rangle$ (k=1,2,3) denotes a time-bin quantum state and 's' and 'i' denote the signal and idler photon, respectively. Here, the pulse-to-pulse phase θ_{CEO} is described by $\frac{2\pi f_{CEO}}{f_{rep}}$ where f_{CEO} corresponds to the carrier-envelope offset frequency (see Section 2.2, sweepable via a radiofrequency input into the Menlo system), and f_{rep} corresponds to the pulse repetition rate (here, set constant to 250 MHz). Both the signal and idler interferometer phases are kept constant at 0 rad (relative to a CW-based reference signal), θ is then swept by changing the radiofrequency input over an accessible range of 10-115 MHz. After exiting the interferometers, the photons are routed to two independent single-photon detectors.

It is important to note that while previous quantum measurements using this interferometer stabilization scheme [73, 41] exploited a common optical reference across both state preparation and characterization stages, for this measurement we use independent optical sources for state preparation (a pulsed, commercial frequency comb source) and interferometer stabilization (a separate, i.e., out-of-loop, CW source with low frequency jitter). In particular, the frequency comb's parameters are stabilized with respect to atomically-referenced, tunable radiofrequencies (as part of a turn-key system). The laser sources used for state preparation and interferometer stabilization demonstrate a maximum relative frequency drift rate of ≈270 kHz/hour, corresponding to a $<0.01\pi$ rad/hour interferometer drift (which is negligible relative to the total two-hour integration time for each of our quantum interference measurements).

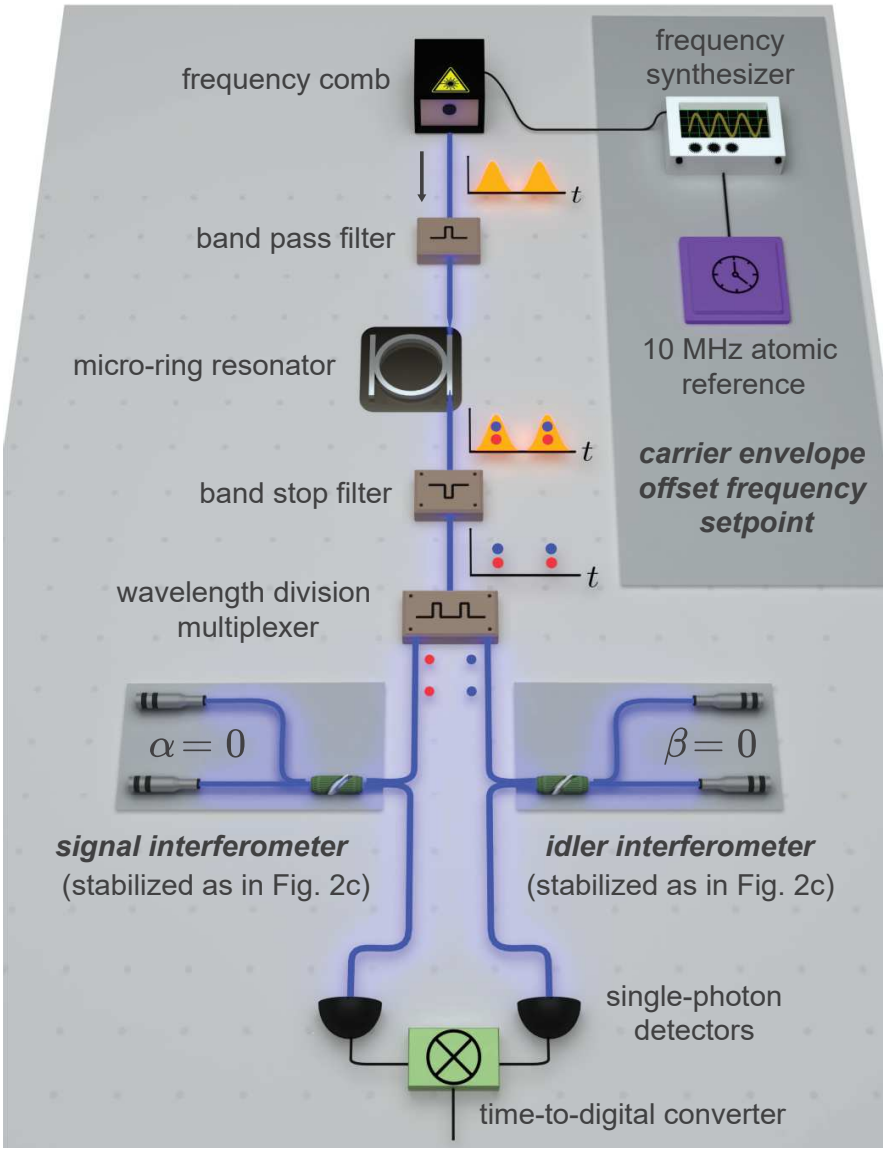

Figure 5.1: Setup for the radiofrequency-controlled quantum interference of high-dimensional time-bin entangled states. A frequency comb is used to excite a single resonance of an integrated microcavity to generate time-bin entangled photon pairs via spontaneous four-wave mixing [73]. The signal and idler are then split and interfere in fiber interferometers stabilized (using the scheme presented in Section 4.2) on a constant, zero phase. Projections on $|1\rangle + |2\rangle$ versus $|1\rangle + |3\rangle$ are made available by switching the interferometer arm fibers to access different length imbalances (4 ns and 8 ns respectively, corresponding to 1x and 2x the frequency comb pulse period). The frequency comb repetition rate and carrier-envelope offset frequencies are both stabilized with respect to a Rubidium reference clock. The continuous-wave laser used to stabilize the two interferometers is not referenced or locked to the frequency comb or atomic reference – the two sources are independent (i.e., out-of-loop).

5.2.2 Results

As mentioned above, when the mode-locked excitation is used as a pump to prepare a time-bin entangled state, the phase encoded in the qudits linearly corresponds to the pulse-to-pulse phase θ_{CEO} [73, 41, 186]; thus, radiofrequencies (particularly, the carrier-envelope offset (CEO) frequency

reference, which defines θ_{CEO} [102]) may be important degrees of freedom for, e.g., quantum optical metrology [187]. Using this comb source for the excitation of signal-idler photon pairs, together with the independent CW source to stabilize the interferometer phase at 0π (Figure 5.1), we show that the CEO radiofrequency is an accessible degree-of-freedom to demonstrate quantum interference (Figures 5.2 and 5.3).

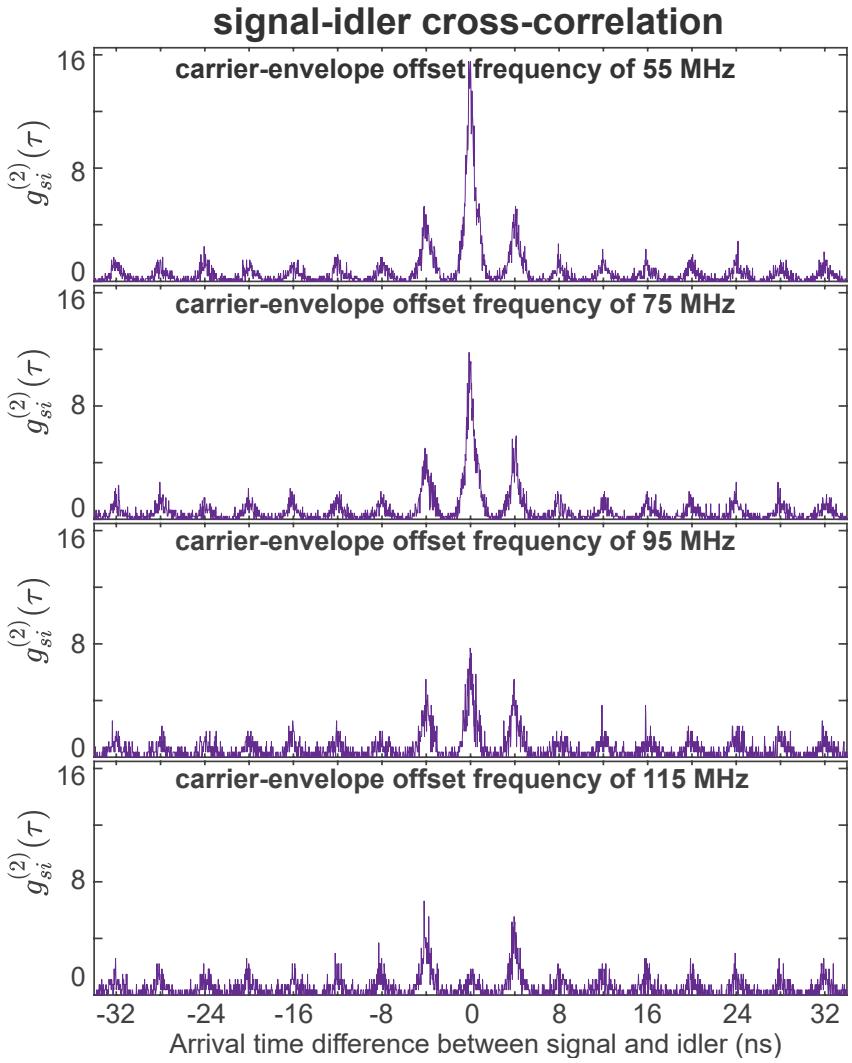

Figure 5.2: Quantum interference in the signal-idler coincidence events. The coincidences between the signal and idler channels are measured and correlated using single-photon detectors and time-to-digital conversion electronics. The carrier-envelope offset frequency setpoint (given by a radiofrequency tone) is swept in order to produce quantum interference, visible in the signal-idler cross-correlation.

Specifically, the quantum interference is computed by post-selecting the time-bin for the two channels that corresponds to the projection measurement, cross-correlating these counts to determine the second-order correlation function ($g^2_{si}(\tau)$, Figure 5.2), and then using Glauber and Gaus-

sian function fits (signal and background, respectively, see Section 2.4) to determine the normalized counts (Figure 5.3).

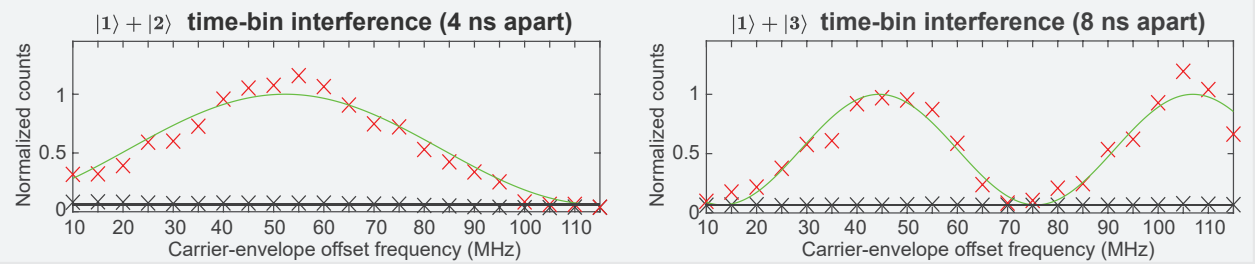

Figure 5.3: Quantum interference measurements for the time-bin encoded photon states, accomplished by sweeping the carrier-envelope offset frequency of the comb source. The raw visibilities for the interference between quantum time-bins one and two periods apart are, in this case, 88.4% and 87.3%, respectively (without any locking of the pump and reference lasers).

Note that the associated interference periodicity depends on whether the interferometer arm length corresponds to 1x or 2x the repetition rate, i.e., a delay of 4 ns or 8 ns in our case (Figure 5.3). The potential use of such low-power interference measurements for the stabilization and perhaps the direct extraction of mode-locked laser CEO frequencies bears further investigation. The successful demonstration of quantum interference using independent optical sources for the pump and interferometer reference (albeit with very high stability metrics) also suggests that constraints for such quantum system designs may be relaxed.

5.3 Single-photon spectra

5.3.1 Technical Approach

The characterization of single-photon signals today is greatly indebted to the classical applications that drove the development of mature and accessible fiber and free-space optics infrastructures. Two different setups are investigated for the characterization of the emitted spectral profile from an on-chip quantum frequency comb [73].

First, a tunable grating-based monochromator with an operating range from 1470 to 1620 nm is used in combination with a single photon detector. The raw single photon counts are measured as a function of the monochromator wavelength (which was in turn calibrated in the classical domain, using a broadband source and optical spectrum analyzer). The optical losses through this

setup, compensated for in our analysis, correspond to 7.3 dB (1.6 dB coupling, 1.5 dB polarization control, 4.2 dB monochromator). Temporal gating is enacted digitally following detection, using the repetition rate of the quantum frequency comb emission as a clock signal. This combination of temporal and spectral filtering also enhances the signal-to-noise ratio of the measurement [188].

Second, a higher-resolution digital tunable wavelength filter, limited to the telecommunications C-band (conventional band: 1530-1565 nm), is employed to similarly sweep across the spectrum (followed again by a single-photon detector). Using the digital wavelength filter, the optical losses are estimated at 7.3 dB (1.6 dB coupling, 5.7 dB digital filter).

The detection stage is comprised of an ID Quantique ID210 single photon detector at 5% quantum efficiency (corresponding to 13 dB detection loss), 10 μs dead time, 500 ps timing jitter, and 1.3 kHz dark count rates. The detector signals are acquired with a time-to-digital converter (PicoQuant HydraHarp 400) with 1 ps timing resolution.

5.3.2 Results

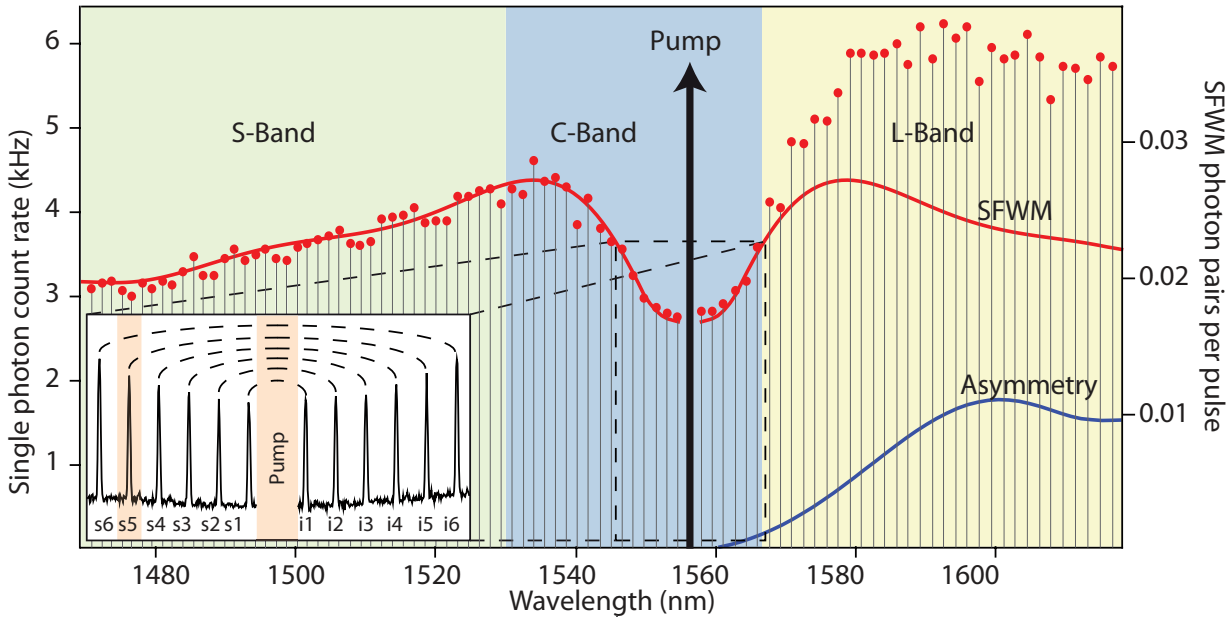

Figure 5.4: Measured single-photon spectrum for an integrated quantum frequency comb. Single-photon spectrum (red circles) emitted by the micro-ring resonator, measured using a grating-based spectrum analyzer and a high-resolution digital tunable filter in the C band (bottom inset). The S, C, and L telecommunications bands are indicated. The red curve shows the symmetric contribution generated through spontaneous four-wave mixing, whereas the blue curve shows the spectral asymmetry, which can be explained by Raman scattering (see Section 2.4).

The emission spectra reconstructed using the above-described methods can be seen in Figure 5.4. The quantum frequency comb produced in the measurement can be seen to span the S, C, and L telecommunications bands, providing quantum resources that can potentially be frequency-filtered to address multiple different users. Such a measurement is useful for determining the approximate spectral location of resonances, as necessary for the design of quantum signal processing steps that can follow such a source (e.g., filtering resonances for cross-correlation, interference, or tomography measurements).

6 | Conclusion and Perspectives

In response to the reported weakness of the quantum photonics supply chain [63], and the underdevelopment of standardized quantum system components compatible with mature infrastructures, the objectives of this thesis were the development of low-footprint quantum source architectures, low-loss quantum signal processing techniques, and fiber-compatible quantum signal characterization methods. The completion of these objectives was successful, with the main results and potential future work summarized below.

1. **Development of low-footprint quantum source architectures (Chapter 3):**
   In this objective, we targeted the development of a new class of portable sources, i.e., a hybrid system merging the pump laser and quantum source into one compact setup. Our findings illustrate a scalable concept that exploits the resonance pass-band characteristic of a micro-cavity to drive a bandwidth-matched (energy-efficient) and stable excitation of the micro-cavity and the associated SFWM photon generation process. When compared to external excitation schemes, this solution allows for a simple and versatile tuning of the repetition rate at which the QFC is emitted, either electronically by changing the RF modulation signal or by changing the external cavity length. Moreover, in this setup, higher pump repetition rates were shown to enable increased pair production rates while maintaining photon purity and CAR. Furthermore, as advances to the scheme will enable stable pulsing at higher harmonic mode-locking repetition rates, fewer external frequency modes will be excited within the resonance, leading to new prospects for fundamental studies in the transitory regime between pulsed and continuous-wave excitation (e.g., the scaling of photon-pair properties like purity and mode-locking dynamics as a function of fewer excited modes). Future extensions of the scheme, such as the inclusion of noise-suppression techniques [104, 105, 106, 107, 108], could potentially also

enable the pulse-to-pulse phase coherence required for the realization of a high repetition rate time-bin entangled quantum frequency comb source, as well as higher pump repetition rates for increased photon signal rates.

The source approach can be applied to a wide range of resonant structures besides third-order nonlinear micro-ring resonators, e.g., photonic crystal waveguides [140] and resonators [141], micro-disks [142], coupled resonator optical waveguides [143], and second-order nonlinear micro-cavities [144] (as long as an input-drop configuration is accessible). The bandwidth-matched excitation also gives access to higher-power pumping regimes, useful for, e.g., multi-photon state generation [73]. While we observed mode-locking when the amplitude modulator was replaced with a phase modulator, a higher sensitivity to the RF driving frequency and the occasional operational instability were observed. We thus used a more robust amplitude-modulated setup; however, the scheme can likely make use of phase modulators if coupled with active synchronization methods, e.g. regenerative feedback circuits [147].

Further, highly attractive research lines towards improving our solutions include: realizing a practical pulsed QFC scheme in a passive lasing setup (see Refs. [103] and [139] for potential routes); making use of pulse-shaping to further enhance quantum properties (e.g., by using atypical temporal profiles [189, 190]); and employing a two-port resonator where an input-drop configuration is inaccessible (e.g., by pursuing pulse-carving techniques [191]).

2. **Development of low-loss quantum signal processing techniques (Chapter 4):**
   In this objective, we targeted the development of fiber-based devices and setups for the processing of quantum signals. Firstly, we targeted the realization of a suite of tools for phase-retrieval in fiber-based interferometers. Secondly, we targeted the development of a scheme for the versatile, coherent control of quantum states hyper-entangled in frequency and time.

   The fiber interferometer scheme was found to be experimentally practical and to enable the unambiguous retrieval of phase in the fiber interferometer platform, without the need to dither or sweep the stabilizing laser frequency. Moreover, it enabled the demonstration of long-term stability and the ability to access all phase values. We also characterized the use of the scheme with dim and pulsed reference beams, presenting strategies towards reduced background photon counts, alongside an analysis of the operational considerations for the use of such references. In extensions of the scheme, we expect that single-photon-level, quadrature-encoded reference signals may also find appropriate use cases where it is mandatory to avoid

stimulated processes (e.g., high-power signals, complex photonic chips) or where minimal system disturbances are important (e.g., quantum ranging [131]).

The phase-retrieval method presented in this thesis is currently limited to unbalanced interferometer applications (as equal arm lengths cannot provide the required phase-offset in reference signal components, making other schemes [150] more suitable for balanced interferometer stabilization); it is not suited for use with reference lasers with unstable optical powers unless forced calibration steps or algorithmic upgrades are included (in contrast to, e.g., methods based on minimizing dither tones [161]); and it is best suited towards Michelson-like configurations, as extending our method to others, e.g., the Mach–Zehnder, would require supplementary polarization control.

Future work on this method will focus on further increasing stability and phase resolution through the use of higher bit-depth and faster electronics, performing out-of-loop stability measurements using additional optical sources and longer fiber (determining scheme appropriateness beyond coherent signal processing), extending the scope of the demonstrated scheme to interferometers with more arms (as required for, e.g., high-dimensional state manipulation without cascading two-arm interferometers) as well as to integrated interferometers [192, 193].

As another part of this objective, we targeted the coherent control of time-frequency hyperentangled states. Such states show great compatibility with fiber optics, make use of well-developed degrees of freedom, and have great scalability potential in terms of state dimensionality (i.e., many frequency and time bins can be employed to make large states). The design, based on a self-referenced fiber loop comprised of fiber Bragg gratings for frequency-to-time mapping and electro-optics for enacting temporal phase/amplitude masks, was successful in the realization of high-dimensional cluster states [41]. It is worth noting that while many of the motivations for using integrated sources come from reasons of compactness, the use of a chip-based resonator here enables new functionality - the GHz-range frequency spacings that here allow addressing individual frequency modes can only be accessed in such microscopic size scales. Moreover, the ability to use a self-referenced loop for the operation is extremely advantageous for reducing scheme complexity, with the only inputs being radiofrequency-based and the entire device being passive (besides optical losses) when no such inputs are provided[1].

[1] Note that if amplitude modulators were to be included in such a loop, drift in their voltage response may necessitate active feedback.

3. **Development of fiber-coupled quantum signal characterization techniques (Chapter 5):**
   In this objective, we targeted characterization techniques for quantum signals that make use of infrastructure or degrees of freedom compatible with fiber photonics. Towards this end, we demonstrated the radiofrequency-controlled quantum interference of high-dimensional time-bin entangled states prepared using an integrated source. While radiofrequencies have been used for quantum interference, e.g., in the processing of frequency-bin entangled photons using electro-optic phase modulators [55], the use of a radiofrequency in this manner is atypical for the field. We successfully demonstrated interference using projections in the $|1\rangle+|2\rangle$ and in the $|1\rangle+|3\rangle$ bases. As the extraction of pulsed laser carrier-envelope frequency is the foundation for its stabilization and the development of high-precision frequency combs, the use of quantum interference to determine and stabilize this frequency would be a highly attractive avenue of future research.

   Second, we made use of fiber-compatible setups for the characterization of few-photon level spectra. Towards this end, we used both grating-based monochromators built from mature free-space components (coupled to fiber), as well as telecommunications-based programmable spectral filters. With both setups, we were able to resolve the output from an integrated frequency comb and use the results to pinpoint the spectral location of its resonances. Since the introduction of this technique in our laboratory, it has become a routine step for building every new setup and verifying proper source operation. One of the main detriments of the technique in its current state, however, is the relatively low resolution accessible (10's GHz). Future work should target the use of optical and electronic signal processing, e.g., through the use of dispersive components and temporal gating, for achieving higher resolutions while maintaining ease-of-use and fiber compatibility.

Finally, it is also worth noting that **several of the developments presented here may hold relevance outside of quantum photonic systems**. For example, the source architecture presented may be of interest for compact and tightly-timed narrowband lasers (as required, e.g., for spectroscopy [194] and molecular excitation [195]). Accurate techniques for phase-retrieval may be relevant to fields such as sensing [196] and optical coherence tomography [118], with the ability to use few-photon signals potentially relevant for applications where high power lasers cannot be used (e.g., avoiding stimulated emission or the perturbation of samples under test).

Furthermore, the demonstrated techniques are particularly **well-suited towards the generation, processing, and characterization of high-dimensional and hyper-entangled time-frequency quantum states**. The key benefit of quantum photonics systems based on such approaches is the ability to scale the Hilbert space size by increasing dimensionality, while maintaining high state detection rates (which diminish with the number of photons used) and the ability to propagate the state within a single spatial mode, e.g., that of an optical fiber or waveguide [55, 41]. The Hilbert space size is associated both with the amount of data and the complexity of the data processing possible for a system. Thus, the ability of such approaches to store more information in a smaller number of photons addresses some of the key limitations of quantum photonic systems based on qubits. In the future, by using broad microcavity spectra with resonance spacings on the order of 10's of GHz, alongside the stabilization of pump pulse-to-pulse phases, we expect that the generation of time-frequency high-dimensional hyper-entangled states of massive scale may be achievable. For example, access to a similar bandwidth as shown in Figure 5.4, in combination with a denser resonance spacing (25 GHz, corresponding to D≈320 resonance pairs) excited by a train of (D≈320) coherent pulses, would already correspond to a four-partite Hilbert space (320^4) in excess of 10.5 billion - in just two photons.

In closing, our work has focused on several different aspects of quantum systems, spanning sources, signal processing, and characterization. While much further development remains for the realization of scalable and deployable quantum photonic technologies, the aforementioned objectives of this thesis were successfully completed and hopefully move this goal forward. We believe the work was particularly successful in **leveraging infrastructure from telecommunications and integrated photonics**. This is significant, as it allowed us to make use of robust supply chains and standardized off-the-shelf components, towards creating systems compatible with optical fiber networks (a similar leveraging of complementary infrastructures is behind the rise of integrated photonics [197]). The work presented here confirms that **such components can often be used easily, with minimal customization, towards advanced quantum photonics applications**.

References

[1] A. Einstein, B. Podolsky, and N. Rosen, "Can quantum-mechanical description of physical reality be considered complete?," Physical Review, vol. 47, pp. 777–780, may 1935.

[2] M. O. Scully and M. S. Zubairy, Quantum optics. Cambridge University Press, 1997.

[3] NobelPrize.org, "The Nobel Prize in Physics 1956," 1956.

[4] NobelPrize.org, "The Nobel Prize in Physics 1964," 1964.

[5] NobelPrize.org, "The Nobel Prize in Physiology or Medicine 2003," 2003.

[6] R. Damadian, "Tumor detection by nuclear magnetic resonance," Science, vol. 171, pp. 1151–1153, mar 1971.

[7] NobelPrize.org, "The Nobel Prize in Physics 1921," 1921.

[8] S. Wiesner, "Conjugate coding," ACM SIGACT News, vol. 15, pp. 78–88, jan 1983.

[9] C. H. Bennett and G. Brassard, "Quantum cryptography: Public key distribution and coin tossing," Theoretical Computer Science, vol. 560, pp. 7–11, dec 2014.

[10] F. Xu, X. Ma, Q. Zhang, H.-K. Lo, and J.-W. Pan, "Secure quantum key distribution with realistic devices," Reviews of Modern Physics, vol. 92, p. 025002, may 2020.

[11] P. Benioff, "The computer as a physical system: A microscopic quantum mechanical Hamiltonian model of computers as represented by Turing machines," Journal of Statistical Physics, vol. 22, pp. 563–591, may 1980.

[12] R. P. Feynman, "Simulating physics with computers," International Journal of Theoretical Physics, vol. 21, pp. 467–488, jun 1982.

[13] L. Gyongyosi and S. Imre, "A survey on quantum computing technology," Computer Science Review, vol. 31, pp. 51–71, feb 2019.

[14] C. L. Degen, F. Reinhard, and P. Cappellaro, "Quantum sensing," Reviews of Modern Physics, vol. 89, p. 035002, jul 2017.

[15] S. Pirandola, B. R. Bardhan, T. Gehring, C. Weedbrook, and S. Lloyd, "Advances in photonic quantum sensing," Nature Photonics, vol. 12, pp. 724–733, dec 2018.

[16] F. Arute, K. Arya, R. Babbush, D. Bacon, J. C. Bardin, R. Barends, R. Biswas, S. Boixo, F. G. S. L. Brandao, D. A. Buell, B. Burkett, Y. Chen, Z. Chen, B. Chiaro, R. Collins, W. Courtney, A. Dunsworth, E. Farhi, B. Foxen, A. Fowler, C. Gidney, M. Giustina, R. Graff, K. Guerin, S. Habegger, M. P. Harrigan, M. J. Hartmann, A. Ho, M. Hoffmann, T. Huang, T. S. Humble, S. V. Isakov, E. Jeffrey, Z. Jiang, D. Kafri, K. Kechedzhi, J. Kelly, P. V. Klimov, S. Knysh, A. Korotkov, F. Kostritsa, D. Landhuis, M. Lindmark, E. Lucero, D. Lyakh, S. Mandrà, J. R. McClean, M. McEwen, A. Megrant, X. Mi, K. Michielsen, M. Mohseni, J. Mutus, O. Naaman, M. Neeley, C. Neill, M. Y. Niu, E. Ostby, A. Petukhov, J. C. Platt, C. Quintana, E. G. Rieffel, P. Roushan, N. C. Rubin, D. Sank, K. J. Satzinger, V. Smelyanskiy, K. J. Sung, M. D. Trevithick, A. Vainsencher, B. Villalonga, T. White, Z. J. Yao, P. Yeh, A. Zalcman, H. Neven, and J. M. Martinis, "Quantum supremacy using a programmable superconducting processor," Nature, vol. 574, pp. 505–510, oct 2019.

[17] H.-S. Zhong, H. Wang, Y.-H. Deng, M.-C. Chen, L.-C. Peng, Y.-H. Luo, J. Qin, D. Wu, X. Ding, Y. Hu, P. Hu, X.-Y. Yang, W.-J. Zhang, H. Li, Y. Li, X. Jiang, L. Gan, G. Yang, L. You, Z. Wang, L. Li, N.-L. Liu, C.-Y. Lu, and J.-W. Pan, "Quantum computational advantage using photons," Science, vol. 370, pp. 1460–1463, dec 2020.

[18] Qureca Ltd., "Overview on quantum initiatives worldwide – update mid 2021," 2021.

[19] M. H. S. Amin, A. N. Omelyanchouk, and A. M. Zagoskin, "Mechanisms of spontaneous current generation in an inhomogeneous d -wave superconductor," Physical Review B, vol. 63, p. 212502, apr 2001.

[20] J. M. Arrazola, V. Bergholm, K. Brádler, T. R. Bromley, M. J. Collins, I. Dhand, A. Fumagalli, T. Gerrits, A. Goussev, L. G. Helt, J. Hundal, T. Isacsson, R. B. Israel, J. Izaac, S. Jahangiri, R. Janik, N. Killoran, S. P. Kumar, J. Lavoie, A. E. Lita, D. H. Mahler, M. Menotti, B. Morrison, S. W. Nam, L. Neuhaus, H. Y. Qi, N. Quesada, A. Repingon, K. K. Sabapathy, M. Schuld, D. Su, J. Swinarton, A. Száva, K. Tan, P. Tan, V. D. Vaidya, Z. Vernon, Z. Zabaneh, and Y. Zhang, "Quantum circuits with many photons on a programmable nanophotonic chip," Nature, vol. 591, pp. 54–60, mar 2021.

[21] S. Bartolucci, P. Birchall, H. Bombin, H. Cable, C. Dawson, M. Gimeno-Segovia, E. Johnston, K. Kieling, N. Nickerson, M. Pant, and Others, "Fusion-based quantum computation," arXiv preprint arXiv:2101.09310, jan 2021.

[22] M. Mirhosseini, A. Sipahigil, M. Kalaee, and O. Painter, "Superconducting qubit to optical photon transduction," Nature, vol. 588, pp. 599–603, dec 2020.

[23] Y. Cao, J. Romero, and A. Aspuru-Guzik, "Potential of quantum computing for drug discovery," IBM Journal of Research and Development, vol. 62, pp. 6:1–6:20, nov 2018.

[24] H. Yu, L. McCuller, M. Tse, N. Kijbunchoo, L. Barsotti, N. Mavalvala, J. Betzwieser, C. D. Blair, S. E. Dwyer, A. Effler, M. Evans, A. Fernandez-Galiana, P. Fritschel, V. V. Frolov, F. Matichard, D. E. McClelland, T. McRae, A. Mullavey, D. Sigg, B. J. J. Slagmolen, C. Whittle, A. Buikema, Y. Chen, T. R. Corbitt, R. Schnabel, R. Abbott, C. Adams, R. X. Adhikari, A. Ananyeva, S. Appert, K. Arai, J. S. Areeda, Y. Asali, S. M. Aston, C. Austin, A. M. Baer, M. Ball, S. W. Ballmer, S. Banagiri, D. Barker, J. Bartlett, B. K. Berger, D. Bhattacharjee, G. Billingsley, S. Biscans, R. M. Blair, N. Bode, P. Booker, R. Bork, A. Bramley, A. F. Brooks, D. D. Brown, C. Cahillane, K. C. Cannon, X. Chen, A. A. Ciobanu, F. Clara, S. J. Cooper, K. R. Corley, S. T. Countryman, P. B. Covas, D. C. Coyne, L. E. H. Datrier, D. Davis, C. Di

Fronzo, K. L. Dooley, J. C. Driggers, P. Dupej, T. Etzel, T. M. Evans, J. Feicht, P. Fulda, M. Fyffe, J. A. Giaime, K. D. Giardina, P. Godwin, E. Goetz, S. Gras, C. Gray, R. Gray, A. C. Green, A. Gupta, E. K. Gustafson, R. Gustafson, J. Hanks, J. Hanson, T. Hardwick, R. K. Hasskew, M. C. Heintze, A. F. Helmling-Cornell, N. A. Holland, J. D. Jones, S. Kandhasamy, S. Karki, M. Kasprzack, K. Kawabe, P. J. King, J. S. Kissel, R. Kumar, M. Landry, B. B. Lane, B. Lantz, M. Laxen, Y. K. Lecoeuche, J. Leviton, J. Liu, M. Lormand, A. P. Lundgren, R. Macas, M. MacInnis, D. M. Macleod, G. L. Mansell, S. Márka, Z. Márka, D. V. Martynov, K. Mason, T. J. Massinger, R. McCarthy, S. McCormick, J. McIver, G. Mendell, K. Merfeld, E. L. Merilh, F. Meylahn, T. Mistry, R. Mittleman, G. Moreno, C. M. Mow-Lowry, S. Mozzon, T. J. N. Nelson, P. Nguyen, L. K. Nuttall, J. Oberling, R. J. Oram, C. Osthelder, D. J. Ottaway, H. Overmier, J. R. Palamos, W. Parker, E. Payne, A. Pele, C. J. Perez, M. Pirello, H. Radkins, K. E. Ramirez, J. W. Richardson, K. Riles, N. A. Robertson, J. G. Rollins, C. L. Romel, J. H. Romie, M. P. Ross, K. Ryan, T. Sadecki, E. J. Sanchez, L. E. Sanchez, T. R. Saravanan, R. L. Savage, D. Schaetzl, R. M. S. Schofield, E. Schwartz, D. Sellers, T. Shaffer, J. R. Smith, S. Soni, B. Sorazu, A. P. Spencer, K. A. Strain, L. Sun, M. J. Szczepańczyk, M. Thomas, P. Thomas, K. A. Thorne, K. Toland, C. I. Torrie, G. Traylor, A. L. Urban, G. Vajente, G. Valdes, D. C. Vander-Hyde, P. J. Veitch, K. Venkateswara, G. Venugopalan, A. D. Viets, T. Vo, C. Vorvick, M. Wade, R. L. Ward, J. Warner, B. Weaver, R. Weiss, B. Willke, C. C. Wipf, L. Xiao, H. Yamamoto, H. Yu, L. Zhang, M. E. Zucker, and J. Zweizig, "Quantum correlations between light and the kilogram-mass mirrors of LIGO," Nature, vol. 583, pp. 43–47, jul 2020.

[25] NIST, "Post-Quantum Cryptography | CSRC," 2016.

[26] D. Kielpinski, C. Monroe, and D. J. Wineland, "Architecture for a large-scale ion-trap quantum computer," Nature, vol. 417, pp. 709–711, jun 2002.

[27] B. Hensen, H. Bernien, A. E. Dréau, A. Reiserer, N. Kalb, M. S. Blok, J. Ruitenberg, R. F. L. Vermeulen, R. N. Schouten, C. Abellán, W. Amaya, V. Pruneri, M. W. Mitchell, M. Markham, D. J. Twitchen, D. Elkouss, S. Wehner, T. H. Taminiau, and R. Hanson, "Loophole-free Bell inequality violation using electron spins separated by 1.3 kilometres," Nature, vol. 526, pp. 682–686, oct 2015.

[28] S. Pezzagna and J. Meijer, "Quantum computer based on color centers in diamond," Applied Physics Reviews, vol. 8, p. 011308, mar 2021.

[29] J. J. Pla, K. Y. Tan, J. P. Dehollain, W. H. Lim, J. J. L. Morton, F. A. Zwanenburg, D. N. Jamieson, A. S. Dzurak, and A. Morello, "High-fidelity readout and control of a nuclear spin qubit in silicon," Nature, vol. 496, pp. 334–338, apr 2013.

[30] A. Chatterjee, P. Stevenson, S. De Franceschi, A. Morello, N. P. de Leon, and F. Kuemmeth, "Semiconductor qubits in practice," Nature Reviews Physics, vol. 3, pp. 157–177, mar 2021.

[31] X. Ma, X. Yuan, Z. Cao, B. Qi, and Z. Zhang, "Quantum random number generation," npj Quantum Information, vol. 2, p. 16021, nov 2016.

[32] D. Drahi, N. Walk, M. J. Hoban, A. K. Fedorov, R. Shakhovoy, A. Feimov, Y. Kurochkin, W. S. Kolthammer, J. Nunn, J. Barrett, and I. A. Walmsley, "Certified quantum random numbers from untrusted light," Physical Review X, vol. 10, p. 041048, dec 2020.

[33] P. J. Bustard, D. Moffatt, R. Lausten, G. Wu, I. A. Walmsley, and B. J. Sussman, "Quantum random bit generation using stimulated Raman scattering," Optics Express, vol. 19, p. 25173, dec 2011.

[34] F. Appas, F. Baboux, M. I. Amanti, A. Lemaítre, F. Boitier, E. Diamanti, and S. Ducci, "Flexible entanglement-distribution network with an AlGaAs chip for secure communications," npj Quantum Information, vol. 7, p. 118, dec 2021.

[35] S. Lloyd, "Enhanced sensitivity of photodetection via quantum illumination," Science, vol. 321, pp. 1463–1465, sep 2008.

[36] E. Knill, R. Laflamme, and G. J. Milburn, "A scheme for efficient quantum computation with linear optics," Nature, vol. 409, pp. 46–52, jan 2001.

[37] R. Raussendorf and H. J. Briegel, "A one-way quantum computer," Physical Review Letters, vol. 86, pp. 5188–5191, may 2001.

[38] D. Bonneau, J. W. Silverstone, and M. G. Thompson, "Silicon quantum photonics," in Silicon Photonics III (L. Pavesi and D. J. Lockwood, eds.), vol. 122 of Topics in Applied Physics, pp. 41–82, Berlin, Heidelberg: Springer Berlin Heidelberg, 2016.

[39] D. Rauch, J. Handsteiner, A. Hochrainer, J. Gallicchio, A. S. Friedman, C. Leung, B. Liu, L. Bulla, S. Ecker, F. Steinlechner, R. Ursin, B. Hu, D. Leon, C. Benn, A. Ghedina, M. Cecconi, A. H. Guth, D. I. Kaiser, T. Scheidl, and A. Zeilinger, "Cosmic Bell test using random measurement settings from high-redshift quasars," Physical Review Letters, vol. 121, p. 080403, aug 2018.

[40] U. Madhow, Introduction to communication systems. Cambridge University Press, 2014.

[41] C. Reimer, S. Sciara, P. Roztocki, M. Islam, L. Romero Cortés, Y. Zhang, B. Fischer, S. Loranger, R. Kashyap, A. Cino, S. T. Chu, B. E. Little, D. J. Moss, L. Caspani, W. J. Munro, J. Azaña, M. Kues, and R. Morandotti, "High-dimensional one-way quantum processing implemented on d-level cluster states," Nature Physics, vol. 15, pp. 148–153, dec 2019.

[42] H. Takesue and K. Inoue, "1.5-μm band quantum-correlated photon pair generation in dispersion-shifted fiber: suppression of noise photons by cooling fiber," Optics Express, vol. 13, p. 7832, oct 2005.

[43] J. Claudon, J. Bleuse, N. S. Malik, M. Bazin, P. Jaffrennou, N. Gregersen, C. Sauvan, P. Lalanne, and J.-M. Gérard, "A highly efficient single-photon source based on a quantum dot in a photonic nanowire," Nature Photonics, vol. 4, pp. 174–177, mar 2010.

[44] R. Bedington, J. M. Arrazola, and A. Ling, "Progress in satellite quantum key distribution," npj Quantum Information, vol. 3, p. 30, dec 2017.

[45] L.-J. Wang, K.-H. Zou, W. Sun, Y. Mao, Y.-X. Zhu, H.-L. Yin, Q. Chen, Y. Zhao, F. Zhang, T.-Y. Chen, and J.-W. Pan, "Long-distance copropagation of quantum key distribution and terabit classical optical data channels," Physical Review A, vol. 95, p. 012301, jan 2017.

[46] W. Chen, Z.-F. Han, T. Zhang, H. Wen, Z.-Q. Yin, F.-X. Xu, Q.-L. Wu, Yun-Liu, Y. Zhang, X.-F. Mo, Y.-Z. Gui, G. Wei, and G.-C. Guo, "Field experimental "star type" metropolitan quantum key distribution network," IEEE Photonics Technology Letters, vol. 21, pp. 575–577, aug 2007.

[47] C. Cahall, K. L. Nicolich, N. T. Islam, G. P. Lafyatis, A. J. Miller, D. J. Gauthier, and J. Kim, "Multi-photon detection using a conventional superconducting nanowire single-photon detector," Optica, vol. 4, p. 1534, dec 2017.

[48] G. J. Mendoza, R. Santagati, J. Munns, E. Hemsley, M. Piekarek, E. Martín-López, G. D. Marshall, D. Bonneau, M. G. Thompson, and J. L. O'Brien, "Active temporal and spatial multiplexing of photons," Optica, vol. 3, p. 127, feb 2016.

[49] J. L. Park, "The concept of transition in quantum mechanics," Foundations of Physics, vol. 1, pp. 23–33, mar 1970.

[50] G. Ghirardi, "Entanglement, nonlocality, superluminal signaling and cloning," in Advances in Quantum Mechanics, InTech, apr 2013.

[51] W. K. Wootters and W. H. Zurek, "A single quantum cannot be cloned," Nature, vol. 299, pp. 802–803, oct 1982.

[52] D. Dieks, "Communication by EPR devices," Physics Letters A, vol. 92, pp. 271–272, nov 1982.

[53] E. Diamanti, H.-K. Lo, B. Qi, and Z. Yuan, "Practical challenges in quantum key distribution," npj Quantum Information, vol. 2, p. 16025, nov 2016.

[54] D. Collins, N. Gisin, N. Linden, S. Massar, and S. Popescu, "Bell inequalities for arbitrarily high-dimensional systems," Physical Review Letters, vol. 88, p. 040404, jan 2002.

[55] M. Kues, C. Reimer, P. Roztocki, L. R. Cortés, S. Sciara, B. Wetzel, Y. Zhang, A. Cino, S. T. Chu, B. E. Little, D. J. Moss, L. Caspani, J. Azaña, and R. Morandotti, "On-chip generation of high-dimensional entangled quantum states and their coherent control," Nature, vol. 546, pp. 622–626, jun 2017.

[56] J. T. Barreiro, N. K. Langford, N. A. Peters, and P. G. Kwiat, "Generation of hyperentangled photon pairs," Physical Review Letters, vol. 95, pp. 1–4, dec 2005.

[57] K. Azuma, K. Tamaki, and H.-K. Lo, "All-photonic quantum repeaters," Nature Communications, vol. 6, p. 6787, nov 2015.

[58] A. Kuhn, M. Hennrich, and G. Rempe, "Deterministic single-photon source for distributed quantum networking," Physical Review Letters, vol. 89, p. 067901, jul 2002.

[59] R. Uppu, F. T. Pedersen, Y. Wang, C. T. Olesen, C. Papon, X. Zhou, L. Midolo, S. Scholz, A. D. Wieck, A. Ludwig, and P. Lodahl, "Scalable integrated single-photon source," Science Advances, vol. 6, dec 2020.

[60] D. R. Hamel, L. K. Shalm, H. Hübel, A. J. Miller, F. Marsili, V. B. Verma, R. P. Mirin, S. W. Nam, K. J. Resch, and T. Jennewein, "Direct generation of three-photon polarization entanglement," Nature Photonics, vol. 8, pp. 801–807, oct 2014.

[61] E. Y. Zhu, Z. Tang, L. Qian, L. G. Helt, M. Liscidini, J. E. Sipe, C. Corbari, A. Canagasabey, M. Ibsen, and P. G. Kazansky, "Direct generation of polarization-entangled photon pairs in a poled fiber," Physical Review Letters, vol. 108, p. 213902, may 2012.

[62] A. Riazi, C. Chen, E. Y. Zhu, A. V. Gladyshev, P. G. Kazansky, J. E. Sipe, and L. Qian, "Biphoton shaping with cascaded entangled-photon sources," npj Quantum Information, vol. 5, p. 77, dec 2019.

[63] J. Broz and C. Merzbacher, "Quantum Economic Development Consortium (QED-C)," 2020.

[64] M. Lucamarini, Z. L. Yuan, J. F. Dynes, and A. J. Shields, "Overcoming the rate–distance limit of quantum key distribution without quantum repeaters," Nature, vol. 557, pp. 400–403, may 2018.

[65] E. Y. Zhu, C. Corbari, A. Gladyshev, P. G. Kazansky, H.-K. Lo, and L. Qian, "Toward a reconfigurable quantum network enabled by a broadband entangled source," Journal of the Optical Society of America B, vol. 36, pp. B1–B6, mar 2019.

[66] J. C. Chapman, T. M. Graham, C. K. Zeitler, H. J. Bernstein, and P. G. Kwiat, "Time-bin and polarization superdense teleportation for space applications," arXiv:1901.07181, pp. 1–33, jan 2019.

[67] R. Kaltenbaek, G. Hechenblaikner, N. Kiesel, O. Romero-Isart, K. C. Schwab, U. Johann, and M. Aspelmeyer, "Macroscopic quantum resonators (MAQRO): Testing quantum and gravitational physics with massive mechanical resonators," Experimental Astronomy, vol. 34, pp. 123–164, mar 2012.

[68] H. J. Briegel and R. Raussendorf, "Persistent entanglement in arrays of interacting particles," Physical Review Letters, vol. 86, pp. 910–913, jan 2001.

[69] C. Schaeff, R. Polster, R. Lapkiewicz, R. Fickler, S. Ramelow, and A. Zeilinger, "Scalable fiber integrated source for higher-dimensional path-entangled photonic quNits," Optics Express, vol. 20, p. 16145, jul 2012.

[70] J. Wang, S. Paesani, Y. Ding, R. Santagati, P. Skrzypczyk, A. Salavrakos, J. Tura, R. Augusiak, L. Mančinska, D. Bacco, D. Bonneau, J. W. Silverstone, Q. Gong, A. Acín, K. Rottwitt, L. K. Oxenløwe, J. L. O'Brien, A. Laing, and M. G. Thompson, "Multidimensional quantum entanglement with large-scale integrated optics," Science, vol. 360, pp. 285–291, apr 2018.

[71] R. T. Thew, A. Acin, H. Zbinden, and N. Gisin, "Experimental realization of entangled qutrits for quantum communication," Quantum Information and Computation, vol. 4, p. 093, feb 2004.

[72] M. Kues, C. Reimer, J. M. Lukens, W. J. Munro, A. M. Weiner, D. J. Moss, and R. Morandotti, "Quantum optical microcombs," Nature Photonics, vol. 13, pp. 170–179, mar 2019.

[73] C. Reimer, M. Kues, P. Roztocki, B. Wetzel, F. Grazioso, B. E. Little, S. T. Chu, T. Johnston, Y. Bromberg, L. Caspani, D. J. Moss, and R. Morandotti, "Generation of multiphoton entangled quantum states by means of integrated frequency combs," Science, vol. 351, pp. 1176–1180, mar 2016.

[74] P. Imany, J. A. Jaramillo-Villegas, O. D. Odele, K. Han, D. E. Leaird, J. M. Lukens, P. Lougovski, M. Qi, and A. M. Weiner, "50-GHz-spaced comb of high-dimensional frequency-bin entangled photons from an on-chip silicon nitride microresonator," Optics Express, vol. 26, p. 1825, jan 2018.

[75] P. Roztocki, S. Sciara, C. Reimer, L. Romero Cortes, Y. Zhang, B. Wetzel, M. Islam, B. Fischer, A. Cino, S. T. Chu, B. E. Little, D. J. Moss, L. Caspani, J. Azana, M. Kues, and R. Morandotti, "Complex quantum state generation and coherent control based on integrated frequency combs," Journal of Lightwave Technology, vol. 37, pp. 338–344, jan 2019.

[76] C. Reimer, Optical quantum state generation with integrated frequency comb sources. Doctorat en sciences de l'énergie et des matériaux, Université du Québec, 2017.

[77] S. Sciara, Investigation, realization, and entanglement characterization of complex optical quantum states. PhD thesis, University of Quebec, 2020.

[78] N. Picqué and T. W. Hänsch, "Frequency comb spectroscopy," Nature Photonics, vol. 13, pp. 146–157, mar 2019.

[79] NobelPrize.org, "The Nobel Prize in Physics 2005," 2005.

[80] P. Del'Haye, A. Schliesser, O. Arcizet, T. Wilken, R. Holzwarth, and T. J. Kippenberg, "Optical frequency comb generation from a monolithic microresonator," Nature, vol. 450, pp. 1214–1217, dec 2007.

[81] D. J. Moss, R. Morandotti, A. L. Gaeta, and M. Lipson, "New CMOS-compatible platforms based on silicon nitride and Hydex for nonlinear optics," Nature Photonics, vol. 7, pp. 597–607, jul 2013.

[82] M. Peccianti, A. Pasquazi, Y. Park, B. E. Little, S. T. Chu, D. J. Moss, and R. Morandotti, "Demonstration of a stable ultrafast laser based on a nonlinear microcavity," Nature communications, vol. 3, p. 765, jan 2012.

[83] K. Saha, Y. Okawachi, B. Shim, J. S. Levy, R. Salem, A. R. Johnson, M. A. Foster, M. R. E. Lamont, M. Lipson, and A. L. Gaeta, "Modelocking and femtosecond pulse generation in chip-based frequency combs," Optics Express, vol. 21, p. 1335, jan 2013.

[84] V. Brasch, M. Geiselmann, T. Herr, G. Lihachev, M. H. P. Pfeiffer, M. L. Gorodetsky, and T. J. Kippenberg, "Photonic chip-based optical frequency comb using soliton Cherenkov radiation," Science, vol. 351, pp. 357–360, jan 2016.

[85] A. L. Gaeta, M. Lipson, and T. J. Kippenberg, "Photonic-chip-based frequency combs," Nature Photonics, vol. 13, pp. 158–169, mar 2019.

[86] C. Reimer, L. Caspani, M. Clerici, M. Ferrera, M. Kues, M. Peccianti, A. Pasquazi, L. Razzari, B. E. Little, S. T. Chu, D. J. Moss, and R. Morandotti, "Integrated frequency comb source of heralded single photons," Optics Express, vol. 22, p. 6535, mar 2014.

[87] C. Reimer, M. Kues, L. Caspani, B. Wetzel, P. Roztocki, M. Clerici, Y. Jestin, M. Ferrera, M. Peccianti, A. Pasquazi, B. E. Little, S. T. Chu, D. J. Moss, and R. Morandotti, "Cross-polarized photon-pair generation and bi-chromatically pumped optical parametric oscillation on a chip," Nature Communications, vol. 6, p. 8236, dec 2015.

[88] R. W. Boyd, Nonlinear optics. Elsevier, 3 ed., 2008.

[89] E. Engin, D. Bonneau, C. M. Natarajan, A. S. Clark, M. G. Tanner, R. H. Hadfield, S. N. Dorenbos, V. Zwiller, K. Ohira, N. Suzuki, H. Yoshida, N. Iizuka, M. Ezaki, J. L. O'Brien, and M. G. Thompson, "Photon pair generation in a silicon micro-ring resonator with reverse bias enhancement," Optics Express, vol. 21, p. 27826, nov 2013.

[90] D. Grassani, S. Azzini, M. Liscidini, M. Galli, M. J. Strain, M. Sorel, J. E. Sipe, and D. Bajoni, "Micrometer-scale integrated silicon source of time-energy entangled photons," Optica, vol. 2, p. 88, feb 2015.

[91] Y. J. Lu, R. L. Campbell, and Z. Y. Ou, "Mode-locked two-photon states," Physical Review Letters, vol. 91, p. 163602, oct 2003.

[92] Z. Xie, T. Zhong, S. Shrestha, X. Xu, J. Liang, Y.-X. Gong, J. C. Bienfang, A. Restelli, J. H. Shapiro, F. N. C. Wong, and C. Wei Wong, "Harnessing high-dimensional hyperentanglement through a biphoton frequency comb," Nature Photonics, vol. 9, pp. 536–542, aug 2015.

[93] L. Olislager, J. Cussey, A. T. Nguyen, P. Emplit, S. Massar, J.-M. Merolla, and K. P. Huy, "Frequency-bin entangled photons," Physical Review A, vol. 82, p. 013804, jul 2010.

[94] N. Fabre, G. Maltese, F. Appas, S. Felicetti, A. Ketterer, A. Keller, T. Coudreau, F. Baboux, M. I. Amanti, S. Ducci, and P. Milman, "Generation of a time-frequency grid state with integrated biphoton frequency combs," Physical Review A, vol. 102, p. 012607, jul 2020.

[95] G. Maltese, M. I. Amanti, F. Appas, G. Sinnl, A. Lemaître, P. Milman, F. Baboux, and S. Ducci, "Generation and symmetry control of quantum frequency combs," npj Quantum Information, vol. 6, p. 13, dec 2020.

[96] T. Carmon, L. Yang, and K. J. Vahala, "Dynamical thermal behavior and thermal self-stability of microcavities," Optics Express, vol. 12, p. 4742, oct 2004.

[97] A. Pasquazi, M. Peccianti, L. Razzari, D. J. Moss, S. Coen, M. Erkintalo, Y. K. Chembo, T. Hansson, S. Wabnitz, P. Del'Haye, X. Xue, A. M. Weiner, and R. Morandotti, "Micro-combs: a novel generation of optical sources," Physics Reports, vol. 729, pp. 1–81, jan 2018.

[98] M. Karpiński, M. Jachura, L. J. Wright, and B. J. Smith, "Bandwidth manipulation of quantum light by an electro-optic time lens," Nature Photonics, vol. 11, pp. 53–57, jan 2017.

[99] K. A. G. Fisher, D. G. England, J.-P. W. MacLean, P. J. Bustard, K. J. Resch, and B. J. Sussman, "Frequency and bandwidth conversion of single photons in a room-temperature diamond quantum memory," Nature Communications, vol. 7, p. 11200, sep 2016.

[100] F. Mazeas, M. Traetta, M. Bentivegna, F. Kaiser, D. Aktas, W. Zhang, C. A. Ramos, L. A. Ngah, T. Lunghi, É. Picholle, N. Belabas-Plougonven, X. Le Roux, É. Cassan, D. Marris-Morini, L. Vivien, G. Sauder, L. Labonté, and S. Tanzilli, "High-quality photonic entanglement for wavelength-multiplexed quantum communication based on a silicon chip," Optics Express, vol. 24, p. 28731, dec 2016.

[101] D. Rieländer, A. Lenhard, O. Jime'nez Farìas, A. Máttar, D. Cavalcanti, M. Mazzera, A. Acín, and H. de Riedmatten, "Frequency-bin entanglement of ultra-narrow band non-degenerate photon pairs," Quantum Science and Technology, vol. 3, p. 014007, jan 2018.

[102] A. M. Weiner, Ultrafast Optics. Hoboken, NJ, USA: John Wiley & Sons, Inc., jun 2009.

[103] P. Roztocki, M. Kues, C. Reimer, B. E. Little, S. T. Chu, D. J. Moss, and R. Morandotti, "Four-wave mixing photon pair generation statistics for a nonlinear microcavity with chaotic and pulsed excitation," in 2017 Conference on Lasers and Electro-Optics (CLEO), (San Jose, CA, USA), IEEE, 2017.

[104] X. Shan, D. Cleland, and A. Ellis, "Stabilising Er fibre soliton laser with pulse phase locking," Electronics Letters, vol. 28, p. 182, jan 1992.

[105] X. Shan and D. Spirit, "Novel method to suppress noise in harmonically modelocked erbium fibre lasers," Electronics Letters, vol. 29, pp. 979–981, may 1993.

[106] E. R. Thoen, M. E. Grein, E. M. Koontz, E. P. Ippen, H. A. Haus, and L. A. Kolodziejski, "Stabilization of an active harmonically mode-locked fiber laser using two-photon absorption," Optics Letters, vol. 25, p. 948, jul 2000.

[107] G. T. Harvey and L. F. Mollenauer, "Harmonically mode-locked fiber ring laser with an internal Fabry–Perot stabilizer for soliton transmission," Optics Letters, vol. 18, p. 107, jan 1993.

[108] S. Gee, F. Quinlan, S. Ozharar, and P. Delfyett, "Simultaneous optical comb frequency stabilization and super-mode noise suppression of harmonically mode-locked semiconductor ring laser using an intracavity etalon," IEEE Photonics Technology Letters, vol. 17, pp. 199–201, jan 2005.

[109] T. Fortier and E. Baumann, "20 years of developments in optical frequency comb technology and applications," Communications Physics, vol. 2, p. 153, dec 2019.

[110] T. T. Tran, A study on flat/Gaussian optical frequency comb generation. Ph.d. degree in electronics engineering, Myongji University, 2019.

[111] T. Ideguchi, "Dual-comb spectroscopy," Optics and Photonics News, vol. 28, p. 32, jan 2017.

[112] A. Regensburger, C. Bersch, M.-A. Miri, G. Onishchukov, D. N. Christodoulides, and U. Peschel, "Parity–time synthetic photonic lattices," Nature, vol. 488, pp. 167–171, aug 2012.

[113] B. P. Abbott, R. Abbott, T. D. Abbott, M. R. Abernathy, F. Acernese, K. Ackley, C. Adams, T. Adams, P. Addesso, R. X. Adhikari, V. B. Adya, C. Affeldt, M. Agathos, K. Agatsuma, N. Aggarwal, O. D. Aguiar, L. Aiello, A. Ain, P. Ajith, B. Allen, A. Allocca, P. A. Altin, S. B. Anderson, W. G. Anderson, K. Arai, M. A. Arain, M. C. Araya, C. C. Arceneaux, J. S. Areeda, N. Arnaud, K. G. Arun, S. Ascenzi, G. Ashton, M. Ast, S. M. Aston, P. Astone, P. Aufmuth, C. Aulbert, S. Babak, P. Bacon, M. K. Bader, P. T. Baker, F. Baldaccini, G. Ballardin, S. W. Ballmer, J. C. Barayoga, S. E. Barclay, B. C. Barish, D. Barker, F. Barone, B. Barr, L. Barsotti, M. Barsuglia, D. Barta, J. Bartlett, M. A. Barton, I. Bartos, R. Bassiri, A. Basti, J. C. Batch, C. Baune, V. Bavigadda, M. Bazzan, B. Behnke, M. Bejger, C. Belczynski, A. S. Bell, C. J. Bell, B. K. Berger, J. Bergman, G. Bergmann, C. P. Berry, D. Bersanetti, A. Bertolini, J. Betzwieser, S. Bhagwat, R. Bhandare, I. A. Bilenko, G. Billingsley, J. Birch, R. Birney, O. Birnholtz, S. Biscans, A. Bisht, M. Bitossi, C. Biwer, M. A. Bizouard, J. K. Blackburn, C. D. Blair, D. G. Blair, R. M. Blair, S. Bloemen, O. Bock, T. P. Bodiya, M. Boer, G. Bogaert, C. Bogan, A. Bohe, P. Bojtos, C. Bond, F. Bondu, R. Bonnand, B. A. Boom, R. Bork, V. Boschi, S. Bose, Y. Bouffanais, A. Bozzi, C. Bradaschia, P. R. Brady, V. B. Braginsky, M. Branchesi, J. E. Brau, T. Briant, A. Brillet, M. Brinkmann, V. Brisson, P. Brockill, A. F. Brooks, D. A. Brown, D. D. Brown, N. M. Brown, C. C. Buchanan, A. Buikema, T. Bulik, H. J. Bulten, A. Buonanno, D. Buskulic, C. Buy, R. L. Byer, M. Cabero, L. Cadonati, G. Cagnoli, C. Cahillane, J. C. Bustillo, T. Callister, E. Calloni, J. B. Camp, K. C. Cannon, J. Cao, C. D. Capano, E. Capocasa, F. Carbognani, S. Caride, J. C. Diaz, C. Casentini,

S. Caudill, M. Cavaglià, F. Cavalier, R. Cavalieri, G. Cella, C. B. Cepeda, L. C. Baiardi, G. Cerretani, E. Cesarini, R. Chakraborty, T. Chalermsongsak, S. J. Chamberlin, M. Chan, S. Chao, P. Charlton, E. Chassande-Mottin, H. Y. Chen, Y. Chen, C. Cheng, A. Chincarini, A. Chiummo, H. S. Cho, M. Cho, J. H. Chow, N. Christensen, Q. Chu, S. Chua, S. Chung, G. Ciani, F. Clara, J. A. Clark, F. Cleva, E. Coccia, P. F. Cohadon, A. Colla, C. G. Collette, L. Cominsky, M. Constancio, A. Conte, L. Conti, D. Cook, T. R. Corbitt, N. Cornish, A. Corsi, S. Cortese, C. A. Costa, M. W. Coughlin, S. B. Coughlin, J. P. Coulon, S. T. Countryman, P. Couvares, E. E. Cowan, D. M. Coward, M. J. Cowart, D. C. Coyne, R. Coyne, K. Craig, J. D. Creighton, T. D. Creighton, J. Cripe, S. G. Crowder, A. M. Cruise, A. Cumming, L. Cunningham, E. Cuoco, T. D. Canton, S. L. Danilishin, S. D'Antonio, K. Danzmann, N. S. Darman, C. F. Da Silva Costa, V. Dattilo, I. Dave, H. P. Daveloza, M. Davier, G. S. Davies, E. J. Daw, R. Day, S. De, D. Debra, G. Debreczeni, J. Degallaix, M. De Laurentis, S. Deléglise, W. Del Pozzo, T. Denker, T. Dent, H. Dereli, V. Dergachev, R. T. Derosa, R. De Rosa, R. Desalvo, S. Dhurandhar, M. C. Díaz, L. Di Fiore, M. Di Giovanni, A. Di Lieto, S. Di Pace, I. Di Palma, A. Di Virgilio, G. Dojcinoski, V. Dolique, F. Donovan, K. L. Dooley, S. Doravari, R. Douglas, T. P. Downes, M. Drago, R. W. Drever, J. C. Driggers, Z. Du, M. Ducrot, S. E. Dwyer, T. B. Edo, M. C. Edwards, A. Effler, H. B. Eggenstein, P. Ehrens, J. Eichholz, S. S. Eikenberry, W. Engels, R. C. Essick, T. Etzel, M. Evans, T. M. Evans, R. Everett, M. Factourovich, V. Fafone, H. Fair, S. Fairhurst, X. Fan, Q. Fang, S. Farinon, B. Farr, W. M. Farr, M. Favata, M. Fays, H. Fehrmann, M. M. Fejer, D. Feldbaum, I. Ferrante, E. C. Ferreira, F. Ferrini, F. Fidecaro, L. S. Finn, I. Fiori, D. Fiorucci, R. P. Fisher, R. Flaminio, M. Fletcher, H. Fong, J. D. Fournier, S. Franco, S. Frasca, F. Frasconi, M. Frede, Z. Frei, A. Freise, R. Frey, V. Frey, T. T. Fricke, P. Fritschel, V. V. Frolov, P. Fulda, M. Fyffe, H. A. Gabbard, J. R. Gair, L. Gammaitoni, S. G. Gaonkar, F. Garufi, A. Gatto, G. Gaur, N. Gehrels, G. Gemme, B. Gendre, E. Genin, A. Gennai, J. George, L. Gergely, V. Germain, A. Ghosh, A. Ghosh, S. Ghosh, J. A. Giaime, K. D. Giardina, A. Giazotto, K. Gill, A. Glaefke, J. R. Gleason, E. Goetz, R. Goetz, L. Gondan, G. González, J. M. Castro, A. Gopakumar, N. A. Gordon, M. L. Gorodetsky, S. E. Gossan, M. Gosselin, R. Gouaty, C. Graef, P. B. Graff, M. Granata, A. Grant, S. Gras, C. Gray, G. Greco, A. C. Green, R. J. Greenhalgh, P. Groot, H. Grote, S. Grunewald, G. M. Guidi, X. Guo, A. Gupta, M. K. Gupta, K. E. Gushwa, E. K. Gustafson, R. Gustafson, J. J. Hacker, B. R. Hall, E. D. Hall, G. Hammond, M. Haney, M. M. Hanke, J. Hanks, C. Hanna, M. D. Hannam, J. Hanson, T. Hardwick, J. Harms, G. M. Harry, I. W. Harry, M. J. Hart, M. T. Hartman, C. J. Haster, K. Haughian, J. Healy, J. Heefner, A. Heidmann, M. C. Heintze, G. Heinzel, H. Heitmann, P. Hello, G. Hemming, M. Hendry, I. S. Heng, J. Hennig, A. W. Heptonstall, M. Heurs, S. Hild, D. Hoak, K. A. Hodge, D. Hofman, S. E. Hollitt, K. Holt, D. E. Holz, P. Hopkins, D. J. Hosken, J. Hough, E. A. Houston, E. J. Howell, Y. M. Hu, S. Huang, E. A. Huerta, D. Huet, B. Hughey, S. Husa, S. H. Huttner, T. Huynh-Dinh, A. Idrisy, N. Indik, D. R. Ingram, R. Inta, H. N. Isa, J. M. Isac, M. Isi, G. Islas, T. Isogai, B. R. Iyer, K. Izumi, M. B. Jacobson, T. Jacqmin, H. Jang, K. Jani, P. Jaranowski, S. Jawahar, F. Jiménez-Forteza, W. W. Johnson, N. K. Johnson-Mcdaniel, D. I. Jones, R. Jones, R. J. Jonker, L. Ju, K. Haris, C. V. Kalaghatgi, V. Kalogera, S. Kandhasamy, G. Kang, J. B. Kanner, S. Karki, M. Kasprzack, E. Katsavounidis, W. Katzman, S. Kaufer, T. Kaur, K. Kawabe, F. Kawazoe, F. Kéfélian, M. S. Kehl, D. Keitel, D. B. Kelley, W. Kells, R. Kennedy, D. G. Keppel, J. S. Key, A. Khalaidovski, F. Y. Khalili, I. Khan, S. Khan, Z. Khan, E. A. Khazanov, N. Kijbunchoo, C. Kim, J. Kim, K. Kim, N. G. Kim, N. Kim, Y. M. Kim, E. J. King, P. J. King, D. L. Kinzel, J. S. Kissel, L. Kleybolte, S. Klimenko, S. M. Koehlenbeck, K. Kokeyama, S. Koley, V. Kondrashov, A. Kontos, S. Koranda, M. Korobko, W. Z. Korth, I. Kowalska, D. B. Kozak, V. Kringel, B. Krishnan, A. Królak, C. Krueger, G. Kuehn, P. Kumar, R. Ku-

mar, L. Kuo, A. Kutynia, P. Kwee, B. D. Lackey, M. Landry, J. Lange, B. Lantz, P. D. Lasky, A. Lazzarini, C. Lazzaro, P. Leaci, S. Leavey, E. O. Lebigot, C. H. Lee, H. K. Lee, H. M. Lee, K. Lee, A. Lenon, M. Leonardi, J. R. Leong, N. Leroy, N. Letendre, Y. Levin, B. M. Levine, T. G. Li, A. Libson, T. B. Littenberg, N. A. Lockerbie, J. Logue, A. L. Lombardi, L. T. London, J. E. Lord, M. Lorenzini, V. Loriette, M. Lormand, G. Losurdo, J. D. Lough, C. O. Lousto, G. Lovelace, H. Lück, A. P. Lundgren, J. Luo, R. Lynch, Y. Ma, T. Macdonald, B. Machenschalk, M. Macinnis, D. M. Macleod, F. Magaña-Sandoval, R. M. Magee, M. Mageswaran, E. Majorana, I. Maksimovic, V. Malvezzi, N. Man, I. Mandel, V. Mandic, V. Mangano, G. L. Mansell, M. Manske, M. Mantovani, F. Marchesoni, F. Marion, S. Márka, Z. Márka, A. S. Markosyan, E. Maros, F. Martelli, L. Martellini, I. W. Martin, R. M. Martin, D. V. Martynov, J. N. Marx, K. Mason, A. Masserot, T. J. Massinger, M. Masso-Reid, F. Matichard, L. Matone, N. Mavalvala, N. Mazumder, G. Mazzolo, R. McCarthy, D. E. McClelland, S. McCormick, S. C. McGuire, G. McIntyre, J. McIver, D. J. McManus, S. T. McWilliams, D. Meacher, G. D. Meadors, J. Meidam, A. Melatos, G. Mendell, D. Mendoza-Gandara, R. A. Mercer, E. Merilh, M. Merzougui, S. Meshkov, C. Messenger, C. Messick, P. M. Meyers, F. Mezzani, H. Miao, C. Michel, H. Middleton, E. E. Mikhailov, L. Milano, J. Miller, M. Millhouse, Y. Minenkov, J. Ming, S. Mirshekari, C. Mishra, S. Mitra, V. P. Mitrofanov, G. Mitselmakher, R. Mittleman, A. Moggi, M. Mohan, S. R. Mohapatra, M. Montani, B. C. Moore, C. J. Moore, D. Moraru, G. Moreno, S. R. Morriss, K. Mossavi, B. Mours, C. M. Mow-Lowry, C. L. Mueller, G. Mueller, A. W. Muir, A. Mukherjee, D. Mukherjee, S. Mukherjee, N. Mukund, A. Mullavey, J. Munch, D. J. Murphy, P. G. Murray, A. Mytidis, I. Nardecchia, L. Naticchioni, R. K. Nayak, V. Necula, K. Nedkova, G. Nelemans, M. Neri, A. Neunzert, G. Newton, T. T. Nguyen, A. B. Nielsen, S. Nissanke, A. Nitz, F. Nocera, D. Nolting, M. E. Normandin, L. K. Nuttall, J. Oberling, E. Ochsner, J. O'Dell, E. Oelker, G. H. Ogin, J. J. Oh, S. H. Oh, F. Ohme, M. Oliver, P. Oppermann, R. J. Oram, B. O'Reilly, R. O'Shaughnessy, C. D. Ott, D. J. Ottaway, R. S. Ottens, H. Overmier, B. J. Owen, A. Pai, S. A. Pai, J. R. Palamos, O. Palashov, C. Palomba, A. Pal-Singh, H. Pan, Y. Pan, C. Pankow, F. Pannarale, B. C. Pant, F. Paoletti, A. Paoli, M. A. Papa, H. R. Paris, W. Parker, D. Pascucci, A. Pasqualetti, R. Passaquieti, D. Passuello, B. Patricelli, Z. Patrick, B. L. Pearlstone, M. Pedraza, R. Pedurand, L. Pekowsky, A. Pele, S. Penn, A. Perreca, H. P. Pfeiffer, M. Phelps, O. Piccinni, M. Pichot, M. Pickenpack, F. Piergiovanni, V. Pierro, G. Pillant, L. Pinard, I. M. Pinto, M. Pitkin, J. H. Poeld, R. Poggiani, P. Popolizio, A. Post, J. Powell, J. Prasad, V. Predoi, S. S. Premachandra, T. Prestegard, L. R. Price, M. Prijatelj, M. Principe, S. Privitera, R. Prix, G. A. Prodi, L. Prokhorov, O. Puncken, M. Punturo, P. Puppo, M. Pürrer, H. Qi, J. Qin, V. Quetschke, E. A. Quintero, R. Quitzow-James, F. J. Raab, D. S. Rabeling, H. Radkins, P. Raffai, S. Raja, M. Rakhmanov, C. R. Ramet, P. Rapagnani, V. Raymond, M. Razzano, V. Re, J. Read, C. M. Reed, T. Regimbau, L. Rei, S. Reid, D. H. Reitze, H. Rew, S. D. Reyes, F. Ricci, K. Riles, N. A. Robertson, R. Robie, F. Robinet, A. Rocchi, L. Rolland, J. G. Rollins, V. J. Roma, J. D. Romano, R. Romano, G. Romanov, J. H. Romie, D. Rosińska, S. Rowan, A. Rüdiger, P. Ruggi, K. Ryan, S. Sachdev, T. Sadecki, L. Sadeghian, L. Salconi, M. Saleem, F. Salemi, A. Samajdar, L. Sammut, L. M. Sampson, E. J. Sanchez, V. Sandberg, B. Sandeen, G. H. Sanders, J. R. Sanders, B. Sassolas, B. S. Sathyaprakash, P. R. Saulson, O. Sauter, R. L. Savage, A. Sawadsky, P. Schale, R. Schilling, J. Schmidt, P. Schmidt, R. Schnabel, R. M. Schofield, A. Schönbeck, E. Schreiber, D. Schuette, B. F. Schutz, J. Scott, S. M. Scott, D. Sellers, A. S. Sengupta, D. Sentenac, V. Sequino, A. Sergeev, G. Serna, Y. Setyawati, A. Sevigny, D. A. Shaddock, T. Shaffer, S. Shah, M. S. Shahriar, M. Shaltev, Z. Shao, B. Shapiro, P. Shawhan, A. Sheperd, D. H. Shoemaker, D. M. Shoemaker, K. Siellez, X. Siemens, D. Sigg, A. D. Silva, D. Simakov, A. Singer, L. P. Singer, A. Singh, R. Singh,

A. Singhal, A. M. Sintes, B. J. Slagmolen, J. R. Smith, M. R. Smith, N. D. Smith, R. J. Smith, E. J. Son, B. Sorazu, F. Sorrentino, T. Souradeep, A. K. Srivastava, A. Staley, M. Steinke, J. Steinlechner, S. Steinlechner, D. Steinmeyer, B. C. Stephens, S. P. Stevenson, R. Stone, K. A. Strain, N. Straniero, G. Stratta, N. A. Strauss, S. Strigin, R. Sturani, A. L. Stuver, T. Z. Summerscales, L. Sun, P. J. Sutton, B. L. Swinkels, M. J. Szczepańczyk, M. Tacca, D. Talukder, D. B. Tanner, M. Tápai, S. P. Tarabrin, A. Taracchini, R. Taylor, T. Theeg, M. P. Thirugnanasambandam, E. G. Thomas, M. Thomas, P. Thomas, K. A. Thorne, K. S. Thorne, E. Thrane, S. Tiwari, V. Tiwari, K. V. Tokmakov, C. Tomlinson, M. Tonelli, C. V. Torres, C. I. Torrie, D. Töyrä, F. Travasso, G. Traylor, D. Trifirò, M. C. Tringali, L. Trozzo, M. Tse, M. Turconi, D. Tuyenbayev, D. Ugolini, C. S. Unnikrishnan, A. L. Urban, S. A. Usman, H. Vahlbruch, G. Vajente, G. Valdes, M. Vallisneri, N. Van Bakel, M. Van Beuzekom, J. F. Van Den Brand, C. Van Den Broeck, D. C. Vander-Hyde, L. Van Der Schaaf, J. V. Van Heijningen, A. A. Van Veggel, M. Vardaro, S. Vass, M. Vasúth, R. Vaulin, A. Vecchio, G. Vedovato, J. Veitch, P. J. Veitch, K. Venkateswara, D. Verkindt, F. Vetrano, A. Viceré, S. Vinciguerra, D. J. Vine, J. Y. Vinet, S. Vitale, T. Vo, H. Vocca, C. Vorvick, D. Voss, W. D. Vousden, S. P. Vyatchanin, A. R. Wade, L. E. Wade, M. Wade, S. J. Waldman, M. Walker, L. Wallace, S. Walsh, G. Wang, H. Wang, M. Wang, X. Wang, Y. Wang, H. Ward, R. L. Ward, J. Warner, M. Was, B. Weaver, L. W. Wei, M. Weinert, A. J. Weinstein, R. Weiss, T. Welborn, L. Wen, P. Weßels, T. Westphal, K. Wette, J. T. Whelan, S. E. Whitcomb, D. J. White, B. F. Whiting, K. Wiesner, C. Wilkinson, P. A. Willems, L. Williams, R. D. Williams, A. R. Williamson, J. L. Willis, B. Willke, M. H. Wimmer, L. Winkelmann, W. Winkler, C. C. Wipf, A. G. Wiseman, H. Wittel, G. Woan, J. Worden, J. L. Wright, G. Wu, J. Yablon, I. Yakushin, W. Yam, H. Yamamoto, C. C. Yancey, M. J. Yap, H. Yu, M. Yvert, A. Zadrożny, L. Zangrando, M. Zanolin, J. P. Zendri, M. Zevin, F. Zhang, L. Zhang, M. Zhang, Y. Zhang, C. Zhao, M. Zhou, Z. Zhou, X. J. Zhu, M. E. Zucker, S. E. Zuraw, and J. Zweizig, "Observation of gravitational waves from a binary black hole merger," Physical Review Letters, vol. 116, pp. 1–16, feb 2016.

[114] J. M. Dudley, G. Genty, and S. Coen, "Supercontinuum generation in photonic crystal fiber," Reviews of Modern Physics, vol. 78, pp. 1135–1184, oct 2006.

[115] R. Trebino, Frequency-resolved optical gating: the measurement of ultrashort laser pulses. Boston, MA: Springer US, 2000.

[116] C. K. Hong, Z. Y. Ou, and L. Mandel, "Measurement of subpicosecond time intervals between two photons by interference," Physical Review Letters, vol. 59, pp. 2044–2046, nov 1987.

[117] T. Y. Fan, "Laser beam combining for high-power, high-radiance sources," IEEE Journal on Selected Topics in Quantum Electronics, vol. 11, pp. 567–577, oct 2005.

[118] W. Drexler, U. Morgner, R. K. Ghanta, F. X. Kärtner, J. S. Schuman, and J. G. Fujimoto, "Ultrahigh-resolution ophthalmic optical coherence tomography," Nature Medicine, vol. 7, pp. 502–506, apr 2001.

[119] K. Kikuchi, "Coherent optical communications: historical perspectives and future directions," in High Spectral Density Optical Communication Technologies, pp. 11–49, Berlin, Heidelberg: Springer Berlin Heidelberg, 2010.

[120] N. Gisin and R. Thew, "Quantum communication," Nature Photonics, vol. 1, pp. 165–171, mar 2007.

[121] P. Kultavewuti, E. Y. Zhu, L. Qian, V. Pusino, M. Sorel, and J. Stewart Aitchison, "Correlated photon pair generation in AlGaAs nanowaveguides via spontaneous four-wave mixing," Optics Express, vol. 24, p. 3365, feb 2016.

[122] X. Zhang, Y. Zhang, C. Xiong, and B. J. Eggleton, "Correlated photon pair generation in low-loss double-stripe silicon nitride waveguides," Journal of Optics, vol. 18, p. 074016, jul 2016.

[123] Z. Y. Ou and Y. J. Lu, "Cavity enhanced spontaneous parametric down-conversion for the prolongation of correlation time between conjugate photons," Physical Review Letters, vol. 83, pp. 2556–2559, sep 1999.

[124] J. F. Clauser, M. A. Horne, A. Shimony, and R. A. Holt, "Proposed experiment to test local hidden-variable theories," Physical Review Letters, vol. 23, pp. 880–884, oct 1969.

[125] C. K. Law, I. A. Walmsley, and J. H. Eberly, "Continuous frequency entanglement: effective finite Hilbert space and entropy control," Physical Review Letters, vol. 84, pp. 5304–5307, jun 2000.

[126] M. Fedorov and N. Miklin, "Schmidt modes and entanglement," Contemporary Physics, vol. 55, pp. 94–109, apr 2014.

[127] M. Liscidini and J. E. Sipe, "Stimulated emission tomography," Physical Review Letters, vol. 111, p. 193602, nov 2013.

[128] A. Eckstein, G. Boucher, A. Lemaître, P. Filloux, I. Favero, G. Leo, J. E. Sipe, M. Liscidini, and S. Ducci, "High-resolution spectral characterization of two photon states via classical measurements," Laser and Photonics Reviews, vol. 8, pp. L76–L80, sep 2014.

[129] A. Christ, K. Laiho, A. Eckstein, K. N. Cassemiro, and C. Silberhorn, "Probing multimode squeezing with correlation functions," New Journal of Physics, vol. 13, p. 033027, mar 2011.

[130] M. Förtsch, J. U. Fürst, C. Wittmann, D. Strekalov, A. Aiello, M. V. Chekhova, C. Silberhorn, G. Leuchs, and C. Marquardt, "A versatile source of single photons for quantum information processing," Nature Communications, vol. 4, p. 1818, may 2013.

[131] D. G. England, B. Balaji, and B. J. Sussman, "Quantum-enhanced standoff detection using correlated photon pairs," Physical Review A, vol. 99, p. 023828, feb 2019.

[132] S. Takeuchi, "Recent progress in single-photon and entangled-photon generation and applications," Japanese Journal of Applied Physics, vol. 53, p. 030101, mar 2014.

[133] T. Pittman, "It's a good time for time-bin qubits," Physics, vol. 6, p. 110, oct 2013.

[134] J. Brendel, N. Gisin, W. Tittel, and H. Zbinden, "Pulsed energy-time entangled twin-photon source for quantum communication," Physical Review Letters, vol. 82, p. 2594, mar 1999.

[135] L. G. Helt, Z. Yang, M. Liscidini, and J. E. Sipe, "Spontaneous four-wave mixing in microring resonators," Optics Letters, vol. 35, p. 3006, sep 2010.

[136] A. Pasquazi, M. Peccianti, B. E. Little, S. T. Chu, D. J. Moss, and R. Morandotti, "Stable, dual mode, high repetition rate mode-locked laser based on a microring resonator," Optics Express, vol. 20, p. 27355, nov 2012.

[137] A. Pasquazi, L. Caspani, M. Peccianti, M. Clerici, M. Ferrera, L. Razzari, D. Duchesne, B. E. Little, S. T. Chu, D. J. Moss, and R. Morandotti, "Self-locked optical parametric oscillation in a CMOS compatible microring resonator: a route to robust optical frequency comb generation on a chip," Optics Express, vol. 21, p. 13333, jun 2013.

[138] A. R. Johnson, Y. Okawachi, M. R. E. Lamont, J. S. Levy, M. Lipson, and A. L. Gaeta, "Microresonator-based comb generation without an external laser source," Optics Express, vol. 22, p. 1394, jan 2014.

[139] M. Kues, C. Reimer, B. Wetzel, P. Roztocki, B. E. Little, S. T. Chu, T. Hansson, E. A. Viktorov, D. J. Moss, and R. Morandotti, "Passively mode-locked laser with an ultra-narrow spectral width," Nature Photonics, vol. 11, pp. 159–162, jan 2017.

[140] C. Xiong, C. Monat, A. S. Clark, C. Grillet, G. D. Marshall, M. J. Steel, J. Li, L. O'Faolain, T. F. Krauss, J. G. Rarity, and B. J. Eggleton, "Slow-light enhanced correlated photon pair generation in a silicon photonic crystal waveguide," Optics Letters, vol. 36, p. 3413, sep 2011.

[141] S. Azzini, D. Grassani, M. Galli, D. Gerace, M. Patrini, M. Liscidini, P. Velha, and D. Bajoni, "Stimulated and spontaneous four-wave mixing in silicon-on-insulator coupled photonic wire nano-cavities," Applied Physics Letters, vol. 103, p. 031117, jul 2013.

[142] W. C. Jiang, X. Lu, J. Zhang, O. Painter, and Q. Lin, "Silicon-chip source of bright photon pairs," Optics Express, vol. 23, p. 20884, aug 2015.

[143] M. Davanço, J. R. Ong, A. B. Shehata, A. Tosi, I. Agha, S. Assefa, F. Xia, W. M. J. Green, S. Mookherjea, and K. Srinivasan, "Telecommunications-band heralded single photons from a silicon nanophotonic chip," Applied Physics Letters, vol. 100, p. 261104, jun 2012.

[144] X. Guo, C.-l. Zou, C. Schuck, H. Jung, R. Cheng, and H. X. Tang, "Parametric down-conversion photon-pair source on a nanophotonic chip," Light: Science and Applications, vol. 6, p. e16249, nov 2016.

[145] R. H. Brown and R. Q. Twiss, "Correlation between photons in two coherent beams of light," Nature, vol. 177, pp. 27–29, jan 1956.

[146] M. Becker, D. Kuizenga, and A. Siegman, "Harmonic mode locking of the Nd:YAG laser," IEEE Journal of Quantum Electronics, vol. 8, pp. 687–693, aug 1972.

[147] G. R. Huggett, "Mode-locking of CW lasers by regenerative RF feedback," Applied Physics Letters, vol. 13, pp. 186–187, sep 1968.

[148] A. A. Freschi and J. Frejlich, "Adjustable phase control in stabilized interferometry," Optics Letters, vol. 20, p. 635, mar 1995.

[149] A. Dandridge, A. Tveten, and T. Giallorenzi, "Homodyne demodulation scheme for fiber optic sensors using phase generated carrier," IEEE Transactions on Microwave Theory and Techniques, vol. 30, pp. 1635–1641, oct 1982.

[150] G. Jotzu, T. J. Bartley, H. B. Coldenstrodt-Ronge, B. J. Smith, and I. A. Walmsley, "Continuous phase stabilization and active interferometer control using two modes," Journal of Modern Optics, vol. 59, pp. 42–45, oct 2012.

[151] V. V. Krishnamachari, E. R. Andresen, S. R. Keiding, and E. O. Potma, "An active interferometer-stabilization scheme with linear phase control," Optics Express, vol. 14, p. 5210, jun 2006.

[152] D. Grassani, M. Galli, and D. Bajoni, "Active stabilization of a Michelson interferometer at an arbitrary phase with subnanometer resolution," Optics Letters, vol. 39, p. 2530, apr 2014.

[153] K. Liu and R. M. Measures, "Signal processing techniques for interferometric fiber-optic strain sensors," Journal of Intelligent Material Systems and Structures, vol. 3, pp. 432–461, jul 1992.

[154] O. B. Wright, "Stabilized dual-wavelength fiber-optic interferometer for vibration measurement," Optics Letters, vol. 16, pp. 56–58, jan 1991.

[155] C. Ma, W. D. Sacher, Z. Tang, J. C. Mikkelsen, Y. Yang, F. Xu, T. Thiessen, H.-K. Lo, and J. K. S. Poon, "Silicon photonic transmitter for polarization-encoded quantum key distribution," Optica, vol. 3, p. 1274, oct 2016.

[156] Y. Pilnyak, P. Zilber, L. Cohen, and H. S. Eisenberg, "Quantum tomography of photon states encoded in polarization and picosecond time bins," Physical Review A, vol. 100, p. 43826, oct 2019.

[157] F. Steinlechner, S. Ecker, M. Fink, B. Liu, J. Bavaresco, M. Huber, T. Scheidl, and R. Ursin, "Distribution of high-dimensional entanglement via an intra-city free-space link," Nature Communications, vol. 8, pp. 1–7, jul 2017.

[158] S. J. Nowierski, N. N. Oza, P. Kumar, and G. S. Kanter, "Tomographic reconstruction of time-bin-entangled qudits," Physical Review A, vol. 94, p. 042328, oct 2016.

[159] S.-B. Cho and T.-G. Noh, "Stabilization of a long-armed fiber-optic single-photon interferometer," Optics Express, vol. 17, p. 19027, oct 2009.

[160] D. Pulford, C. Robillard, and E. Huntington, "Single photon locking of an all-fiber interferometer," Review of Scientific Instruments, vol. 76, jun 2005.

[161] P. Toliver, J. M. Dailey, A. Agarwal, and N. A. Peters, "Continuously active interferometer stabilization and control for time-bin entanglement distribution," Optics Express, vol. 23, p. 4135, feb 2015.

[162] H. Guo, A. Gnanapandithan, Y. Liu, C. Zhou, Z. Zheng, Y. Ou, X. Zeng, and L. Qian, "Single-arm frequency-shifted interferometry using a bidirectional electro-optic modulator," Journal of Lightwave Technology, vol. 37, pp. 1310–1316, jan 2019.

[163] M. Song, S. Yin, and P. B. Ruffin, "Fiber Bragg grating strain sensor demodulation with quadrature sampling of a Mach–Zehnder interferometer," Applied Optics, vol. 39, p. 1106, mar 2000.

[164] S. Rogers, D. Mulkey, X. Lu, W. C. Jiang, and Q. Lin, "High visibility time-energy entangled photons from a silicon nanophotonic chip," ACS Photonics, vol. 3, pp. 1754–1761, oct 2016.

[165] H. Martin and X. Jiang, "Rapid phase-shifting fiber interferometer with optical stylus," Optics Letters, vol. 35, p. 655, feb 2010.

[166] X.-T. Fang, P. Zeng, H. Liu, M. Zou, W. Wu, Y.-L. Tang, Y.-J. Sheng, Y. Xiang, W. Zhang, H. Li, Z. Wang, L. You, M.-J. Li, H. Chen, Y.-A. Chen, Q. Zhang, C.-Z. Peng, X. Ma, T.-Y. Chen, and J.-W. Pan, "Implementation of quantum key distribution surpassing the linear rate-transmittance bound," Nature Photonics, vol. 14, pp. 422–425, jul 2020.

[167] M. Wada, S. Okubo, K. Kashiwagi, F. L. Hong, K. Hosaka, and H. Inaba, "Evaluation of fiber noise induced in ultrastable environments," IEEE Transactions on Instrumentation and Measurement, vol. 68, pp. 2246–2252, nov 2019.

[168] K. Chen, C. M. Li, Q. Zhang, Y. A. Chen, A. Goebel, S. Chen, A. Mair, and J. W. Pan, "Experimental realization of one-way quantum computing with two-photon four-qubit cluster states," Physical Review Letters, vol. 99, pp. 1–4, sep 2007.

[169] G. Vallone, E. Pomarico, P. Mataloni, F. De Martini, and V. Berardi, "Realization and characterization of a two-photon four-qubit linear cluster state," Physical Review Letters, vol. 98, p. 180502, may 2007.

[170] W.-B. Gao, C.-Y. Lu, X.-C. Yao, P. Xu, O. Gühne, A. Goebel, Y.-A. Chen, C.-Z. Peng, Z.-B. Chen, and J.-W. Pan, "Experimental demonstration of a hyper-entangled ten-qubit Schrödinger cat state," Nature Physics, vol. 6, pp. 331–335, may 2010.

[171] D. Allan, "Statistics of atomic frequency standards," Proceedings of the IEEE, vol. 54, pp. 221–230, feb 1966.

[172] M. Mičuda, E. Doláková, I. Straka, M. Miková, M. Dušek, J. Fiurášek, and M. Ježek, "Highly stable polarization independent Mach-Zehnder interferometer," Review of Scientific Instruments, vol. 85, aug 2014.

[173] X. Ma and M. Razavi, "Alternative schemes for measurement-device-independent quantum key distribution," Physical Review A, vol. 86, p. 062319, dec 2012.

[174] B. J. Vakoc, S. H. Yun, J. F. de Boer, G. J. Tearney, and B. E. Bouma, "Phase-resolved optical frequency domain imaging," Optics Express, vol. 13, p. 5483, jul 2005.

[175] D. Loterie, S. Farahi, D. Psaltis, and C. Moser, "Complex pattern projection through a multimode fiber," in Adaptive Optics and Wavefront Control for Biological Systems (T. G. Bifano, J. Kubby, and S. Gigan, eds.), vol. 9335, p. 93350I, mar 2015.

[176] P. R. Saulson, Fundamentals of interferometric gravitational wave detectors. World Scientific, 2nd ed., apr 2017.

[177] K.-N. Joo and S.-W. Kim, "Absolute distance measurement by dispersive interferometry using a femtosecond pulse laser," Optics Express, vol. 14, p. 5954, jun 2006.

[178] J. Howard and H. Landgraf, "Quadrature sampling phase detection," Review of Scientific Instruments, vol. 65, pp. 2130–2133, jun 1994.

[179] J. Saniie and M. Luukkala, "Digital phase detection based on in-phase and quadrature sampling," Journal of Physics E: Scientific Instruments, vol. 16, pp. 606–607, jul 1983.

[180] S. Sciara, C. Reimer, M. Kues, P. Roztocki, A. Cino, D. J. Moss, L. Caspani, W. J. Munro, and R. Morandotti, "Universal N-partite d-level pure-state entanglement witness based on realistic measurement settings," Physical Review Letters, vol. 122, p. 120501, mar 2019.

[181] J. L. O'Brien, G. J. Pryde, A. G. White, T. C. Ralph, and D. Branning, "Demonstration of an all-optical quantum controlled-NOT gate," Nature, vol. 426, pp. 264–267, nov 2003.

[182] D. F. V. James, P. G. Kwiat, W. J. Munro, and A. G. White, "Measurement of qubits," Physical Review A, vol. 64, p. 052312, oct 2001.

[183] R. T. Thew, K. Nemoto, A. G. White, and W. J. Munro, "Qudit quantum-state tomography," Physical Review A, vol. 66, p. 012303, jul 2002.

[184] E. Y. Zhu, C. Corbari, P. G. Kazansky, and L. Qian, "Self-calibrating fiber spectrometer for the measurement of broadband downconverted photon pairs," arXiv:1505.01226, may 2015.

[185] N. Fabre, "Spectral single photons characterization using generalized Hong, Ou and Mandel interferometry," arXiv:2110.03564, oct 2021.

[186] J. D. Franson, "Bell inequality for position and time," Physical Review Letters, vol. 62, pp. 2205–2208, may 1989.

[187] N. Picqué and T. W. Hänsch, "Single-photon interferometry and spectroscopy with two laser frequency combs," arXiv:1906.03706, pp. 1–9, jun 2019.

[188] F. Bouchard, D. England, P. J. Bustard, K. L. Fenwick, E. Karimi, K. Heshami, and B. Sussman, "Achieving ultimate noise tolerance in quantum communication," Physical Review Applied, vol. 15, p. 024027, feb 2021.

[189] S. Heugel, A. S. Villar, M. Sondermann, U. Peschel, and G. Leuchs, "On the analogy between a single atom and an optical resonator," Laser Physics, vol. 20, pp. 100–106, jan 2010.

[190] A. Aadhi, A. V. Kovalev, M. Kues, P. Roztocki, C. Reimer, Y. Zhang, T. Wang, B. E. Little, S. T. Chu, Z. Wang, D. J. Moss, E. A. Viktorov, and R. Morandotti, "Highly reconfigurable hybrid laser based on an integrated nonlinear waveguide," Optics Express, vol. 27, p. 25251, sep 2019.

[191] M. Savanier and S. Mookherjea, "Generating photon pairs from a silicon microring resonator using an electronic step recovery diode for pump pulse generation," Applied Physics Letters, vol. 108, p. 251102, jun 2016.

[192] F. Ceccarelli, S. Atzeni, A. Prencipe, R. Farinaro, and R. Osellame, "Thermal phase shifters for femtosecond laser written photonic integrated circuits," Journal of Lightwave Technology, vol. 37, pp. 4275–4281, jun 2019.

[193] H. Wang, J. Qin, X. Ding, M.-C. Chen, S. Chen, X. You, Y.-M. He, X. Jiang, L. You, Z. Wang, C. Schneider, J. J. Renema, S. Höfling, C.-Y. Lu, and J.-W. Pan, "Boson sampling with 20 input photons and a 60-mode interferometer in a 10^{14} -dimensional Hilbert space," Physical Review Letters, vol. 123, p. 250503, dec 2019.

[194] J. Mandon, G. Guelachvili, and N. Picqué, "Fourier transform spectroscopy with a laser frequency comb," Nature Photonics, vol. 3, pp. 99–102, feb 2009.

[195] G. Wrigge, I. Gerhardt, J. Hwang, G. Zumofen, and V. Sandoghdar, "Efficient coupling of photons to a single molecule and the observation of its resonance fluorescence," Nature Physics, vol. 4, pp. 60–66, jan 2008.

[196] M. Pisco, F. A. Bruno, D. Galluzzo, L. Nardone, G. Gruca, N. Rijnveld, F. Bianco, A. Cutolo, and A. Cusano, "Opto-mechanical lab-on-fibre seismic sensors detected the Norcia earthquake," Scientific Reports, vol. 8, p. 6680, dec 2018.

[197] R. Soref, "The past, present, and future of silicon photonics," IEEE Journal of Selected Topics in Quantum Electronics, vol. 12, pp. 1678–1687, nov 2006.

A | Summary of tabletop-scale, state-of-the-art interferometer stabilization methods

Ref. No.	Reconstructed Phase: Standard Deviation (rad)	Reconstructed Phase: Allan Deviation (rad)	Optical Platform	Stabilization Type	Notes
[148] Freschi et al.	0.017	N/A	Free-space	Active	Based on arm dithering, 532 nm reference laser
[150] Jotzu et al.	0.052	N/A	Free-space	Active	Based on polarization multiplexed reference, 632 nm reference laser
[151] Krishnamachari et al.	0.050	N/A	Free-space	Active	Based on non-collinear propagation, 822 nm reference laser
[152] Grassani et al.	0.007	N/A	Free-space	Active	Based on non-collinear propagation, 633 nm reference laser, 40 Hz sample rate
[172] Mičuda et al.	N/A	$\sigma(\tau) < 0.052$ rad for all $\tau <$ 2 hours	Free-space	Passive	Based on displaced-Sagnac design, 816 nm reference laser
[159] Cho et al.	0.060	N/A	Fiber	Active	Based on a single-color scheme with a tunable delay line, 1553 nm reference laser, 100 kHz sampling rate

Ref. No.	**Reconstructed Phase: Standard Deviation (rad)**	**Reconstructed Phase: Allan Deviation (rad)**	**Optical Platform**	**Stabilization Type**	**Notes**
[160] Pulford et al.	N/A	N/A	Fiber	Active	Based on a single-color scheme with single-photon level reference signal at 1550 nm
[161] Toliver et al.	0.003	N/A	Fiber	Active	Based on arm dithering, 1550 nm reference laser, 34 ms integration time
[164] Rogers et al.	N/A	N/A	Fiber	Active	Based on a variant of the Pound-Drever-Hall technique
[165] Martin et al.	0.045	N/A	Fiber	Active	Based on phase-shifting interferometry, 1550 nm reference laser, 11 nm peak-to-peak variation in path length difference
[167] Wada et al.	$\sim$0.1216 rad drift over 14 hours.	N/A	Fiber	Passive	Employs an ultrastable environment, 1525 nm reference laser. Without intricate isolation, phase drift is $\sim$182.5 rad drift over 14 h
Section 4.2 of this thesis	0.0037	$\sigma(\tau) <$ 0.0041 rad for all $\tau <$ 1 hour	Fiber	Active	The standard deviation value was obtained with integration window and measurement duration settings from Ref. [161]

B | Candidate's Works

Journal Publications

[J.22] S. Sciara, **P. Roztocki**, et al. "Scalable and effective multi-level entangled photon states: a promising tool to boost quantum technologies," Nanophotonics 10, 4447-4465 (2021).

[J.21] B. Fischer, M. Chemnitz, B. MacLellan, **P. Roztocki**, et al. "Autonomous on-chip interferometry for reconfigurable optical waveform generation," Optica 8, 1268-1276 (2021).

[J.20] **P. Roztocki**, B. MacLellan, et al. "Arbitrary phase access for stable fiber interferometers", Laser & Photonics Reviews 15, 2000524 (2021). *Chosen for the issue cover.*

[J.19] Y. Zhang, M. Kues, **P. Roztocki**, et al. "Induced Photon Correlations Through the Overlap of Two Four-Wave Mixing Processes in Integrated Cavities", Laser & Photonics Reviews 14, 2000128 (2020).

[J.18] M. Kues, C. Reimer, S. Sciara, **P. Roztocki**, et al. "Cluster States Go High-Dimensional", Optics & Photonics News Special Issue: Optics in 2019 (2019). *Highlighted as one of the most exciting peer-reviewed optics research results to have emerged over the past 12 months, alongside being chosen for the issue cover.*

[J.17] S. Sciara, **P. Roztocki**, et al. "Generation and Processing of Complex Photon States with Quantum Frequency Combs", IEEE Photonics Technology Letters, DOI: 10.1109/LPT.2019.2944564 (2019).

[J.16] S. Sciara, C. Reimer, M. Kues, **P. Roztocki**, et al. "Universal N-Partite d-Level Pure-State Entanglement Witness Based on Realistic Measurement Settings", Physical Review Letters 122, 120501 (2019).

[J.15] A. Aadhi, A.V. Kovalev, M. Kues, **P. Roztocki**, et al. "Highly Reconfigurable Hybrid Laser based on an Integrated Nonlinear Waveguide", Optics Express 18, 25251 (2019).

[J.14] C. Reimer, S. Sciara, **P. Roztocki**, et al. "High-dimensional One-way Quantum Processing Implemented on d-Level Cluster States", Nature Physics 15, 2 (2019).

[J.13] B. MacLellan, **P. Roztocki**, et al. "Generation and Coherent Control of Pulsed Quantum Frequency Combs", Journal of Visualized Experiments 136, e57517 (2018).

[J.12] C. Reimer, Y. Zhang, **P. Roztocki**, et al. "On-chip Frequency Combs and Telecommunications Signal Processing meets Quantum Optics", Frontiers of Optoelectronics 11, 134 (2018). *Invited review.*

[J.11] B. Wetzel, M. Kues, **P. Roztocki**, et al. "Customizing Supercontinuum Generation via On-chip Adaptive Temporal Pulse-splitting", Nature Communications 9, 4884 (2018).

[J.10] **P. Roztocki**, S. Sciara, et al. "Complex Quantum State Generation and Coherent Control Based on Integrated Frequency Combs", Journal of Lightwave Technology 2, 338 (2018). *Invited review.*

[J.9] M. Kues, C. Reimer, **P. Roztocki**, et al. "Scaling On-Chip Entangled Photon States to Higher Dimensions", Optics & Photonics News Special Issue: Optics in 2017 (2017). *Highlighted as one of the most exciting peer-reviewed optics research results to have emerged over the past 12 months, alongside being chosen for the issue cover.*

[J.8] Y. Zhang, C. Reimer, J. Wu, **P. Roztocki**, et al. "Multichannel Phase-Sensitive Amplification in a Low-loss CMOS-compatible Spiral Waveguide", Optics Letters 21, 4391 (2017).

[J.7] **P. Roztocki**, M. Kues, et al. "Practical System for the Generation of Pulsed Quantum Frequency Combs", Optics Express 16, 18941 (2017).

[J.6] M. Kues, C. Reimer, **P. Roztocki**, et al. "On-chip Generation of High-Dimensional Entangled Quantum States and their Coherent Control", Nature 546, 622 (2017).

[J.5] M. Kues, C. Reimer, B. Wetzel, **P. Roztocki**, et al. "Passively Mode-locked Laser with an Ultra-Narrow Spectral Width", Nature Photonics 11, 159 (2017).

[J.4] C. Reimer, M. Kues, **P. Roztocki**, et al. "On-chip Quantum Frequency Combs", Optics & Photonics News Special Issue: Optics in 2016 (2016). *Highlighted as one of the most exciting peer-reviewed optics research results to have emerged over the past 12 months.*

[J.3] L. Caspani, C. Reimer, M. Kues, **P. Roztocki**, et al. "Multifrequency Sources of Quantum Correlated Photon Pairs on-Chip: A Path Towards Integrated Quantum Frequency Combs", Nanophotonics, 5, 351 (2016). *Invited review.*

[J.2] C. Reimer, M. Kues, **P. Roztocki**, et al. "Generation of Multiphoton Entangled Quantum States by Means of Integrated Frequency Combs", Science 351, 1176 (2016).

[J.1] C. Reimer, M. Kues, L. Caspani, B. Wetzel, **P. Roztocki**, et al. "Cross-Polarized Photon-Pair Generation and Bi-Chromatically Pumped Optical Parametric Oscillation on a Chip", Nature Communications 6, 8236 (2015).

Patents

[P.10] B. Fischer, **P. Roztocki**, M. Chemnitz, C. Rimoldi, B. MacLellan, L. Romero Cortes, M. Kues, J. Azana, Y. Jestin, R. Morandotti, "System and method for optical information processing with a reconfigurable nonlinear optical network", US63/051,435 (application) (filed on July 15, 2020).

[P.9] S. Shankar Bharadwaj, J. van Howe, **P. Roztocki**, Y. Jestin, J. Azana, R. Morandotti, "Method and system for extractable scaling in quantum random number generator", US63/051,539 (application) (filed on July 14, 2020).

[P.8] B. MacLellan, **P. Roztocki**, J. van Howe, L. Romero Cortes, B. Fischer, Y. Jestin, J. Azana, R. Morandotti, "Method for automated design of optical systems" US 63/034,974 (application) (filed on June 4, 2020).

[P.7] M. Islam, **P. Roztocki**, M. Kues, C. Reimer, B. Fischer, S. Sciara, R. Helsten, Y. Zhang, Y. Jestin, R. Morandotti, "System and Method for Phase-Readout of Multi-Path Optical Interferometers" US62/893,288 (application) (filed on August 29, 2019).

[P.6] B. Wetzel, M. Kues, C. Reimer, R. Helsten, **P. Roztocki**, R. Morandotti, and Y. Jestin, "Method And System For Nonlinear Optical Process Optimization Via Temporal Pulse Splitting" PCT/CA2019/050144 (application) (filed on February 05, 2019).

[P.5] M. Kues, C. Reimer, S. Sciara, **P. Roztocki**, L. Romero Cortes, J. Azana, Y. Jestin, R. Morandotti, "Method and system for the generation and control of high-dimensional multi-partite quantum states", CA3,084,024 (application) US16/768,667 (application) (filed on November 28, 2018)

[P.4] **P. Roztocki**, C. Reimer, M. Kues, R. Helsten, Y. Jestin, and R. Morandotti, "System and Method for Phase-readout and Active Stabilization of Optical Interferometers", CA2,989,040 (application) US15/735,430 (granted) (filed on September 08, 2016).

[P.3] C. Reimer, M. Kues, B. Wetzel, **P. Roztocki**, F. Grazioso, Y. Jestin, and R. Morandotti, "Method and System for the Generation of Optical Multipartite Quantum States", CA2,983,035 (application) EU16782417.6 (application) US15/560,614 (granted) (filed in April 12, 2016).

[P.2] C. Reimer, M. Kues, B. Wetzel, **P. Roztocki**, Y. Jestin, and R. Morandotti, "Passive Mode-locked Laser System and Method for Generation of Long Pulses", CA2,978,362 (application) US10/177,525 (granted) (filed on March 15, 2016).

[P.1] M. Kues, C. Reimer, B. Wetzel, **P. Roztocki**, Y. Jestin, and R. Morandotti, "Method and System for Pulsed Excitation of a Nonlinear Medium for Photon Pair Generation", CA2,978,360 (application) US15/552,061 (granted) (filed on March 15, 2016).

Book Chapters

[B.2] B. Fischer, **P. Roztocki**, C. Reimer, et al., "Nonlinear and Quantum Effects in Integrated Microcavities", in Nonlinear Meta-Optics, Taylor & Francis, DOI:10.1201/b22515 (2020).

[B.1] **P. Roztocki**, M. Kues, et al. "Quantum State Generation via Frequency Combs", in Foundations of Quantum Theory, IOS Press (2019).

Invited Talks in Refereed International Conferences

[I.38] S. Sciara, **P. Roztocki**, C. Reimer, B. MacLellan, B. Fischer, L. Romero Cortes, D.J. Moss, L. Caspani, W.J. Munro, J. Azana, M. Kues, and R. Morandotti, "On-chip Quantum Frequency Combs for The Generation of Complex Entangled Photon States in the Time and Spectral Domains", Photonics North, Canada, Virtual conference (2020).

[I.37] M. Kues, S. Sciara, **P. Roztocki**, B. Fischer, C. Reimer, M. Islam, L. Romero Cortés, Y. Zhang, A. Cino, S.T. Chu, B.E. Little, D.J. Moss, L. Caspani, W. Munro, J. Azaña, and R. Morandotti, "On-chip Quantum Frequency Comb for Complex Photon State Generation", SPIE Photonics West, San Francisco, USA (2020).

[I.36] B. Fischer, C. Reimer, S. Sciara, **P. Roztocki**, M. Islam, L. Romero Cortés, Y. Zhang, S. Loranger, R. Kashyap, A. Cino, S.T. Chu, B.E. Little, D.J. Moss, L. Caspani, W. Munro, J. Azaña, M. Kues, and R. Morandotti, "High-dimensional d-level Cluster States with On-Chip Frequency Combs", SPIE Photonics West OPTO, San Francisco, USA (2020).

[I.35] M. Kues, C. Reimer, S. Sciara, **P. Roztocki**, M. Islam, L. Romero Cortés, Y. Zhang, B. Fischer, S. Loranger, R. Kashyap, A. Cino, S.T. Chu, B.E. Little, D.J. Moss, L. Caspani, W.J. Munro, J. Azaña, and R. Morandotti, "D-dimensional Frequency-time Entangled Cluster States with On-chip Frequency Combs", OSA Advanced Photonics Congress Integrated Photonics Research, Silicon and Nanophotonics, Burlingame, USA (2019).

[I.34] **P. Roztocki**, C. Reimer, S. Sciara, L. Romero Cortés, Y. Zhang, B. Wetzel, M. Islam, A. Cino, S.T. Chu, B.E. Little, D.J. Moss, L. Caspani, J. Azaña, M. Kues, and R. Morandotti, "Microcavity-based Frequency Combs for Quantum State Generation and Coherent Control", Photonics West, San Francisco, USA (2019).

[I.33] S. Sciara, C. Reimer, M. Kues, **P. Roztocki**, M. Islam, L. Romero Cortes, Y. Zhang, B. Fischer, S. Loranger, R. Kashyap, A. Cino, S.T. Chu, B.E. Little, D.J. Moss, L. Caspani, W.J. Munro, J. Azaña, and R. Morandotti, "On-chip Generation, Coherent Control and Processing of Complex Entangled Photon States", IEEE Photonics Society Summer Topicals Meeting Series, Ft. Lauderdale, USA, (2019).

[I.32] S. Sciara, M. Kues, C. Reimer, **P. Roztocki**, M. Islam, L. Romero Cortes, Y. Zhang, B. Fischer, S. Loranger, R. Kashyap, A. Cino, S.T. Chu, B.E. Little, D.J. Moss, L. Caspani, W. J. Munro, J. Azaña, and R. Morandotti, "Quantum Frequency Combs for the On-chip Generation, Coherent Control and Processing of Complex Entangled Photon States", Canadian Semiconductor Science and Technology Conference, Saskatoon, Canada, (2019).

[I.31] L. Caspani, S. Sciara, C. Reimer, **P. Roztocki**, M. Islam, L. Romero Cortés, Y. Zhang, B. Fischer, S. Loranger, R. Kashyap, A. Cino, S.T. Chu, B.E. Little, D.J. Moss, W.J. Munro, J. Azaña, M. Kues, and R. Morandotti, "Generation of On-chip D-dimensional Entangled Cluster States and their Characterization via Optimal Entanglement Witnesses", International Conference on Metamaterials, Photonic Crystals and Plasmonics (META), Lisbon, Portugal (2019).

[I.30] S. Sciara, M. Kues, C. Reimer, **P. Roztocki**, B. Wetzel, B.E. Little, S.T. Chu, D.J. Moss, L. Caspani, and R. Morandotti, "Integrated Frequency Combs for the On-chip Generation of Optical Quantum States", International Conference on Metamaterials, Photonic Crystals and Plasmonics (META), Lisbon, Portugal (2019).

[I.29] **P. Roztocki**, C. Reimer, M. Kues, S. Sciara, M. Islam, L. Romero Cortés, Y. Zhang, B. Fischer, S. Loranger, R. Kashyap, A. Cino, S.T. Chu, B.E. Little, D.J. Moss, L. Caspani, W.J. Munro, J. Azaña, B. Wetzel, and R. Morandotti, "Kerr Combs and Telecommunications Components for the Generation and High-dimensional Quantum Processing of D-level Cluster States", International Conference on Transparent Optical Networks ICTON 2019, Angers, France (2019).

[I.28] S. Sciara, M. Kues, C. Reimer, **P. Roztocki**, L. Romero Cortés, B. Wetzel, Y. Zhang, A. Cinio, S.T. Chu, B.E. Little, D.J. Moss, L. Caspani, J. Azaña, and R. Morandotti, "Generation and Coherent Manipulation of Complex Quantum States Based on Integrated Frequency Combs", Photonics in Switching and Computing, Limassol, Cyprus (2018).

[I.27] M. Kues, C. Reimer, **P. Roztocki**, L. Romero Cortés, S. Sciara, B. Wetzel, Y. Zhang, A. Cino, S.T. Chu, B.E. Little, D.J. Moss, L. Caspani, J. Azaña, and R. Morandotti, "Complex Entangled Photon States on a Chip", Foundations & Advances in Nonlinear Science and 4nd International Symposium Advances in Nonlinear Photonics, Minsk, Belarus (2018). *Keynote*

[I.26] M. Kues, C. Reimer, S. Sciara, **P. Roztocki**, B. Wetzel, L. Caspani, S. T. Chu, D. J. Moss, and R. Morandotti, "Generation of Correlated Photons", Photonics North, Montreal, Canada (2018).

[I.25] **P. Roztocki**, M. Kues, C. Reimer, L. Romero Cortés, S. Sciara, B. Wetzel, Y. Zhang, A. Cino, S.T. Chu, B.E. Little, D.J. Moss, L. Caspani, J. Azaña, and R. Morandotti, "Scalable On-chip Generation and Coherent Control of Complex Optical Quantum States", CLEO, San Francisco, USA (2018).

[I.24] S. Sciara, M. Kues, **P. Roztocki**, C. Reimer, L. Romero Cortés, B. Wetzel, Y. Zhang, A. Cino, B. E. Little, S. T. Chu, D. J. Moss, L. Caspani, J. Azãna, and R. Morandotti, "Integrated Frequency Combs for On-Chip Generation of High-Dimensional Entangled Photon States and Their Coherent Control", SPIE Photonics Europe, Strasbourg, France (2018).

[I.23] M. Kues, C. Reimer, **P. Roztocki**, L. Romero Cortés, S. Sciara, B. Wetzel, Y. Zhang, A. Cino, B.E. Little, S.T. Chu, D.J. Moss, L. Caspani, J. Azaña, and R. Morandotti, "High-dimensional Optical Quantum States from Integrated Frequency Combs and Their Coherent Control", Photonics West, San Francisco, USA (2018).

[I.22] **P. Roztocki**, M. Kues, C. Reimer, B. Wetzel, S. Sciara, Y. Zhang, A. Cino, S.T. Chu, B.E. Little, D.J. Moss, and R. Morandotti, "Practical Excitation Schemes for Integrated Micro-Cavity Based Quantum Frequency Combs", Photonics West, San Francisco, USA (2018).

[I.21] M. Kues, C. Reimer, **P. Roztocki**, B. Wetzel, F. Grazioso, B.E. Little, S.T. Chu, T. Johnston, Y. Bromberg, L. Caspani, D.J. Moss, and R. Morandotti, "On-chip Frequency Combs for Scalable Quantum State Generation", META, Seoul, Korea (2017).

[I.20] S. Sciara, M. Kues, C. Reimer, **P. Roztocki**, B. Wetzel, Y. Bromberg, B.E. Little, S.T. Chu, D.J. Moss, L. Caspani, and R. Morandotti, "On-chip Quantum State Generation by Means of Integrated Frequency Combs", Photonics Society Summer Topicals Meeting Series, San Juan, Puerto Rico (2017).

[I.19] **P. Roztocki**, C. Reimer, M. Kues, B. Wetzel, Y. Bromberg, B.E. Little, S.T. Chu, D.J. Moss, L. Caspani, and R. Morandotti, "Integrated Frequency Combs for Quantum State Generation", CCMR 2017, Jeju Island, Korea (2017).

[I.18] **P. Roztocki**, M. Kues, C. Reimer, B. Wetzel, B.E. Little, S.T. Chu, D.J. Moss, and R. Morandotti, "Pulsed Quantum Frequency Combs from an Actively Mode-Locked Intra-Cavity Generation Scheme", CLEO Europe, Munich, Germany (2017).

[I.17] S. Sciara, M. Kues, C. Reimer, **P. Roztocki**, B. Wetzel, F. Grazioso, B.E. Little, S.T. Chu, T. Johnston, Y. Bromberg, L. Caspani, D.J. Moss, and R. Morandotti, "On-chip Frequency Combs for Scalable Quantum State Generation", Photonics North, Ottawa, Canada (2017).

[I.16] M. Kues, C. Reimer, B. Wetzel, **P. Roztocki**, B.E. Little, S.T. Chu, T. Hansson, E.A. Viktorov, D.J. Moss, and R. Morandotti, “Transform-limited Nanosecond Passively Mode-locked Laser”, Photonics North, Ottawa, Canada (2017).

[I.15] C. Reimer, M. Kues, **P. Roztocki**, B. Wetzel, B.E. Little, S.T. Chu, L. Caspani, D.J. Moss and R. Morandotti, "Generation of Complex Quantum States via Integrated Frequency Combs", Date 17, Lausanne, Switzerland (2017).

[I.14] **P. Roztocki**, M. Kues, C. Reimer, B. Wetzel, F. Grazioso, B.E. Little, S.T. Chu, T. Johnston, Y. Bromberg, L. Caspani, D.J. Moss, and R. Morandotti, “Quantum State Generation via Integrated Frequency Combs”, SPIE Photonics West, San Francisco, USA (2017).

[I.13] R. Morandotti, M. Kues, C. Reimer, **P. Roztocki**, B. Wetzel, F. Grazioso, B.E. Little, S.T. Chu, T. Johnston, Y. Bromberg, L. Caspani, and D.J. Moss, "Complex Quantum State on a Chip", Congreso Nacional de Ingenieria Fisica, Medellin, Colombia (2016). *Keynote*

[I.12] C. Reimer, M. Kues, **P. Roztocki**, B. Wetzel, B.E. Little, S.T. Chu, T. Johnston, Y. Bromberg, L. Caspani, D.J. Moss, and R. Morandotti, “Quantum State Generation with Integrated Frequency Combs”, Photonics North, Quebec City, Canada (2016).

[I.11] **P. Roztocki**, M. Kues, C. Reimer, B. Wetzel, F. Grazioso, B.E. Little, S.T. Chu, T. Johnston, Y. Bromberg, L. Caspani, D.J. Moss, and R. Morandotti, “Quantum Entangled Frequency Comb Sources”, Integrated Photonics Research, Silicon and Nanophotonics, Vancouver, Canada (2016).

[I.10] M. Kues, C. Reimer, **P. Roztocki**, B. Wetzel, L. Caspani, Y. Bromberg, F. Grazioso, B.E. Little, S.T. Chu, T. Johnston, D.J. Moss, and R. Morandotti, “On-Chip Kerr Frequency Combs for Scalable Quantum State Generation”, 20th Slovak - Czech - Polish Optical Conference On Wave and Quantum Aspects of Contemporary Optics, Jasna, Slovakia (2016).

[I.9] M. Kues, C. Reimer, **P. Roztocki**, B. Wetzel, Y. Bromberg, B.E. Little, S.T. Chu, D.J. Moss, L. Caspani, and R. Morandotti, ”Integrated Quantum Frequency Comb Source of Entangled Qubits”, META’16, 7th International Conference on Metamaterials, Photonic Crystals and Plasmonics, Torremolinos (Malaga), Spain (2016).

[I.8] **P. Roztocki**, M. Kues, C. Reimer, B. Wetzel, B.E. Little, S.T. Chu, T. Johnston, Y. Bromberg, L. Caspani, D.J. Moss, and R. Morandotti, “Quantum State Generation via Integrated Frequency Combs”, International Conference on Optical, Optoelectronic and Photonic Materials and Applications, Montreal, Canada (2016).

[I.7] M. Kues, C. Reimer, **P. Roztocki**, L. Caspani, B. Wetzel, Y. Bromberg, B.E. Little, S.T. Chu, D.J. Moss, and R. Morandotti, “Quantum Combs in Integrated Optics”, Emerging Technologies 2016, Montreal, Canada (2016).

[I.6] M. Kues, C. Reimer, **P. Roztocki**, L. Caspani, B. Wetzel, M. Clerici, M. Ferrera, M. Peccianti, A. Pasquazi, B.E. Little, S.T. Chu, D.J. Moss, and R. Morandotti, "On-Chip Quantum Frequency Comb Source”, SPIE DSS, Baltimore, USA (2016).

[I.5] R. Morandotti, **P. Roztocki**, C. Reimer, M. Kues, B. Wetzel, L. Caspani, F. Grazioso, Y. Bromberg, M. Clerici, M. Ferrera, M. Peccianti, A. Pasquazi, L. Razzari, B.E. Little, S.T. Chu, and D.J. Moss, “Integrated Optical Combs: Towards Quantum Optical Applications”, SPIE Photonics West, San Francisco, USA (2016).

[I.4] **P. Roztocki**, M. Kues, C. Reimer, B. Wetzel, L. Caspani, Y. Bromberg, F. Grazioso, B.E. Little, S.T. Chu, T. Johnston, D.J. Moss, and R. Morandotti, "Quantum State Generation via Integrated Frequency Combs", ECIO 2016, Warsaw, Poland (2016). *Plenary*

[I.3] **P. Roztocki**, C. Reimer, M. Kues, L. Caspani, M. Clerici, M. Ferrera, M. Peccianti, A. Pasquazi, L. Razzari, B.E. Little, S.T. Chu, D.J. Moss, and R. Morandotti, "Integrated Optical Combs: Towards Single Photon Applications", Photonics North, Ottawa, Canada (2015).

[I.2] C. Reimer, M. Kues, L. Caspani, B. Wetzel, **P. Roztocki**, M. Clerici, Y. Jestin, M. Ferrera, M. Peccianti, A. Pasquazi, B.E. Little, S.T. Chu, D.J. Moss, and R. Morandotti, "Novel Classical and Quantum Phenomena in Nonlinear Ring Resonators", Energy Materials Nanotechnology (EMN) on Optoelectronics, Beijing, China (2015).

[I.1] **P. Roztocki**, C. Reimer, L. Caspani, M. Clerici, M. Ferrera, M. Kues, M. Peccianti, A. Pasquazi, L. Razzari, B.E. Little, S.T. Chu, D.J. Moss, and R. Morandotti, "Integrated Optical Combs: Towards Single Photon Applications", The International Conference on Optics, Photonics & Photosciences (CIOFF), Havana, Cuba (2014).

Post-Deadline Talks in Refereed International Conferences

[D.1] M. Kues, C. Reimer, **P. Roztocki**, B. Wetzel, F. Grazioso, B.E. Little, S.T. Chu, D.J. Moss, L. Caspani, and R. Morandotti, "Frequency Comb of Time-Bin Entangled Photon Pairs on a Chip", CLEO/Europe - EQEC, Munich, Germany (2015).

Research Seminars

[S.3] **P. Roztocki**, "Generation and Control of Optical Quantum States using Photonics Silicon Chip and Fiber Technology", McMaster University, Hamilton, Canada (2018).

[S.2] **P. Roztocki**, "On-Chip Generation of Complex Optical Quantum States and their Coherent Control", University of Sussex, Brighton, UK (2017).

[S.1] **P. Roztocki**, "Quantum State Generation via Integrated Frequency Combs", University of Warsaw, Warsaw, Poland (2016).

Articles in Refereed International Conferences (Selected)

[A.73] S. Sciara, H. Yu, M. Chemnitz, B. Fischer, **P. Roztocki**, B. Crockett, C. Reimer, B.E. Little, S.T. Chu, L. Caspani, W.J. Munro, D.J. Moss, M. Kues, J. Azana, Z. Wang, and R. Morandotti, "On-Chip Time and Frequency Modes for the Generation and Processing of Complex Photon States", IEEE Photonics Conference (IPC), Virtual conference (2021).

[A.72] M. Chemnitz, B. Fischer, B. MacLellan, **P. Roztocki**, R. Helsten, B. Wetze, B.E. Little, S.T. Chu, D.J. Moss, J. Azana, and R. Morandotti, "All-Optical Sampling for Adaptive on-chip Picosecond Pulse Shaping", OSA Advanced Photonics Congress, Virtual conference (2021).

[A.71] S. Sciara, C. Reimer, **P. Roztocki**, D.J. Moss, L. Caspani, W.J. Munro, M. Kues, and R. Morandotti, "Two-Photon Multipartite D-Level Cluster States and Witness Operators for Their Practical Entanglement Detection", OSA Advanced Photonics Congress, Virtual conference (2021).

[A.70] H. Yu, M. Chemnitz, S. Sciara, B. Fischer, B. Crockett, **P. Roztocki**, B.E. Little, S.T. Chu, D.J. Moss, J. Azana, Z. Wang, and R. Morandotti, "On-Chip Generation and Characterization of Densely-Spaced Time-Bin Entangled Qubits", Photonics North, Virtual conference (2021).

[A.69] H. Yu, M. Chemnitz, S. Sciara, B. Fischer, B. Crockett, **P. Roztocki**, B.E. Little, S.T. Chu, D.J. Moss, J. Azana, Z. Wang, and R. Morandotti, "Generation of Densely Spaced Time-Bin Entangled Qubit on Chip", Photonics North, Virtual conference (2021).

[A.68] S. S. Bharadwaj, J. van Howe, S. Atzeni, **P. Roztocki**, R. Narayanan, R. Osellame, J. Azaña, J. W. Munro, and R. Morandotti, "A Scalable Design for Photonic Quantum Random Number Generators", CLEO, Virtual conference (2021).

[A.67] H. Yu, M. Chemnitz, S. Sciara, B. Fischer, B. Crockett, **P. Roztocki**, B. Little, S. T. Chu, D. Moss, J. Azana, Z. Wang, and R. Morandotti, "On-Chip Generation of Telecommunications-Compatible Ultrafast Time-Bin Entangled Qubits", CLEO, Virtual conference (2021).

[A.66] S. Sciara, C. Reimer, **P. Roztocki**, D.J. Moss, L. Caspani, W.J. Munro, M. Kues, and R. Morandotti, "Multipartite d-Level Photon Cluster States and Practical Entanglement Detection Through Witness Operators", CLEO, Virtual conference (2021)

[A.65] S. Sciara, C. Reimer, **P. Roztocki**, B. Fischer, L.R. Cortes, D.J. Moss, L. Caspani, W.J. Munro, J. Azana, M. Kues, and R. Morandotti, "Generation and Coherent Manipulation of Complex Entangled Photon States Based on Integrated Quantum Frequency Combs", OSA Advanced Photonics Congress, Canada, Virtual conference (2020).

[A.64] M. Kues, **P. Roztocki**, Y. Zhang, C. Reimer, B. Fischer, B. MacLellan, B.E. Little, S.T. Chu, D.J. Moss, L. Caspani, and R. Morandotti, "Photon Correlation Control in Integrated Quantum Frequency Combs", OSA Advanced Photonics Congress, Canada, Virtual conference (2020).

[A.63] S. Sciara, C. Reimer, **P. Roztocki**, D.J. Moss, L. Caspani, W.J. Munro, M. Kues, and R. Morandotti, "Multipartite d-level Two-Photon Cluster States and their Entanglement Detection via Feasible Witness Operators", OSA Advanced Photonics Congress, Canada, Virtual conference (2020).

[A.62] S.S. Bharadwaj, J. van Howe, S. Atzeni, **P. Roztocki**, R. Narayanan, R. Osellame, J. Azana, and R. Morandotti, "Entropy Scaling in Trusted-Device Photonic Quantum Random Number Generators", OSA Advanced Photonics Congress, Canada, Virtual conference (2020).

[A.61] **P. Roztocki**, B. MacLellan, M. Islam, C. Reimer, B. Fischer, S. Sciara, R. Helsten, Y. Jestin, A. Cino, S.T. Chu, B. Little, D.J. Moss, M. Kues, and R. Morandotti, "Unambiguous Phase Retrieval in Fiber-based Interferometers", OSA Advanced Photonics Congress, Canada, Virtual conference (2020).

[A.60] **P. Roztocki**, M. Kues, Y. Zhang, C. Reimer, B. Fischer, B. MacLellan, A. Bisianov, U. Peschel, B.E. Little, S.T. Chu, D.J. Moss, L. Caspani, and R. Morandotti, "Induced Photon Correlations by the Superposition of Two Four-Wave Mixing Processes on a Photonic Chip", OSA Advanced Photonics Congress, Canada, Virtual conference (2020).

[A.59] A. Aadhi, **P. Roztocki**, A.V. Kovalev, M. Kues, B. Fischer, C. Reimer, Y. Zhang, T. Wang, B.E. Little, S.T. Chu, Z. Wang, D.J. Moss, E.A. Viktorov, and R. Morandotti, "Distinct Laser Dynamics from a Single Figure-Eight Laser with an Integrated Nonlinear Waveguide", OSA Advanced Photonics Congress, Canada, Virtual conference (2020).

[A.58] B. Fischer, A. Aadhi, C. Rimoldi, **P. Roztocki**, L. di Lauro, M. Chemnitz, A.V. Kovalev, S. Chu, B. Little, D.J. Moss, E.A. Viktorov, M. Kues, and R. Morandotti, "Optical Frequency Comb Generation by Hybrid Mode-Locking in a Nested Cavity Scheme", OSA Advanced Photonics Congress, Canada, Virtual conference (2020).

[A.57] **P. Roztocki**, M. Kues, Y. Zhang, C. Reimer, B. Fischer, B. MacLellan, A. Bisianov, U. Peschel, B.E. Little, S.T. Chu, D.J. Moss, L. Caspani, and R. Morandotti, "Induced photon correlations by the superposition of two four-wave mixing processes on a photonic chip", Photonics North, Online Conference (2020).

[A.56] B. MacLellan, **P. Roztocki**, S. Sciara, C. Reimer, L. Romero Cortes, A. Cino, S.T. Chu, B.E. Little, D.J. Moss, L. Caspani, W.J. Munro, J. Azana, M. Kues, and R. Morandotti, "Scalability of high-dimensional quantum operations in the spectral domain", Photonics North, Online Conference (2020).

[A.55] B. Fischer, A.A. Rahim, C. Rimoldi, **P. Roztocki**, L. di Lauro, M. Chemnitz, S.T. Chu, B.E. Little, D.J. Moss, R. Morandotti, "Hybrid mode-locking with a nested cavity scheme", Photonics North, Online Conference (2020).

[A.54] B. Fischer, **P. Roztocki**, M. Islam, C. Reimer, S. Sciara, Y. Zhang, D.J. Moss, M. Kues, and R. Morandotti, "Phase Retrieval in Fiber-Based Interferometers", Photonics North, Quebec, Canada (2019).

[A.53] S. Sciara, C. Reimer, M. Kues, **P. Roztocki**, A. Cino, D.J. Moss, L. Caspani, W.J. Munro, and R. Morandotti, "Universal Multipartite D-Level Entanglement Witnesses for Realistic Measurement Settings", Photonics North, Quebec, Canada (2019).

[A.52] **P. Roztocki**, C. Reimer, S. Sciara, M. Islam, L.R. Cortes, Y. Zhang, B. Fischer, S. Loranger, R. Kashyap, A. Cino, S.T. Chu, B.E. Little, D.J. Moss, L. Caspani, W.J. Munro, J. Azana, M. Kues, and R. Morandotti, "Optical D-Level Frequency-Time-Based Cluster States", Photonics North, Quebec, Canada (2019).

[A.51] **P. Roztocki**, M. Islam, C. Reimer, B. Fischer, S. Sciara, Y. Zhang, D.J. Moss, M. Kues, and R. Morandotti, "Removing Phase Ambiguity in Fiber-Based Interferometers for Coherent Time-Bin Operations", CLEO/Europe-EQEC, Munich, Germany (2019).

[A.50] S. Sciara, C. Reimer, M. Kues, **P. Roztocki**, A. Cino, D.J. Moss, L. Caspani, W.J. Munro, and R. Morandotti, "Universal Multipartite D-Level Entanglement Witnesses for Realistic Measurement Settings", CLEO/Europe, Munich, Germany (2019).

[A.49] **P. Roztocki**, C. Reimer, S. Sciara, M. Islam, L. Romero Cortés, Y. Zhang, B. Fischer, S. Loranger, R. Kashyap, A. Cino, S.T. Chu, B.E. Little, D.J. Moss, L. Caspani, W.J. Munro,

J. Azaña, M. Kues, and R. Morandotti, “Hyper-Entanglement in Time and Frequency”, CLEO/Europe, Munich, Germany (2019).

[A.48] Y. Zhang, M. Kues, **P. Roztocki**, C. Reimer, B. Fischer, B. MacLellan, L. Caspani, B. Little, S.T. Chu, D.J. Moss, and R. Morandotti, “Single-Photon Induced Correlation with Integrated Quantum Frequency Combs”, CLEO/Europe, Munich, Germany (2019).

[A.47] B. Wetzel, M. Kues, **P. Roztocki**, C. Reimer, P.L. Godin, M. Rowley, B.E. Little, S.T. Chu, E.A. Viktorov, D.J. Moss, A. Pasquazi, M. Peccianti, and R. Morandotti, “Customizing Supercontinuum Generation via Adaptive On-Chip Pulse Splitting”, CLEO/Europe, Munich, Germany (2019).

[A.46] M. Kues, C. Reimer, S. Sciara, **P. Roztocki**, M. Islam, L. Romero Cortés, Y. Zhang, B. Fischer, S. Loranger, R. Kashyap, A. Cino, S.T. Chu, B.E. Little, D.J. Moss, L. Caspani, W.J. Munro, J. Azaña, and R. Morandotti, “Optical D-Level Frequency Time-Based Cluster States”, CLEO/Europe, Munich, Germany (2019).

[A.45] C. Reimer, M. Kues, S. Sciara, **P. Roztocki**, M. Islam, L. Romero Cortés, Y. Zhang, B. Fischer, S. Loranger, R. Kashyap, A. Cino, S.T. Chu, B.E. Little, D.J. Moss, L. Caspani, W.J. Munro, J. Azaña, and R. Morandotti, “High-Dimensional One-Way Quantum Computation Operations with On-Chip Optical D-Level Cluster States”, CLEO, San Diego, USA (2019).

[A.44] M. Kues, C. Reimer, S. Sciara, **P. Roztocki**, M. Islam, L. Romero Cortés, Y. Zhang, B. Fischer, S. Loranger, R. Kashyap, A. Cino, S.T. Chu, B.E. Little, D.J. Moss, L. Caspani, W.J. Munro, J. Azaña, and R. Morandotti, “High-Dimensional One-Way Quantum Processing Enabled by Optical D-Level Cluster States”, Quantum Information and Measurement, Rome, Italy (2019).

[A.43] **P. Roztocki**, S. Sciara, M. Kues, C. Reimer, L.R. Cortes, B. Wetzel, Y. Zhang, A. Cino, S.T. Chu, B.E. Little, D.J. Moss, L. Caspani, J. Azaña, and R. Morandotti, “On-Chip Generation and Coherent Control of D-Level Entangled Photon States Through Integrated Frequency Combs”, Quantum Technology International Conference, Paris, France (2018).

[A.42] **P. Roztocki**, C. Reimer, M. Kues, S. Sciara, L. Romero Cortés, Y. Zhang, B. Wetzel, M. Islam, A. Cino, A. Cino, S.T. Chu, B.E. Little, D.J. Moss, L. Caspani, J. Azaña, M. Kues, and R. Morandotti, “Framework for Complex Quantum State Generation and Coherent Control Based On On-Chip Frequency Combs”, Frontiers in Optics, Washington, USA (2018).

[A.41] A.V. Kovalev, A. Aadhi, M. Kues, **P. Roztocki**, C. Reimer, Y. Zhang, T. Wang, A. Matuhina, B.E. Little, S.T. Chu, D.J. Moss, Z. Wang, E.A. Viktorov, and R. Morandotti, "Figure-eight Laser with an Integrated Nonlinear Waveguide: All Optical Square-Wave Generation", International Conference on Laser Optics, St. Petersburg, Russia (2018).

[A.40] **P. Roztocki**, M. Kues, C. Reimer, L. Romero Cortés, S. Sciara, B. Wetzel, Y. Zhang, A. Cino, S.T. Chu, B.E. Little, D.J. Moss, L. Caspani, J. Azaña, and R. Morandotti, "On-chip Generation and Coherent Control of Complex Optical Quantum States", URSI AT-RASC, Gran Canaria, Spain (2018).

[A.39] A. Aadhi, A.V. Kovalev, **P. Roztocki**, M. Kues, C. Reimer, Y. Zhang, T. Wang, B.E. Little, S.T. Chu, D.J. Moss, Z. Wang, E. Viktorov, and R. Morandotti, "Tunable Field Dynamics from a Figure-Eight Laser Featuring an On-Chip Nonlinear Waveguide", Photonics North, Montreal, Canada (2018).

[A.38] S. Sciara, M. Kues, C. Reimer, **P. Roztocki**, L. Romero Cortés, B. Wetzel, Y. Zhang, L. Caspani, A. Cino, S. T. Chu, D. J. Moss, J. Azaña, and R. Morandotti, "On-chip Generation and Coherent Control of Entangled d-level Biphoton States", Photonics North, Montreal, Canada (2018).

[A.37] Y. Zhang, M. Islam, **P. Roztocki**, C. Reimer, S. Sciara, B. Fischer, Y. Bromberg, L. Caspani, S.T. Chu, B.E. Little, D.J. Moss, M. Kues, and R. Morandotti, "Noise Contributions in On-chip Four-photon States", Photonics North, Montreal, Canada (2018).

[A.36] A. Aadhi, A. V. Kovalev, M. Kues, **P. Roztocki**, C. Reimer, Y. Zhang, T. Wang, B.E. Little, S.T. Chu, D.J. Moss, Z. Wang, E. Viktorov, and R. Morandotti, "Dynamics of Laser with an Integrated Nonlinear Waveguide", CLEO, San Jose, USA (2018).

[A.35] M. Kues, C. Reimer, **P. Roztocki**, L. Romero Cortés, S. Sciara, B. Wetzel, Y. Zhang, A. Cino, S.T. Chu, B.E. Little, D.J. Moss, L. Caspani, J. Azaña, and R. Morandotti, "On-chip Entangled D-level Photon States – Scalable Generation and Coherent Processing", CLEO, San Jose, USA (2018).

[A.34] A. Aadhi, A.V. Kovalev, M. Kues, **P. Roztocki**, C. Reimer, Y. Zhang, T. Wang, B.E. Little, S.T. Chu, D.J. Moss, Z. Wang, E. Viktorov, and R. Morandotti, "Optical Square Waves from a Nonlinear Amplifying Loop Mirror Laser", SPIE Photonics West, San Francisco, USA (2018).

[A.33] C. Reimer, M. Kues, **P. Roztocki**, S. Sciara, L. Romero Cortés, B. Wetzel, Y. Zhang, A. Cino, S.T. Chu, B. Little, D.J. Moss, L. Caspani, J. Azaña, and R. Morandotti, "On-chip Quantum Optical Frequency Comb Sources", Optical Fiber Communication Conference, USA (2018).

[A.32] **P. Roztocki**, M. Kues, C. Reimer, L. Romero Cortés, S. Sciara, B. Wetzel, Y. Zhang, A. Cino, S.T. Chu, B.E. Little, D.J. Moss, L. Caspani, J. Azaña, and R. Morandotti, "Integrated Generation of Complex Optical Quantum States and Their Coherent Control", Nanophotonics Australasia, Melbourne, Australia (2017).

[A.31] C. Reimer, M. Kues, **P. Roztocki**, L.R. Cortes, S. Sciara, B. Wetzel, Y. Zhang, A. Cino, S.T. Chu, B.E. Little, D.J. Moss, L. Caspani, J. Azaña, and R. Morandotti, "Integrated Generation of High-dimensional Entangled Photon States and Their Coherent Control", Frontiers in Optics, Washington, USA (2017).

[A.30] C. Reimer, M. Kues, **P. Roztocki**, B. Wetzel, Y. Bromberg, B.E. Little, S.T. Chu, D.J. Moss, L. Caspani, and R. Morandotti, "Entanglement Generation with Integrated Optical Frequency Sources", OSA Nonlinear Optics, Waikoloa, Hawaii, USA (2017).

[A.29] **P. Roztocki**, M. Kues, C. Reimer, B.E. Little, S.T. Chu, D.J. Moss, and R. Morandotti, "Four-Wave Mixing Photon Pair Generation Statistics for a Nonlinear Microcavity with Chaotic and Pulsed Excitation", CLEO Europe, Munich, Germany (2017).

[A.28] M. Kues, C. Reimer, B. Wetzel, **P. Roztocki**, B.E. Little, S.T. Chu, T. Hansson, E.A. Viktorov, D.J. Moss, and R. Morandotti, "A Passively Mode-locked Nanosecond Laser with an Ultra-narrow Spectral Width", CLEO Europe, Munich, Germany (2017).

[A.27] **P. Roztocki**, M. Kues, C. Reimer, B. Wetzel, B.E. Little, S.T. Chu, D.J. Moss, and R. Morandotti, "Practical Pulsed Quantum Frequency Comb Generation Scheme", Photonics North, Ottawa, Canada (2017).

[A.26] **P. Roztocki**, M. Kues, C. Reimer, B.E. Little, S.T. Chu, D.J. Moss, and R. Morandotti, "Four-Wave Mixing Photon Pair Generation Statistics for a Nonlinear Microcavity with Chaotic and Pulsed Excitation", Photonics North, Ottawa, Canada (2017).

[A.25] Y. Zhang, C. Reimer, J. Wu, **P. Roztocki**, B. Wetzel, B.E. Little, S.T. Chu, D.J. Moss, M. Kues, and R. Morandotti, "Multi-Channel Phase-Sensitive Amplification in Nonlinear Waveguides", CLEO, San Jose, USA (2017).

[A.24] **P. Roztocki**, M. Kues, C. Reimer, B. Wetzel, B.E. Little, S.T. Chu, D.J. Moss, and R. Morandotti, "Pulsed Quantum Frequency Combs from an Actively Mode-Locked Intra-Cavity Generation Scheme", CLEO, San Jose, USA (2017).

[A.23] **P. Roztocki**, M. Kues, C. Reimer, B.E. Little, S.T. Chu, D.J. Moss, and R. Morandotti, "Four-Wave Mixing Photon Pair Generation Statistics for a Nonlinear Microcavity with Chaotic and Pulsed Excitation", CLEO, San Jose, USA (2017).

[A.22] M. Kues, C. Reimer, B. Wetzel, **P. Roztocki**, B.E. Little, S.T. Chu, T. Hansson, E.A. Viktorov, D.J. Moss, and R. Morandotti, "An Ultra-narrow Spectral Width Passively Mode-locked Laser", CLEO, San Jose, USA (2017).

[A.21] M. Kues, C. Reimer, B. Wetzel, **P. Roztocki**, B. Little, S.T. Chu, D.J. Moss, and R. Morandotti, "Nanosecond Passively Mode-locked Laser with a Hundred Megahertz Spectral Bandwidth", Frontiers in Optics, Rochester, USA (2016).

[A.20] C. Reimer, M. Kues, **P. Roztocki**, L. Caspani, Y. Bromberg, B. Wetzel, B. Little, S.T. Chu, D.J. Moss, and R. Morandotti, "Generation of Multi-photon Entangled States with Integrated Optical Frequency Comb Sources", Frontiers in Optics, Rochester, USA (2016).

[A.19] Y. Zhang, J. Wu, C. Reimer, **P. Roztocki**, B. Wetzel, B. Little, S.T. Chu, D.J. Moss, M. Kues, and R. Morandotti, "Phase-Sensitive Amplification with Net Gain in Low-Loss Integrated Waveguides", Frontiers in Optics, Rochester, USA (2016).

[A.18] C. Reimer, M. Kues, **P. Roztocki**, B. Wetzel, B.E. Little, S.T. Chu, T. Johnston, Y. Bromberg, L. Caspani, D.J. Moss, and R. Morandotti, "On-Chip Generation of Four-Photon Entangled Qubit States", Plasma-Quebec, Montreal, Canada (2016).

[A.17] **P. Roztocki**, C. Reimer, M. Kues, B. Wetzel, F. Grazioso, Y. Bromberg, B.E. Little, S.T. Chu, D.J. Moss, L. Caspani, and R. Morandotti, "Integrated Quantum Frequency Comb of Entangled Qubits", Plasma-Quebec, Montreal, Canada (2016).

[A.16] M. Kues, C. Reimer, **P. Roztocki**, B. Wetzel, F. Grazioso, L. Caspani, Y. Bromberg, W. Munro, S.T. Chu, B.E. Little, D.J. Moss, and R. Morandotti, "Multi-correlated Two-Photon States from a Bi-Modal Integrated Frequency Comb Source", Integrated Photonics Research, Silicon and Nanophotonics, Vancouver, Canada (2016).

[A.15] M. Kues, C. Reimer, **P. Roztocki**, L. Caspani, Y. Bromberg, B. Wetzel, B.E. Little, S.T. Chu, D.J. Moss, and R. Morandotti, "Multi-photon Entangled Quantum State from Integrated Optical Frequency Combs", OSA Latin America Optics and Photonics Conference, Medellin, Colombia (2016).

[A.14] M. Kues, C. Reimer, B. Wetzel, **P. Roztocki**, F. Grazioso, L. Caspani, Y. Bromberg, B.E. Little, W. Munro, S.T. Chu, D.J. Moss, and R. Morandotti, "Two-Photon Multi-Correlated

States from an On-Chip Bi-Modal Micro-Cavity", OSA Latin America Optics and Photonics Conference, Medellin, Colombia (2016).

[A.13] M. Kues, C. Reimer, **P. Roztocki**, B. Wetzel, F. Grazioso, Y. Bromberg, B.E. Little, S.T. Chu, D.J. Moss, L. Caspani, and R. Morandotti, "On-Chip Frequency Comb of Entangled Qubits", OSA Latin America Optics and Photonics Conference, Medellin, Colombia (2016).

[A.12] M. Kues, C. Reimer, B. Wetzel, **P. Roztocki**, L. Caspani, Y. Bromberg, B.E. Little, W.J. Munro, S.T. Chu, D.J. Moss, and R. Morandotti, "Four Mode Multi-correlated Bi-Photon States within an Integrated Quantum Frequency Comb", CLEO, San José, USA (2016).

[A.11] C. Reimer, M. Kues, **P. Roztocki**, L. Caspani, Y. Bromberg, B. Wetzel, B.E. Little, S.T. Chu, D.J. Moss, and R. Morandotti, "On-chip Generation of Four-Photon Entangled Qubit States", CLEO, San José, USA (2016).

[A.10] C. Reimer, M. Kues, **P. Roztocki**, B. Wetzel, Y. Bromberg, F. Grazioso, B.E. Little, S.T. Chu, D.J. Moss, L. Caspani, and R. Morandotti, "Integrated Quantum Frequency Comb Source of Entangled Qubits", CLEO, San José, USA (2016).

[A.9] M. Kues, **P. Roztocki**, C. Reimer, B. Wetzel, L. Caspani, Y. Bromberg, B.E. Little, W.J. Munro, S.T. Chu, D.J. Moss, and R. Morandotti, "Two-Photon Four-Mode Multi-Correlated States within a Bi-Modally Pumped Integrated Kerr Optical Parametric Oscillator", Photonics North, Quebec, Canada (2016).

[A.8] C. Reimer, M. Kues, **P. Roztocki**, B. Wetzel, F. Grazioso, Y. Bromberg, B.E. Little, S.T. Chu, D.J. Moss, L. Caspani, and R. Morandotti, "Integrated Frequency Comb of Time-Bin Entangled Photon Pairs", Frontiers in Optics / Laser Science (FIO/LS), San José, USA (2015).

[A.7] M. Kues, C. Reimer, B. Wetzel, **P. Roztocki**, L. Caspani, F. Grazioso, Y. Bromberg, B.E. Little, W.J. Munro, S.T. Chu, D.J. Moss, and R. Morandotti, "Multi-Correlated Two-Photon States within an Integrated Quantum Frequency Comb", Frontiers in Optics / Laser Science (FIO/LS), San José, USA (2015).

[A.6] C. Reimer, M. Kues, B. Wetzel, **P. Roztocki**, B.E. Little, S.T. Chu, D.J. Moss, and R. Morandotti, "Ultra-low Power Passive Mode-locking Using an Integrated Nonlinear Microring Resonator", Colloque de Plasma-Quebec, Montreal, Canada (2015).

[A.5] C. Reimer, M. Kues, B. Wetzel, **P. Roztocki**, B.E. Little, S.T. Chu, D.J. Moss, and R. Morandotti, "Ultra-Low Power Passive Mode-Locking Using an Integrated Nonlinear Microring Resonator", Photonics North, Ottawa, Canada (2015).

[A.4] C. Reimer, M. Kues, L. Caspani, B. Wetzel, **P. Roztocki**, M. Clerici, Y. Jestin, M. Ferrera, M. Peccianti, A. Pasquazi, B.E. Little, S.T. Chu, D.J. Moss, and R. Morandotti, "Integrated Bichromatically Pumped Optical Parametric Oscillator for Orthogonally Polarized Photon Pair Generation", OSA Integrated Photonics Research, Silicon and Nanophotonics 2015, Boston, USA (2015).

[A.3] C. Reimer, M. Kues, B. Wetzel, **P. Roztocki**, B.E. Little, S.T. Chu, D.J. Moss, and R. Morandotti, "Passive Mode-Locking of Transform-Limited Hundred-ps Long Pulses using an Integrated Nonlinear Microring Resonator", OSA Integrated Photonics Research, Silicon and Nanophotonics 2015, Boston, USA (2015).

[A.2] L. Caspani, C. Reimer, M. Kues, B. Wetzel, **P. Roztocki**, M. Clerici, Y. Jestin, M. Ferrera, M. Peccianti, A. Pasquazi, B.E. Little, S.T. Chu, D.J. Moss, and R. Morandotti, "Direct Generation of Cross-polarized Photons on a Chip", CLEO-Europe, Munich, Germany (2015).

[A.1] C. Reimer, M. Kues, B. Wetzel, **P. Roztocki**, B.E. Little, S.T. Chu, D.J. Moss, and R. Morandotti, "Ultra-Low Power Passive Mode-locking Using an Integrated Nonlinear Microring Resonator", CLEO, San José, USA (2015).

Press Releases (Selected)

[R.5] **P. Roztocki** and R. Morandotti, "Death and Rebirth through Nonlinear Control", Science 372, 6537 (2021).

[R.4] **P. Roztocki** and R. Morandotti, "Astrocombs for Extreme-precision Spectroscopy", Nature Astronomy 2, 135–136 (2019).

[R.3] Y. Zhang, **P. Roztocki**, C. Reimer, M. Kues, D. J. Moss, and R. Morandotti, "Quantum State Generation in Optical Frequency Combs for Quantum Computing", The Bridge 1, 8-17 (2018).

[R.2] M. Kues, C. Reimer, **P. Roztocki**, D. Moss, and R. Morandotti, "Quantum Communications and Computing", Photonics Spectra 1, 76 (2017)

[R.1] M. Kues, C. Reimer, **P. Roztocki**, S. Sciara, L. Caspani, Y. Bromberg, B. Wetzel, F. Grazioso, M. Clerici, M. Peccianti, M. Ferrera, A. Pasquazi, B. E. Little, S. T. Chu, D. J. Moss, and R. Morandotti, "On-chip Frequency Combs for Optical Quantum State Generation", IEEE Photonics Society Newsletter (October 2016) (invited).